

1 **Title:** Longitudinal trajectories of brain development from infancy to school age and their  
2 relationship to literacy development  
3

4  
5 **Authors:** Ted K. Turesky<sup>1</sup>, Elizabeth Escalante<sup>1</sup>, Megan Loh<sup>1</sup>, Nadine Gaab<sup>1,2</sup>  
6  
7  
8  
9

10  
11 **Affiliations**

12 <sup>1</sup>Harvard Graduate School of Education, Cambridge, MA

13 <sup>2</sup>Harvard Medical School, Boston, MA  
14  
15  
16

17 **Correspondence**

18 Ted K. Turesky

19 50 Church Street

20 Cambridge, MA 02139

21 Theodore\_Turesky@gse.harvard.edu  
22  
23  
24  
25  
26  
27  
28

29 **Preprint URL:** <https://doi.org/10.1101/2024.06.29.601366>  
30

31 **Classifications:** Biological Sciences/Neuroscience  
32  
33  
34  
35  
36  
37  
38  
39  
40  
41  
42

43 **Keywords:** brain, development, infant, literacy, longitudinal, MRI  
44

45 **Competing interests:** The authors do not have any competing interests to report.

46 **Abstract**

47 Reading is one of the most complex skills that we utilize daily, and it involves the early  
48 development and interaction of various lower-level subskills, including phonological processing  
49 and oral language. These subskills recruit brain structures, which begin to develop long before  
50 the skill manifests and exhibit rapid development during infancy. However, how longitudinal  
51 trajectories of early brain development in these structures support long-term acquisition of literacy  
52 subskills and subsequent reading is unclear. Children underwent structural and diffusion MRI  
53 scanning at multiple timepoints between infancy and second grade and were tested for literacy  
54 subskills in preschool and decoding and word reading in early elementary school. We developed  
55 and implemented a reproducible pipeline to generate longitudinal trajectories of early brain  
56 development to examine associations between these trajectories and literacy (sub)skills.  
57 Furthermore, we examined whether familial risk of reading difficulty and children's home literacy  
58 environments, two common literacy-related covariates, influenced those trajectories. Results  
59 showed that individual differences in curve features (e.g., intercepts and slopes) for longitudinal  
60 trajectories of volumetric, surface-based, and white matter organization measures were linked  
61 directly to phonological processing and indirectly to first-grade decoding and word reading skills  
62 via phonological processing. Altogether, these findings suggest that the brain bases of  
63 phonological processing, previously identified as the strongest behavioral predictor of reading and  
64 decoding skills, may already begin to develop by birth but undergo further refinement between  
65 infancy and preschool. The present study underscores the importance of considering academic  
66 skill acquisition from the very beginning of life.

67 **Significance Statement**

68 Reading is crucial for academic, vocational, and health outcomes, but acquiring proficient reading  
69 skills is a protracted developmental process involving lower-level subskills and brain structures  
70 that undergo rapid development starting in infancy. We examined how longitudinal trajectories of  
71 early brain development support long-term acquisition of reading using a reproducible pipeline we  
72 developed specifically for infant-to-school-age longitudinal MRI data. Findings suggest that the  
73 brain bases of reading-related skills begin to develop by birth but continue building between  
74 infancy and preschool. This study emphasizes the importance of considering academic skill  
75 acquisition as a dynamic process preceding the emergence of the skill, and it offers a roadmap  
76 for future studies to examine relationships between early brain development and academic skill  
77 acquisition.

## 78 1. Introduction

79 “...the best way to determine how a child learns is to follow them closely while they are learning.”  
80 (1, 2).

81 Reading acquisition is a multifactorial, developmental process that begins long before the  
82 skill manifests. Behaviorally, the acquisition of reading necessitates the acquisition and complex  
83 interplay of lower-level literacy subskills. In turn, these subskills represent waypoint products of  
84 brain development that began in utero. Therefore, understanding how reading skill emerges  
85 requires examining its behavioral subskills and the developmental trajectories of the brain areas  
86 subserving it starting from the very beginnings of life.

87 Literacy development represents a model process through which to examine academic  
88 skill acquisition, because literacy develops hierarchically, with lower-level “subskills” interacting  
89 and driving the emergence of higher-level academic skills (e.g., 3). For instance, phonological  
90 processing, which refers to the ability to detect, understand, and manipulate speech sounds (4–  
91 7), is the most consistent predictor of subsequent decoding and word reading (4, 8–10).  
92 Meanwhile, various studies have shown that both word reading and oral language skills, which  
93 encompass abilities supporting listening comprehension (11); e.g., vocabulary and syntactic  
94 knowledge), are important subskills for reading comprehension (12). However, these subskills  
95 themselves have protracted development and the brain structures that support them begin  
96 developing long before they manifest, with the most rapid development transpiring perinatally (13,  
97 14).

98 Several cross-sectional and prospective studies have been conducted linking  
99 performance of these key literacy subskills to brain architecture. For instance, cross-sectional  
100 studies in preschoolers and kindergarteners have shown that phonological processing is  
101 associated with brain structure and function in left temporoparietal, occipitotemporal, and inferior  
102 frontal regions and tracts (15–20). This set of regions has also been linked with preschool and  
103 kindergarten oral language skills in some studies (21–23), but other studies have not shown  
104 associations (17, 24). Looking to early development, infant brain function and white matter  
105 organization have been shown to relate prospectively to (pre)school-age literacy outcomes (25–  
106 29), including phonological processing and oral language skills (30–32). Taken together, these  
107 studies suggest that certain brain areas may be important for academic skill *performance* at a  
108 particular time during development or as ‘neural scaffolding’ that supports subsequent language  
109 development (33). However, recent work in school-age children using large-scale, multi-site  
110 cross-sectional datasets showed little evidence for stable associations between individual  
111 differences in white matter organization and reading performance. Rather, using a separate

112 longitudinal dataset, investigators found associations between slopes of white matter growth and  
113 reading gains, suggesting a dynamic interplay between brain development and learning to read  
114 (34). Moreover, the brain itself is a dynamic system that undergoes its most rapid development  
115 during infancy and early childhood (13, 14), making cross-sectional and prospective designs  
116 suboptimal to capture individual differences in early skill *acquisition* (2) As such, individual  
117 longitudinal trajectories, which capture heterogenous rates of brain and skill development  
118 between infancy and second grade, are needed to examine the acquisition of (sub)skills important  
119 for literacy.

120 Therefore, the overall goal of the current study is to examine the relationship between  
121 longitudinal trajectories of early brain development and acquisition of reading-related subskills,  
122 which we undertook in four objectives. The first objective was to generate individual longitudinal  
123 trajectories of early brain development spanning infancy to school age. Prior longitudinal studies  
124 have examined trajectories of early brain development but only up to the second year of life (e.g.,  
125 35), while others have examined developmental trajectories of brain structure spanning infancy  
126 to school age but only by harmonizing cross-sectional and longitudinal datasets acquired and  
127 processed with varying methods (e.g., 36). However, to our knowledge, no purely longitudinal  
128 studies have mapped the development of brain structure, including white matter organization,  
129 from infancy to school age, using a consistent processing pipeline and one that is appropriate for  
130 early development. Indeed, methodological challenges associated with infant MRI data have  
131 restricted the number and breadth of longitudinal studies in the early developmental period. This  
132 is not only because acquiring and processing infant MRI data requires specialized procedures  
133 and tools to generate accurate brain estimates (37–42), but also because the use of different  
134 procedures and tools for different developmental stages can introduce bias in developmental  
135 analyses. However, the alternative—to use identical procedures and tools for all developmental  
136 stages—would likely cause estimates to vary in accuracy across ages and could introduce  
137 spurious effects and/or obscure true effects in developmental comparisons (43). Some infant-  
138 specific tools offer age-specific adjustments (e.g., different sets of templates) within the first two  
139 years of life, and the small number of studies that have examined longitudinal trajectories of brain  
140 development in the first two years have opted for a balanced approach, with age-appropriate  
141 adjustments to limited processing steps in a way that does not require fundamentally different  
142 techniques for different ages (e.g., additional sequences or different smoothing kernels; (35, 44).  
143 However, methods to accommodate a wider early developmental range are lacking.

144 In the current study, we extend this work by developing reproducible pipelines for  
145 generating longitudinal trajectories of volumetric, surface-based, and white matter organization

146 brain measures from infancy to school age. To do this, we leveraged both infant-specific and  
147 standard MRI procedures and tools. We then compared among several candidate linear and  
148 nonlinear mixed effects models, varying according to function (e.g., linear, logarithmic) and  
149 random parameters (e.g., intercepts alone versus intercepts and slopes), to identify the model  
150 with the most parsimonious fit (45). In general, prior longitudinal studies have reported rapid  
151 growth at birth that tapers with age (35, 46–48), except for cortical thickness, which peaks  
152 between ages one and two years (49), suggesting logarithmic functions might provide a better fit  
153 compared with other functions for most measures.

154 Our second objective was to examine the association of individual differences in early  
155 brain development to long-term literacy development. As such, we extracted curve features (e.g.,  
156 intercepts and slopes) from individual longitudinal trajectories for brain areas and tracts previously  
157 shown to relate to reading-related skill development in longitudinal studies in older children (34,  
158 50–59) or prospective studies in infants (30–32). We then tested these curve features for  
159 correlations with preschool/early kindergarten phonological processing, a key literacy subskill.  
160 Based on converging evidence from prior neuroimaging (30–32) and genetics studies (60, 61),  
161 we hypothesized that phonological processing skill would relate to curve intercepts (i.e., brain  
162 estimates at birth) and slopes (i.e., rate of brain development). If the foundations of literacy  
163 development are largely present at birth and stable across early development, then we expect  
164 most of these brain-behavior associations to be with curve intercepts, whereas if the brain  
165 development subserving literacy subskills is more protracted or dynamic, as suggested by Roy  
166 and colleagues (34), then we expect brain-behavior associations to be with curve slopes.

167 Our third objective was to examine the roles of risk factors related to literacy skills in  
168 shaping longitudinal trajectories of early brain development. Reading difficulty is heritable, as 40-  
169 60% of children with a familial risk (e.g., first-degree relative with a history) of reading difficulty  
170 (FHD+) themselves develop reading difficulty (62, 63) Brain imaging studies of FHD+  
171 preschoolers show reduced gray matter volume, activation, and fractional anisotropy in left  
172 occipito-temporal and temporo-parietal regions (16–18) and tracts (57) compared with FHD-  
173 preschoolers; these reductions overlap with those observed in children with reading difficulty (20,  
174 64–70), suggesting that the phenotypes characteristic of reading difficulty manifest in some  
175 children before the start of formal reading instruction. Concordantly, similar alterations have been  
176 observed earlier in development, where FHD+ infants exhibited lower fractional anisotropy in left  
177 arcuate fasciculus compared with FHD- infants (71), distinguishable patterns of functional  
178 connectivity in left fusiform gyrus as shown by a support vector machine classifier (72), and  
179 alterations in neural responses to basic speech sounds as measured by event-related potentials

180 (73–75). Possibly underlying this heritability, work in genetics, including recent large-scale  
181 genome-wide studies, has shown that reading-related skills (60) and reading difficulty (76, 77) are  
182 associated with variation in genes involved in early developmental processes, including  
183 neurogenesis and axon guidance (78).

184 Another risk factor repeatedly shown to affect children’s literacy skills is the home literacy  
185 environment, which includes caregiver–child shared reading and reading-related resources, in  
186 preschool literacy skills (79–84) and in infancy/toddlerhood (83, 85–90). Recent work has also  
187 identified links between the home literacy environment and brain architecture in  
188 preschoolers/kindergarteners (21, 24, 91–94) and infants (95, 96). Overall, these studies offer  
189 strong evidence that genetic and environmental factors related to the development of reading-  
190 related skills are likely to affect longitudinal trajectories of brain development starting perinatally.  
191 Therefore, we hypothesized that the FHD status and home literacy environment would  
192 significantly contribute, as covariates, to longitudinal trajectories of brain development in left  
193 hemisphere temporo-parietal, occipito-temporal, and inferior frontal regions and tracts.

194 Our fourth objective was to broaden the scope of our examination of early brain-literacy  
195 associations to other literacy-related subskills and subsequent reading skills. Reading acquisition  
196 is a hierarchical process in which multiple distinct but interacting subskills (including but not limited  
197 to phonological processing) converge to effect higher-order skills. First, we tested the specificity  
198 of associations with phonological processing by examining another subskill important for reading  
199 comprehension, oral language skill. Second, we tested whether phonological processing  
200 mediated relationships between curve features of early brain development and subsequent  
201 measures of decoding and word reading skill. Taken altogether, findings from this study will inform  
202 our understanding of how early brain development contributes to later reading-related skill  
203 acquisition.

204

205

206

207 **2. Methods**

208 2.1. Participants

209 Children examined in this study were obtained from two longitudinal cohorts: the New England  
 210 dataset and the Calgary open-source dataset (<https://osf.io/axz5r/>). Only children with high-quality  
 211 (i.e., post-QC, please see below) MRI data from at least two timepoints between birth and late  
 212 childhood were included. Due to the multi-modal nature of the study, varying numbers of  
 213 longitudinal datasets were used for structural (n = 98 with 276 observations) versus diffusion  
 214 analyses (n = 128 with 396 observations). For the New England cohort, family history (i.e., first-  
 215 degree relative with a history) of reading difficulty was also examined and present in 40 of 80  
 216 children. For children ages  $\leq 24$  months, demographic information was provided by caregivers.  
 217 Please see Table 1 for overall demographic details, Supplementary Table 1 for demographic  
 218 details by modality, and Supplementary Methods for participant information, including race  
 219 demographics, unique to each cohort. This study was approved by the Institutional Review Boards  
 220 of Boston Children’s Hospital (IRB-P00023182), Harvard University (IRB21-0916), and the  
 221 University of Calgary Conjoint Health Research Ethics Board (REB13-0020). Participants’ parents  
 222 gave informed consent, and children gave verbal assent if over 25 months old. Data examined  
 223 here partially overlap with brain images analyzed in previous studies examining infant brain  
 224 development (30–32, 36, 48, 54, 71, 72, 96–102).

225

<i>General information</i>	Numbers participants   observations	137   441
	Number observations per participant	3 ± 1
	Age at literacy-related subskill and cognitive testing (months)	63 ± 5.3
	Age at decoding/word reading testing (months)	82 ± 6.4
<i>Covariates</i>	Biological sex (F/M)	73/64
	Maternal education (years)	17 ± 2.1
	Cohort ([New England]/Calgary)	80/57
	Family history of reading difficulty (+/-)	40/40
	Home literacy environment (a.u.)	0.037 ± 0.41
<i>Literacy-related subskills</i>	Phonological processing standard score	106 ± 14
	Oral language standard score	113 ± 13
<i>Decoding/word reading</i>	Word attack standard score	112 ± 14
	Word identification standard score	110 ± 17
<i>Cognitive abilities</i>	Nonverbal general cognitive ability	106 ± 13

226

## 227 2.2. Environmental variables

228 Socioeconomic status was measured with maternal education, consistent with prior brain imaging  
229 studies on socioeconomic status (103–108). Maternal education measures were collected during  
230 each timepoint, although inter-time-point variability was low, and these were averaged to generate  
231 one socioeconomic status measure across the developmental window. Rather than using ordinal  
232 coding, years of education as a continuous measure ranging from 12 to 20 years were used.

233 For the New England cohort, parents also completed at each time point questionnaires  
234 relating to children’s home literacy environments home literacy environment, which includes the  
235 extent of parent-child shared reading and access to reading-related resources (109). Responses  
236 were indicated using ordinal scales ranging from 1 to 6. As responses were non-normally  
237 distributed ( $p < 0.05$  according to the Shapiro-Wilk normality test; Supplementary Figure 1),  
238 except for “Time read to per week” for all timepoints and “Frequency with which family members  
239 share rhymes or jokes with the child” for one timepoint, they were normalized and then averaged  
240 at each timepoint according to procedure used previously (30). As with maternal education, home  
241 literacy environment estimates, which exhibited low inter-timepoint variability, were averaged to  
242 generate one estimate per individual across the developmental window. These overall home  
243 literacy environment estimates, which were normally distributed (Shapiro-Wilk  $W = 0.99$ ,  $p > 0.05$ ;  
244 Supplementary Figure 2), were used in later statistical analyses.

245

## 246 2.3. Literacy and cognitive measures

247 Two literacy subskills were administered to children prior to the beginning of formal reading  
248 instruction: phonological processing and oral language. These constructs were selected as  
249 representative subskills supporting literacy development (3, 4, 8–10, 12, 110); however, they  
250 constitute a small subset of literacy-related measures collected for this cohort. No outliers were  
251 detected using the *isoutlier* function in MATLAB, which sets an outlier threshold at three scaled  
252 median absolute deviations from the median.

253 Phonological processing was measured in both New England and Calgary cohorts. For  
254 the New England cohort, the *phonological processing* composite was estimated from three  
255 subtests from the WJ-IV Tests of Cognitive Abilities: word access, word fluency, and substitution  
256 (111). Word access measures phonetic coding by asking children to identify words containing  
257 certain sounds. Word fluency measures speed of lexical access by asking children to name as  
258 many words as possible beginning with a certain sound in one minute. Substitution measures  
259 children’s ability to produce a new word by replacing one sound from a provided word with another  
260 sound. Importantly, while the word access and word fluency subtests require some level of lexical

261 access, these subtests, along with the substitution subtest, are well established measures of  
262 phonological/phonemic processing/awareness. For additional details and item examples from the  
263 technical manual, please see the Supplementary Methods. Children in the Calgary cohort were  
264 administered the phonological processing subtest of the NEPSY-II, which measures phonemic  
265 awareness (112). Unlike the New England cohort, each child from the Calgary cohort completed  
266 this subtest multiple times. To harmonize phonological processing scores across the two  
267 datasets, we used NEPSY-II scores from when the child was closest in age to the average age  
268 at which the New England cohort completed the WJ-IV (64 months) and not earlier than 50 months  
269 of age.

270 The composite oral language, which was only measured in the New England cohort, was  
271 estimated from two subtests from the WJ-IV Tests of Oral Language: picture vocabulary and oral  
272 comprehension (113). Picture vocabulary measures lexical knowledge by asking children to  
273 specify a picture corresponding to a given word or naming an object. Oral comprehension  
274 measures oral listening, vocabulary, and reasoning by asking children to identify missing words  
275 from short passages. All assessments were administered and double-scored by testers trained  
276 by a clinical psychologist and then raw scores were converted to standard scores.

277 In addition, we measured decoding and word reading with two untimed subtests from the  
278 Woodcock Reading Mastery Tests III (114): word attack and word identification. For word attack,  
279 children were presented with pseudowords that they needed to *decode* using phonological  
280 abilities. For word identification, children were presented with individual real words that they  
281 needed to *read*. Word attack and word identification subtests were administered at the beginning  
282 of formal reading instruction.

283 Lastly, we measured children's nonverbal general cognitive ability at preschool/early  
284 kindergarten-age using the Matrix Reasoning subtest of the Kaufman Brief Intelligence Test: 2nd  
285 Edition (KBIT-2, (115)). Herein, children were asked to identify the piece missing from a matrix of  
286 visual images.

287 All raw estimates for each of the WJ-IV, NEPSY-II, and WRMT subtests were non-  
288 normally distributed ( $p < 0.05$  according to the Shapiro-Wilk normality test), except for  
289 preschool/early kindergarten picture vocabulary and late kindergarten/grade 1 word attack  
290 (Supplementary Figure 3). All standardized (composite) estimates used in subsequent analyses  
291 were normally distributed ( $p > 0.05$ ; Supplementary Figure 4).

292  
293  
294

## 295 2.4. MRI data acquisition and processing

296 All data were acquired on a 3.0 T scanner with a 32-channel head coil. Please see Supplementary  
297 Methods for cohort-specific acquisition parameters.

298 The rapid brain growth transpiring immediately after birth posed serious challenges for  
299 structural MRI processing because standard methods that are optimal for older children are  
300 suboptimal for infants and vice versa (43). To circumvent bias associated with choosing a single  
301 pipeline for multiple developmental stages, we implemented pipelines that are age-appropriate  
302 but not fundamentally different for each developmental stage.

303

### 304 2.4.1. Structural MRI processing and quality control

305 Raw magnetization-prepared rapid gradient-echo (MPRAGE) images were visually inspected for  
306 artifacts by a trained rater and scored as “fail,” “check,” or “pass” (116). Only images scored as  
307 “check” or “pass” underwent image processing. The standard, unmodified FreeSurfer v7.3  
308 (<https://surfer.nmr.mgh.harvard.edu/>) “recon” pipeline was used for brains > 50 months.  
309 Processing procedures for brains < 50 months were similar in concept to those described in (117).  
310 Namely, Infant FreeSurfer (for brains  $\leq$  24 months) or standard FreeSurfer (for brains 25 to 50  
311 months) was used to extract the brain from the skull, correct for intensity inhomogeneity, and  
312 segment MPRAGE images by tissue class (gray matter, white matter, cerebrospinal fluid) and  
313 subcortical brain region (40); <https://surfer.nmr.mgh.harvard.edu/fswiki/infantFS>). To improve  
314 tissue classification accuracy, MPRAGE images were submitted in parallel to iBEATv2.0 Docker  
315 1.0.0 (118–120); <https://github.com/iBEAT-V2/iBEAT-V2.0-Docker>), has been validated for birth  
316 to age six years (118). Resulting segmentations from each software package were then  
317 hybridized using in-house MATLAB code that combined the cortical pial and white matter  
318 boundaries labelled by iBEATv2.0 with the subcortical parcellations of Infant FreeSurfer (brains  $\leq$   
319 24 months) or standard Freesurfer (brains 25 to 50 months), effectively relabeling cortical gray  
320 and white matter in the FreeSurfer-style segmentation; for details, please see the Supplementary  
321 Methods. Structural processing was finalized by submitting these FreeSurfer-style hybrid  
322 segmentations to a modified version of the standard FreeSurfer v7.3 “recon” pipeline, which, for  
323 brains  $\leq$  24 months, incorporated elements from Infant FreeSurfer. For a schematic of the  
324 structural processing pipeline, please see Supplementary Figure 5.

325 Resulting white and pial surfaces were visually inspected by two (brains > 50 months) or  
326 three (brains  $\leq$  24 months) trained raters on a 3-point scale (0, 1, and 2) and datasets with average  
327 ratings > 1.5 were retained for subsequent analyses. Finally, parcellations were visualized to  
328 ensure accuracy of anatomical labels. For reproducibility purposes, we did not perform manual

329 editing to correct tissue mislabeling in the remaining images; however, structural measures from  
330 edited and unedited pediatric brain images processed with FreeSurfer have been shown to be  
331 highly correlated (121), including in children (122). Measures of gray and white matter volume,  
332 surface area, cortical thickness, and mean curvature, generated in the final FreeSurfer steps,  
333 were extracted from 8 a priori left hemisphere regions delineated with the Desikan-Killiany atlas—  
334 banks of the superior temporal sulcus, fusiform gyrus, inferior parietal lobule, middle temporal  
335 gyrus, pars opercularis, pars triangularis, superior temporal gyrus, and supramarginal gyrus—  
336 based on their reported involvement in reading-related subskills (15–23, 30–32, 54, 60; for  
337 reviews, please see 123, Table 3 and 124).

338

#### 339 2.4.2. Diffusion MRI processing and quality control

340 Preprocessed and tractography for all diffusion-weighted image (DWI) data, regardless of age,  
341 were performed with MRtrix3 based on the pipeline established for the Developing Human  
342 Connectome Project (41, 125). DWI data were first denoised using Marchenko–Pastur principal  
343 component analysis (126–128) and then corrected for susceptibility distortions, eddy currents,  
344 motion, and intensity inhomogeneity using FSL’s topup and eddy (with slice-to-volume correction)  
345 functions (129–133), and Advanced Normalization Tools (ANTs) N4 bias correction tool (134).  
346 Subsequently, three tissue response functions for spherical deconvolution were estimated using  
347 the Dhollander algorithm, a 0.1 fractional anisotropy threshold, and eight maximum harmonic  
348 degrees (135). Fiber orientation densities (FODs) were computed with multi-shell, multi-tissue  
349 constrained spherical deconvolution (136, 137) and then normalized using multi-tissue informed  
350 log-domain intensity normalization.

351 Two million streamlines were tracked from the normalized FOD maps using the  
352 Anatomically Constrained Tractography (ACT) technique. Importantly, ACT has been shown to  
353 greatly improve tractography, but it relies on accurate tissue segmentations, which are typically  
354 challenging to generate with infant brain data. Using the hybrid segmentations generated for  
355 brains  $\leq 50$  months (please see above) circumvented this challenge. Thus, FreeSurfer-style  
356 hybrid segmentations for brains  $\leq 50$  months and standard FreeSurfer segmentations for brains  
357  $> 50$  months were registered to the preprocessed DWI images using ANTs and then converted  
358 to five-tissue-type images for ACT. The remaining whole-brain tractography parameters included  
359 seeding at the gray/white matter boundary and tracking with the iFOD1 probabilistic algorithm;  
360 step size, minimum and maximum length, and maximum step angle were set to default (138, 139).

361 Resulting whole-brain tractography was then submitted to the open-source instantiation  
362 of Automated Fiber Quantification (AFQ; (140) for waypoint- and probabilistic-atlas-based fiber

363 tract segmentation. The standard pyAFQ pipeline was used for brains > 24 months (141), whereas  
364 pyBabyAFQ was used for brains  $\leq$  24 months (142). Please see Supplementary Methods for a  
365 summary of differences between the two AFQ instantiations. Next, tracts were resampled to 100  
366 equidistant nodes, and diffusion properties (fractional anisotropy; mean diffusivity) were quantified  
367 for each node for the left hemisphere tracts of interest—arcuate fasciculus, superior longitudinal  
368 fasciculus, and inferior longitudinal fasciculus. Mean fractional anisotropy and mean diffusivity  
369 values for each tract were used to examine model fits (please see section 2.5.1), whereas a more  
370 fine-grained, node-based approach was taken for brain-behavior analyses (please see section  
371 2.5.2). For the latter, to better align tract cores across participants, five nodes on either end were  
372 removed, reducing the total number of nodes per tract to 90. Finally, tracts of interest were visually  
373 inspected by two trained raters on a 3-point scale (0, 1, and 2) and datasets with average ratings  
374  $\geq$  1 were retained for subsequent analyses. For a schematic of the diffusion processing pipeline,  
375 please see Supplementary Figure 6.

376

## 377 2.5. Statistical analyses

378 An overview of statistical operations, all of which were performed in RStudio version 4.2.2, can  
379 be found in Supplementary Figure 7.

### 380 2.5.1. Longitudinal trajectory estimation

381 Prior to modeling, estimates of brain structure and white matter organization underwent a final  
382 quality control procedure to remove estimates for brain areas/tracts of interest if, for brains > 25  
383 months, they were preceded or followed by  $\geq$  10% annual change (positive or negative) in any  
384 measure and for brains  $\leq$  24 months, inter-observation changes were negative (or positive for  
385 mean diffusivity). To mitigate data loss, we next identified which observation—earlier or later—  
386 was more likely to be inaccurate, using an outlier detection procedure (described in the  
387 Supplementary Methods). All remaining participants after these procedures had multiple  
388 observations.

389 To generate longitudinal trajectories (i.e., growth curves), we next submitted cleaned,  
390 longitudinal structural and white matter organization estimates to linear mixed effects models  
391 using linear, logarithmic, and quadratic functions from the R 'lme4' package. Intercepts and slopes  
392 were modeled as fixed and random effects, and covariates for biological sex, socioeconomic  
393 status, and cohort (New England or Calgary) were entered as fixed effects. Vijayakumar and  
394 colleagues recommends comparing model fits quantitatively (45); consequently, we computed  
395 Bayesian Information Criterion (BIC) metrics and the model (i.e., function and number of random  
396 terms) that provided the best fit (i.e., lowest BIC value) was selected for subsequent analyses.

397 Correlations between intercepts and slopes were tested to ensure associations between random  
398 terms were minimized. Most curve features were normally distributed according to the Shapiro-  
399 Wilk normality test ( $p > 0.05$ ) and histograms depicting their distributions are provided in  
400 Supplementary Figures 9-15.

401

402 2.5.2. Associations between longitudinal trajectories of early brain development and phonological  
403 processing

404 Next, individual-level curve features (i.e., intercepts and slopes) were extracted and tested for  
405 correlations (Pearson) with literacy subskills. The extracted curve features represent individual  
406 variation in intercepts or slopes beyond what would be predicted based on the covariates (e.g.,  
407 biological sex); consequently, we did not include these same covariates in the tests of  
408 correlations. To determine whether curve features of volumetric and surface-based measures  
409 were associated with phonological processing in the full sample after accounting for multiple brain  
410 regions (8 tests), a significance threshold was set to  $p_{FDR} < 0.05$  and applied to measures (e.g.,  
411 gray matter volume) separately. As diffusion analyses were performed node-wise (90 nodes), we  
412 corrected for multiple comparisons at  $p_{FWE} < 0.05$  using a permutation-based, threshold-free  
413 cluster enhancement method (143), implemented in the permuco package in R (144); corrections  
414 were performed separately for each tract. These methods are similar to those used previously  
415 (24, 96, 108). When significant, individual growth curves were separated into three groups  
416 according to scores on their behavioral assessment with low  $< 85$ ,  $85 \leq \text{average} \leq 115$ , and high  
417  $> 115$ , averaged by group, and then plotted.

418

419 2.5.3. Sensitivity analyses

420 We conducted four sensitivity analyses to test the reliability of our results. First, we performed a  
421 replication analysis on gray/white matter volume, surface area, and mean diffusivity with nonlinear  
422 mixed effects models using asymptotic functions from the R 'nlme' package (145), similar to that  
423 described in Alex and colleagues (36); [https://github.com/knickmeyer-lab/ORIGINs\\_ICV-and-](https://github.com/knickmeyer-lab/ORIGINs_ICV-and-Subcortical-volume-development-in-early-childhood)  
424 [Subcortical-volume-development-in-early-childhood](https://github.com/knickmeyer-lab/ORIGINs_ICV-and-Subcortical-volume-development-in-early-childhood)). Intercepts and asymptotes were modeled  
425 as fixed and random effects; rate constants were modeled as fixed effects. Second, instead of  
426 testing correlations between curve features and outcomes, we entered outcomes as main and  
427 interaction terms in linear mixed effects models. Third, adhering to recommendations to report  
428 both raw and TIV-corrected results (45), we recomputed brain-behavior associations for  
429 volumetric and surface-based measures using semipartial correlations (Pearson) with the random  
430 terms from longitudinal modeling with TIV as covariates of no interest. Fourth, we submitted

431 volumetric and surface-based brain-behavior associations to semipartial correlations (Pearson)  
432 with average (across timepoint) Euler numbers, which quantifies topological defects (146). For  
433 additional details on these sensitivity analyses and Euler quantification, please see the  
434 Supplementary Methods.

435

#### 436 2.5.4. Specificity analyses

437 To determine whether brain-behavior effects were specific to certain brain measures, regions,  
438 curve features, and behavioral outcomes, we performed three specificity analyses. First, we  
439 generated whole-brain maps depicting variability in associations with phonological processing  
440 according to brain measures (e.g., gray matter volume), region, and curve feature. Second, we  
441 examined whether brain-behavior associations for diffusion measures persisted in right arcuate  
442 fasciculus, superior longitudinal fasciculus, and inferior longitudinal fasciculus. Third, limited to  
443 the New England children, we tested correlations between curve features of brain development  
444 and oral language skill, another reading subskill, and nonverbal general cognitive abilities. For  
445 subsequent testing of literacy-related covariates, we also reanalyzed brain-behavior associations  
446 with phonological processing in the New England subsample only. For volumetric and surface-  
447 based measures, FDR correction accounted for brain regions and behavioral measures (24 tests).  
448 For diffusion, cluster-level FWE correction accounted for nodes (90 tests).

449

#### 450 2.5.5. Literacy-related factors as fixed effects in models of early brain development

451 We determined whether literacy-related covariates (i.e., home literacy environment and FHD  
452 status) contributed to the fit of the growth curve in two ways. First, we examined each covariate  
453 as fixed effects in models of brain development for measures and regions whose curve features  
454 related to phonological processing (please see brain-behavior associations in 2.5.2). For brain  
455 structure, a significance threshold of  $p_{\text{FDR}} < 0.05$  was applied to correct for the multiple brain  
456 development models that fit this criterion. Diffusion analyses, which were performed node-wise  
457 for each tract separately (90 tests), were corrected for multiple comparisons using a lenient cluster  
458 size threshold of 5 nodes, as threshold-free cluster enhancement method was not available for  
459 the statistical tests applied to covariates. Second, we compared brain development models with  
460 and without each covariate using BIC metrics. For diffusion, BIC metrics were obtained using tract  
461 averages (rather than separately on individual nodes). Correction for multiple comparisons was  
462 again set to  $p_{\text{FDR}} < 0.05$  and applied as described above for brain structure, this time also including  
463 statistics for average diffusion measures.

464 2.5.6. Indirect effects between longitudinal trajectories of early brain development and word  
465 reading outcomes via literacy subskills

466 As with previous work (147), indirect effects were tested when literacy subskills were related to  
467 curve features of brain development and decoding and word reading outcomes (after FDR  
468 correction). Formal indirect effects modeling was conducted using the Mediation package in R  
469 with 20,000 bootstrapped samples, and effects were determined significant when the 95%  
470 confidence interval for the average causal mediation effect did not include 0. All mediation models  
471 included covariates for maternal education, home literacy environment, and family history of  
472 reading difficulty. As in the sensitivity analyses, models were run twice, once without controlling  
473 for TIV and once including TIV curve features. Because mediation testing was limited to data with  
474 significant (after correction for multiple comparisons) brain-behavior associations, no additional  
475 correction for multiple correction was applied; this is consistent with prior literature (36, 147, 148).

476

477

478 2.6. Data availability

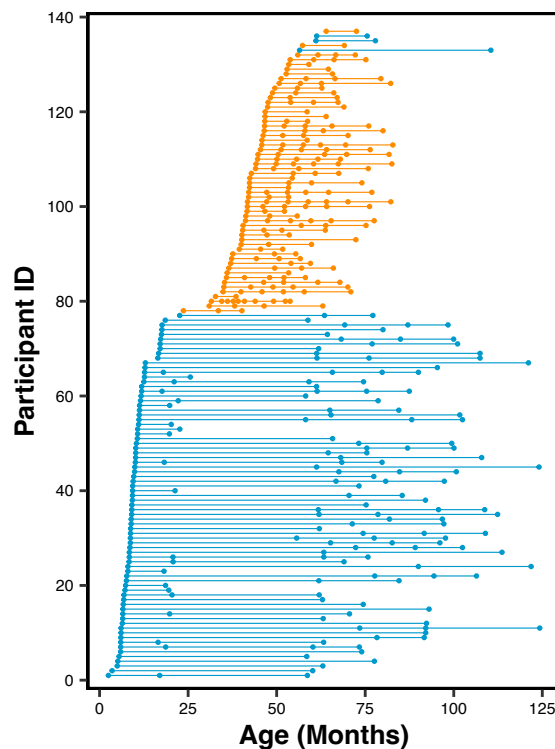
479 All code used to process and analyze has been made openly available at  
480 <https://github.com/TeddyTuresky/Longitudinal-Trajectories-Early-Brain-Development-Language>.  
481 The Calgary dataset is also freely available at <https://osf.io/axz5r/>. All Boston/Cambridge data  
482 used in this study will be made publicly available at upon acceptance of the manuscript.

483

### 484 3. Results

#### 485 3.1. Longitudinal trajectories of brain structure and white matter organization in left hemisphere 486 literacy-related brain regions and tracts

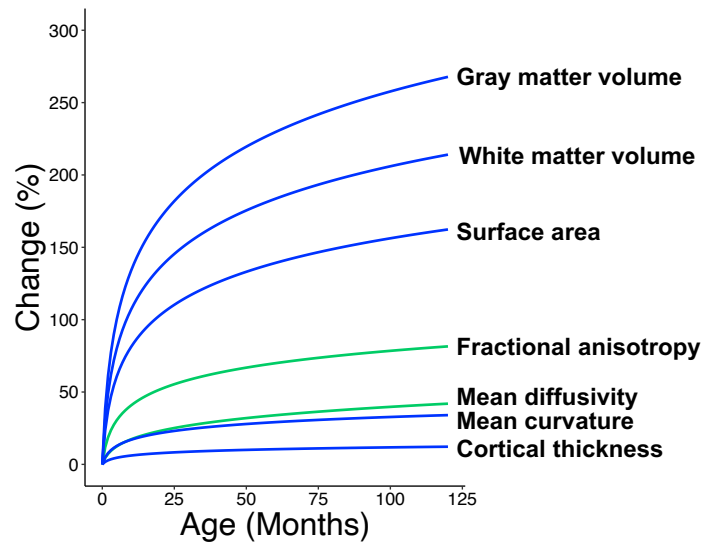
487 Our first objective was to generate accurate longitudinal trajectories of early brain development in  
488 regions and tracts reportedly involved in reading-related subskills (15–23, 30–32, 54, 60; for  
489 reviews, please see 123, Table 3 and 124). Accordingly, growth curves for regional estimates of  
490 gray and white matter volume, surface area, cortical thickness, and mean curvature and for tract  
491 estimates of fractional anisotropy and mean diffusivity were generated from 137 children (F/M =  
492 73/64) with 441 observations. Every child had at least two observations between birth and school  
493 age with 77 having at least one observation in infancy (Figure 1; please see Supplementary Figure  
494 16 for age distributions by modality). Linear mixed effects models included individual-level  
495 intercepts and slopes as well as covariates for biological sex, socioeconomic status, and cohort.  
496 All structural and diffusion measures for all regions and tracts were best fit with logarithmic  
497 functions according to Bayesian Information Criterion (Supplementary Table 2), whereby rates of  
498 development were steeper perinatally and then slowed across the first ten years following birth  
499 (Figure 2; Supplementary Figures 17-22).



500

501 **Figure 1.** Age distribution of longitudinal dataset from infancy to late childhood. All children had  
502 structural and/or diffusion MRI data from at least two observations (dots). Blue, New England  
503 cohort; orange, Calgary cohort.

504



505

506 **Figure 2.** Average longitudinal trajectories from infancy to late childhood by measure. Raw  
507 estimates for each brain region examined and each measure were submitted to linear mixed  
508 effects models using a logarithmic function. Individual growth curves predicted by this model were  
509 averaged to show the overall longitudinal trajectory of the sample for each volumetric/surface-  
510 based (blue lines) and diffusion (green lines) measure. Absolute brain estimates were then  
511 converted to percent change values to visualize all brain measures along a single axis. For growth  
512 curves for separate brain regions and tracts, please see Supplementary Figures 17-22.

513

514

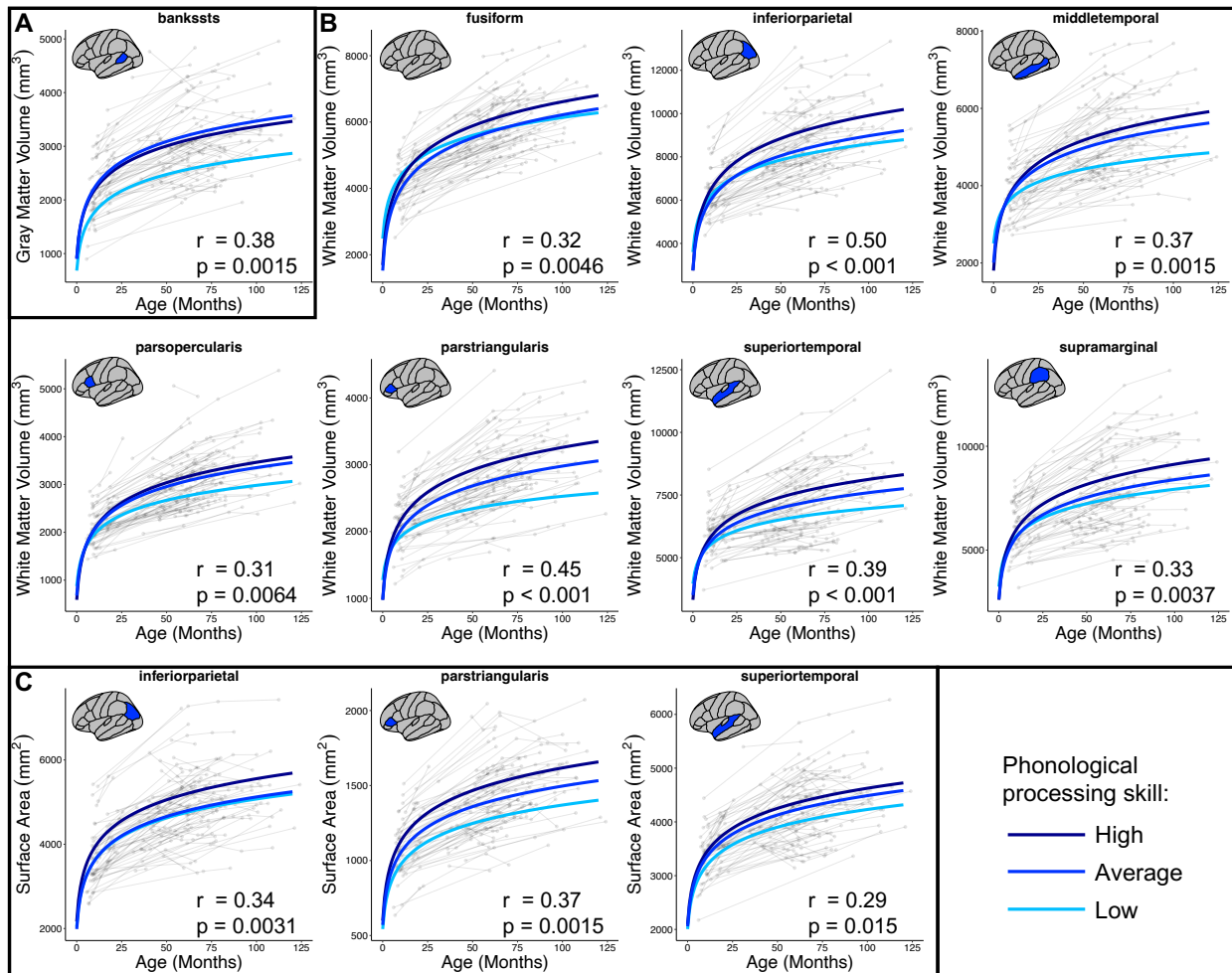
### 515 3.2. Associations between growth curve features and phonological processing

516 Our second objective was to examine whether brain development affects literacy development.  
517 Consequently, curve features (i.e., intercepts and slopes) were extracted from individual-level  
518 growth curves and tested for correlations (Pearson) with preschool/early kindergarten  
519 phonological processing scores, a subskill critical for literacy (3, 8).

520

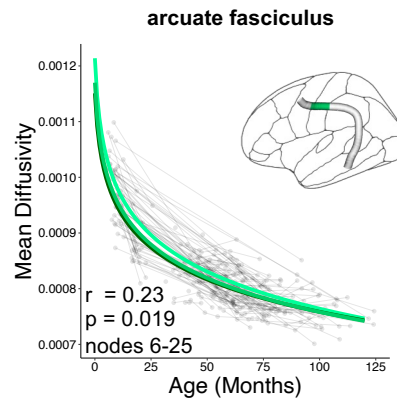
521 For volumetric and surface-based measures, curve features of gray/white matter volume  
522 and surface area in several left hemisphere regions exhibited associations with phonological  
523 processing. Specifically, greater phonological processing was associated with (a) greater  
524 intercepts of gray matter volume in the left banks of the superior temporal sulcus, (b) greater  
525 slopes of white matter volume in left occipitotemporal, temporoparietal, and inferior frontal  
526 regions, and (c) greater surface area intercepts and slopes in inferior parietal lobule, pars  
527 triangularis, and superior temporal gyrus (Supplementary Figure 23). Next, individual growth  
528 curves corresponding to these measures and regions were separated into three groups according  
529 to phonological processing scores with low  $< 85$ ,  $85 \leq \text{average} \leq 115$ , and high  $> 115$ , averaged  
by group, and then plotted to visualize variation in longitudinal trajectories by phonological

530 processing score. Most notably, children with lower phonological processing scores tended to  
 531 have less gray matter volume in left banks of the superior temporal sulcus at birth but maintained  
 532 similar rates of development compared with higher scoring children. At the same time, they had  
 533 lower rates of white matter volume growth in left occipitotemporal, temporoparietal, and inferior  
 534 frontal regions (Figure 3).



535  
 536 **Figure 3.** Longitudinal trajectories of brain structure from infancy to late childhood according to  
 537 phonological processing skill in preschool/early kindergarten. Graphs depict average trajectories  
 538 for children with low (< 85), average (85 – 115), and high (> 115) standardized phonological  
 539 processing scores for measures and regions whose (A) intercepts, (B) slopes, or (C) both  
 540 intercepts and slopes correlated with phonological processing ( $p_{FDR} < 0.05$ ). Correlation statistics  
 541 are reported adjacent to their corresponding plots; intercept and slope statistics for surface area  
 542 averaged here for visualization purposes but reported separately in Supplemental Figure 23. As  
 543 a group, children with low phonological processing in preschool/early kindergarten tended to have  
 544 attenuated longitudinal trajectories, either because they began with lower estimates, as with less  
 545 gray matter volume in the left banks of the superior temporal gyrus at birth (upper left graph), or  
 546 because they had slower rates of development, as with white matter volume in other left  
 547 hemisphere brain regions.

548 Curve features of white matter organization in the left arcuate fasciculus also correlated  
549 with phonological processing outcomes, as greater phonological processing skill was associated  
550 with greater slopes of mean diffusivity (Supplementary Figure 24). When distinguishing  
551 longitudinal trajectories according to literacy subskills (i.e., low < 85, 85 ≤ average ≤ 115, and high  
552 > 115), as with volumetric and surface-based measures above, children with low phonological  
553 processing scores tended to have higher mean diffusivity at birth but greater rates of mean  
554 diffusivity development (i.e., more negative slopes) compared with higher scoring children (Figure  
555 4). No significant associations were observed for the superior or inferior longitudinal fasciculus.  
556



557  
558 **Figure 4.** Longitudinal trajectories of mean diffusivity from infancy to late childhood according to  
559 phonological processing skill in preschool/early kindergarten. Graph depicts average trajectories  
560 for children with low (< 85), average (85 – 115), and high (> 115) standardized phonological  
561 processing scores for the left arcuate fasciculus nodes whose slopes correlated with phonological  
562 processing ( $p_{FWE} < 0.05$ ). Children with low phonological processing tended to exhibit faster  
563 development (i.e., more negative slope) in anterior arcuate fasciculus.  
564

### 565 566 3.3. Sensitivity Analyses

567 We performed four sensitivity analyses to test the robustness of the observed brain-behavior  
568 relationships. For the first sensitivity analysis, we re-fit our volumetric, surface area, and mean  
569 diffusivity estimates with nonlinear mixed effects models using asymptotic functions  
570 (Supplementary Figures 25-28). This alternative model to characterize longitudinal trajectories  
571 was especially important for mean diffusivity findings, where intercepts and slopes from the main  
572 analysis were correlated for many nodes in each tract examined.

573 We observed that greater phonological processing was still associated with greater  
574 intercepts of gray matter volume development in the left banks of the superior temporal sulcus

575 and of surface area in left inferior parietal lobule, pars triangularis, and superior temporal gyrus  
576 (Supplementary Table 3A, C). Interestingly, when trajectories were again split according to low (<  
577 85), average (85 – 115), and high (> 115) standardized phonological processing scores, intercepts  
578 were saliently divided, more so than when using linear models (Supplementary Figure 3A,C).  
579 Whereas our main analyses allowed us to examine relationships between brain development and  
580 literacy subskills directly by using a random slopes term, the nonlinear model used in this  
581 sensitivity analysis replaces the random slopes term with a random asymptote term. As such,  
582 relationships between brain development and language outcomes may only be inferred where  
583 brain measures and regions exhibit asymptote-behavior correlations without corresponding  
584 intercept-behavior correlations. Models for middle and superior temporal cortices and  
585 supramarginal gyrus white matter volume did not converge. However, other brain regions whose  
586 white matter volume and surface area slopes correlated positively with phonological processing  
587 in the main analysis also exhibited significant associations between asymptotes and phonological  
588 processing. Effect sizes in were generally smaller for white matter volume and larger for surface  
589 area compared with the main analysis (Supplementary Tables 3B, C; Supplementary Figure  
590 3B,C). Regarding white matter organization, greater phonological processing was associated with  
591 lower mean diffusivity intercepts in left arcuate fasciculus (Supplementary Tables 3D).

592 Our second sensitivity analysis involved adding phonological processing main and age x  
593 phonological processing interaction terms as covariate analogues to brain-behavior correlations  
594 with intercepts and slopes, respectively. All results for gray and white matter volume and mean  
595 diffusivity present in the main analysis persisted in this sensitivity analysis; however, surface area  
596 effects did not (Supplementary Table 4).

597 For the third sensitivity analysis, we recomputed brain-behavior associations for  
598 volumetric and surface-based measures using semipartial correlations, controlling for curve  
599 features of the longitudinal trajectory for total intracranial volume (TIV). Relative to the results of  
600 the main analysis, effect sizes were reduced when including curve features of TIV. However,  
601 associations with phonological processing remained significant for intercepts of the banks of the  
602 superior temporal sulcus gray matter and inferior parietal lobule, pars triangularis, and superior  
603 temporal gyrus surface area. Slopes of white matter volume development in inferior parietal lobule  
604 and pars triangularis also remained significant (Supplementary Table 5).

605 In the fourth sensitivity analysis, we again recomputed brain-behavior associations, this  
606 time controlling for Euler numbers as a reproducible alternative to manual quality control (149).  
607 On average, effect sizes showed no drop relative to the main analysis ( $r_{\text{avg}} = 0.35$ ). All brain-  
608 behavior associations significant in the main analysis remained significant with the inclusion of

609 Euler numbers, except for the association between phonological processing and slopes of  
610 superior temporal gyrus surface area (Supplementary Table 6).

611

### 612 3.4. *Specificity analyses*

613 We also performed analyses to determine whether brain-behavior associations were limited to  
614 specific brain measures, regions, and curve features or contingent upon specific behavioral  
615 measures. Whole-brain analyses showed higher brain-behavior effects for white matter volume  
616 slopes compared (numerically) to other morphometric measures, especially in left inferior parietal  
617 lobule; however, effects did not appear to be specific to the left hemisphere (Supplementary  
618 Figure 32). In contrast, brain-behavior associations with mean diffusivity did not replicate in right  
619 hemisphere homologue tracts. In a subset of data, we also tested whether associations were  
620 specific to phonological processing, to other reading subskills, or to cognitive measures in  
621 general. Effects with phonological processing persisted in this subset for all brain-behavior  
622 associations except for intercepts of surface area in left inferior parietal and superior temporal  
623 cortices. However, similar effects were not observed for oral language skills or nonverbal general  
624 cognitive ability (Supplementary Table 7).

625

### 626 3.5. *Contributions of literacy-related factors to longitudinal trajectories of brain structure and white 627 matter organization*

628 Next, we sought to examine whether the brain-behavior associations, observed in both the full  
629 sample and the New England cohort only, are driven by two common literacy-related factors:  
630 family history of reading difficulty and the home literacy environment. When modeled as fixed  
631 effects, neither constituted significant contributors to the longitudinal trajectories of early brain  
632 development that predicted phonological processing (Supplementary Table 8). Furthermore, BIC  
633 estimates for models with versus without literacy-related covariates were not significantly different  
634 for any brain measures or regions (Supplementary Table 9).

635

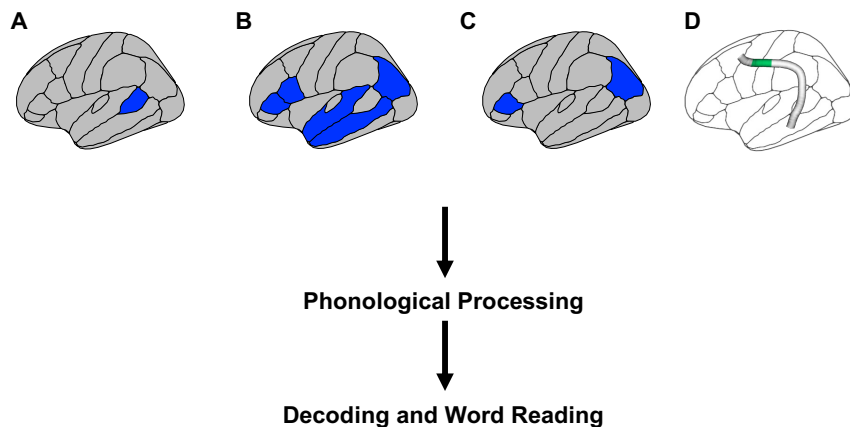
### 636 3.6. *Indirect effects between longitudinal trajectories of early brain development and word 637 reading outcomes via phonological processing*

638 Finally, we examined whether literacy subskills mediated the relationship between brain  
639 development curve features (e.g., intercepts and slopes) and decoding and word reading  
640 outcomes. As a prerequisite for mediation, the mediator (i.e., phonological processing) must be  
641 associated with both the predictor (i.e., brain estimate) and outcome (i.e., word reading). We  
642 limited the potential mediator to phonological processing, which related to both decoding ( $r = 0.48$ ;

643  $p < 0.005$ ) and word reading ( $r = 0.53$ ;  $p < 0.001$ ), as measured by the Woodcock Reading Mastery  
644 Tests III word attack and word identification subtests (114), because brain-behavior associations  
645 with oral language were few and inconsistent in sensitivity analyses, and we limited the potential  
646 predictors to brain measures and regions/tracts surviving FDR correction in the main analysis.  
647 Indirect effects were reported when the 95% confidence intervals, based on 20,000 bootstrapped  
648 samples, for the average causal mediation effect did not include 0 (please see Methods).

649 Phonological processing mediated the relationship between brain and decoding and  
650 between brain and word reading for the following measures and regions: intercepts of gray matter  
651 volume development in the left banks of the superior temporal sulcus (Figure 5A). Phonological  
652 processing skill also mediated associations between decoding/word reading and slopes of white  
653 matter volume development and intercepts and slopes of surface area development in left  
654 temporo-parietal and inferior frontal regions (Figure 5B, C; Supplementary Tables 10, 11). Indirect  
655 effect sizes nominally attenuated when controlling for TIV curve features for decoding (average  
656 estimate with TIV = 0.016, average estimate without TIV = 0.020) and word reading (average  
657 estimate with TIV = 0.024, average estimate without TIV = 0.031; Supplementary Tables 12, 13).  
658 Lastly, phonological processing skill mediated associations between slopes of mean diffusivity  
659 development in left arcuate fasciculus and decoding and word reading (Figure 5D).

660



661

662 **Figure 5.** Phonological processing skill mediates the relationship between early brain  
663 development and decoding and word reading. Indirect effects (filled arrows) were found for (A)  
664 intercepts of gray matter volume in the left banks of the superior temporal sulcus; (B) slopes of  
665 white matter volume and (C) intercepts and slopes of surface area in left temporo-parietal and  
666 inferior frontal regions; and (D) slopes of mean diffusivity in left arcuate fasciculus (nodes 6-25,  
667 green). Note: indirect effects are depicted for surface area slopes only; surface area intercept  
668 effects are reported in Supplementary Tables 10, 11.

669

670

#### 671 **4. Discussion**

672 The brain regions and tracts that eventually support decoding and word reading begin to develop  
673 long before the skills themselves emerge. Here, we examined the relationship between  
674 longitudinal trajectories of early brain development and acquisition of reading-related (sub)skills  
675 in four objectives. First, we generated longitudinal trajectories of early brain structure, including  
676 white matter organization, from infancy to school age in regions and tracts previously linked to  
677 literacy development (30–32, 34, 50–58) using a novel processing and analysis pipeline  
678 appropriate for the early developmental period. Findings showed that longitudinal trajectories  
679 were best modeled using logarithmic, compared with linear and quadratic, functions. Second, we  
680 examined associations between curve features of longitudinal trajectories and a key literacy  
681 subskill: phonological processing. Results showed that curve intercepts (i.e., birth brain estimates)  
682 of gray matter volume and surface area and curve slopes (i.e., early brain development) of white  
683 matter volume, surface area, and mean diffusivity predicted phonological processing measured  
684 in preschool/early kindergarten. While effects were robust in hypothesized left temporo-parietal,  
685 occipito-temporal, and inferior frontal regions and tracts, specificity analyses suggest that these  
686 brain-behavior associations are not limited to these regions. The predominance and magnitude  
687 of slope-outcome associations in comparison with intercept-outcome associations suggests a  
688 less stable, more dynamic relationship between brain and literacy development (34). Third, we  
689 examined whether familial risk of reading difficulty and home literacy environment, two common  
690 literacy-related covariates, influenced those trajectories and found that they did not. Fourth, we  
691 expanded the scope of our inquiry to long-term literacy development, showing that phonological  
692 processing mediated associations between early brain development and decoding and word  
693 reading skills between late kindergarten and second grade. Overall, these findings suggest that  
694 the neural foundations for the subsequent development of phonological processing may be  
695 partially present at birth but are still forming in the years between birth and preschool and  
696 eventually support the development of decoding and word reading skills.

697 Trajectories of early brain development have been generated from longitudinal studies up  
698 to the first two years of life (e.g., 35) and from combined cross-sectional and longitudinal datasets  
699 spanning infancy to school age (e.g., 36). However, methodological challenges associated with  
700 infant MRI and longitudinal designs in general have created a relative vacuum of longitudinal MRI  
701 studies spanning infancy to school age (43). The current study fills this gap as a purely longitudinal  
702 examination of early structural brain development in which longitudinal trajectories are generated  
703 with a pipeline designed for the early developmental period. Overall, longitudinal trajectories of  
704 gray and white matter volume, surface area, fractional anisotropy, and mean diffusivity exhibited

705 rapid postnatal growth that slowed with age, which largely comports with previous early  
706 developmental studies using cross-sectional (150–154) and combined longitudinal and cross-  
707 sectional designs (13, 36, 46, 48, 155, 156). As shown previously (49, 154), the curves for cortical  
708 thickness and mean curvature were generally less steep compared with other brain measures,  
709 both initially following birth and into childhood. Nonetheless, empirical comparisons with linear  
710 and quadratic functions showed that logarithmic models were more parsimonious for all measures  
711 examined.

712         After generating longitudinal trajectories, we examined how this brain development  
713 influenced literacy development by relating curve features of individual trajectories to reading-  
714 related subskills measured in preschool/early kindergarten as well as decoding and word reading  
715 skills measured between kindergarten and second grade. The finding of direct links to  
716 phonological processing and indirect links to decoding and word reading from curve intercepts of  
717 gray matter volume (i.e., gray matter volume at birth) specifically in the left banks of the superior  
718 temporal sulcus is compelling in the context of a recent large-scale genomics study showing  
719 common genetic influences on surface area in this region and reading-related skills (60), including  
720 from a gene involved in neurogenesis and axon formation (78). Combined with observed  
721 intercept-outcome associations for surface area in other left hemisphere regions and prior work  
722 showing an association between reading difficulty and left temporo-parietal sulcal patterns  
723 determined in utero (157), these findings offer convergent evidence for a mechanistic pathway  
724 through which genetic factors shape the foundations of reading development via prenatal left  
725 temporo-parietal brain development. While this intercept-outcome effect remained robust through  
726 all four sensitivity analyses, this interpretation should be viewed with caution, as specificity  
727 analyses suggest intercept-outcome effects may not be limited to the left banks of the superior  
728 temporal sulcus.

729         The intercept-outcome findings also support the hypothesis that school-age literacy skill  
730 builds on an early-developing foundation (33) or ‘neural scaffold’ (30–32). However, the paucity  
731 of intercept-outcome associations in contrast to the multitude and magnitude of slope-outcome  
732 associations suggests that this neural scaffold develops substantially over the first several years  
733 of life. While the mechanisms driving these divergent associations with outcomes will ultimately  
734 require further investigation, it is conceivable that they reflect links to distinct early precursors of  
735 phonological skills. For instance, the intercept-outcome associations may reflect stable relations  
736 with foundational perception skills that develop earlier (e.g., prosody, differentiating phonemes)  
737 and remain necessary for the development of more advanced phonological processing skills,  
738 whereas slope-outcome associations reflect dynamic associations with more advanced

739 phonological processing skills such as syllable or phoneme deletion or substitution. Overall, the  
740 presence of slope-outcome associations offers insights into the early development of a neural  
741 scaffold for literacy and in doing so, underscores the importance of examining individual  
742 longitudinal trajectories (2), as opposed to cross-sectional and prospective associations.

743 It was also interesting that most of the slope-outcome findings were with white matter  
744 properties, and nearly all of these remained significant in all sensitivity analyses, with some effects  
745 becoming even more robust (e.g., please see inferior parietal white matter in second sensitivity  
746 analysis). While no prior study has examined the relationship between long-term literacy subskills  
747 and longitudinal trajectories of white matter development beginning in infancy (or early  
748 development of surface-based measures), there is a small corpus of literature that has linked  
749 reading-related skill performance to short-term, school-age developmental changes in left  
750 temporo-parietal white matter volume (158) and organization, most consistently in the left arcuate  
751 fasciculus (34, 56, 57, 158). This is especially compelling when considering that the slope-  
752 outcome relationship we observed with white matter organization was specific to the left arcuate  
753 fasciculus and to phonological processing, which is highly predictive of subsequent word reading  
754 and decoding performance (4, 8–10). Work from genomics might offer further explanation for the  
755 dominance of white matter associations, as genes involved in axon guidance (159), axon  
756 formation (78), and oligodendrocyte maturation (160) have also been linked to reading-related  
757 skills (60) and reading disability (76, 77). Although white matter volume and organization are not  
758 strongly associated and thought to be sensitive to different properties (161), their reliance on  
759 myelination, the primary function of oligodendrocytes, and other axonal properties suggests that  
760 they may represent another mechanism through which genetic factors may shape early brain  
761 development.

762 Interestingly, specificity analyses showed direct brain-behavior associations with  
763 phonological processing but not with oral language skills or nonverbal general cognitive abilities.  
764 Prior brain imaging studies in preschoolers/kindergarteners comport with this finding as  
765 phonological processing seems to exhibit more consistent associations with brain architecture  
766 (15–20), compared with oral language skills (21–23); c.f., (17, 24). While both subskills are  
767 considered critical for higher-level reading-related skills, they are thought to function on two  
768 distinguishable developmental pathways, whereby phonological processing is more involved in  
769 recognizing and decoding printed words and oral language skills are more essential for the  
770 development of reading comprehension skills (please see Scarborough’s Reading Rope; (8). It  
771 should be noted that this framework also fits with our mediation findings, which show indirect  
772 relations between early brain development and decoding and (printed) word reading via

773 phonological processing. Furthermore, whereas phonological processing is limited in its scope,  
774 as specifically one's ability to recognize and manipulate sounds in a word (4–7), oral language  
775 was measured in the current study as a composite of vocabulary and oral comprehension  
776 subtests, with the latter requiring children to engage with semantic and syntactic cues. As different  
777 brain regions may be more specialized for certain component language skills (e.g., pars  
778 opercularis may be more involved in syntactic processing while pars triangularis and middle  
779 temporal gyrus may be more involved in semantics; (162, 163)), aggregating distinct oral  
780 language skills may have obscured brain-behavior associations. Conversely, it is also conceivable  
781 that oral language acquisition requires additional, moderating factors that were not modeled in  
782 the present study (e.g., social interactions (164) or conversational turn-taking (21)). Nevertheless,  
783 the necessity of phonological processing for literacy development and its relation to early brain  
784 development reported here underscore the importance of examining reading-related subskills at  
785 the very beginnings of life.

786 Turning to literacy-related covariates, familial history of reading difficulty (FHD) was  
787 hypothesized to influence longitudinal trajectories of early brain development, based on previous  
788 findings showing FHD-related alterations in brain architecture in infancy (71, 72) and preschool  
789 (16, 18, 57). Consequently, the observation that FHD status did not influence longitudinal  
790 trajectories in any regions or tracts examined was initially unexpected. However, it is important to  
791 recognize that a child who has an older sibling or parent with a reading difficulty (FHD+) does not  
792 necessarily have a genetic susceptibility for reading difficulty (165), nor will they necessarily  
793 develop reading challenges given the multifactorial nature of reading difficulties. Rather, FHD  
794 status should be considered one of multiple risk factors that can contribute to long-term literacy  
795 development (166, 167), either through intergenerational transmission of genes or environment  
796 (168). Consistent with this, roughly half of FHD+ children develop typical reading skills (62, 63),  
797 and those who do develop typical reading skills have, as a group, been shown to recruit right- and  
798 inter-hemispheric compensatory pathways (169, 170), a pattern similar to children with reading  
799 difficulty who subsequently show improvements (171). Although the specificity analysis examining  
800 brain-behavior effects in non-a-priori brain regions did not point to literacy-related effects solely in  
801 the left hemisphere, right hemisphere regions and tracts were not thoroughly assayed in the  
802 current study. Therefore, it may behoove future studies with larger sample sizes to examine the  
803 development of right hemisphere regions and tracts in the context of FHD status and to distinguish  
804 FHD+ children who develop typical reading skills from FHD+ children who do not.

805 The home literacy environment also did not significantly influence longitudinal trajectories  
806 in the regions and tracts examined, despite reported links to brain structure and function in infants

807 (95, 96) and preschoolers/kindergarteners (21, 24, 91–94). However, with few exceptions (e.g.,  
808 common associations to arcuate fasciculus fractional anisotropy in infants (96) and kindergarten  
809 (24)), specific brain measures and regions/tracts linked to home literacy environment variables  
810 identified at the infant time point were not also identified at the preschool/kindergarten time point,  
811 suggesting that brain-home literacy environment relations may vary across this developmental  
812 window. Future longitudinal studies with more frequent sampling of observations will be needed  
813 to test whether this explanation is accurate. Also, as examination of home literacy was limited to  
814 longitudinal trajectories for brain measures and regions/tracts that were associated with  
815 phonological processing, it is likely that measures and regions/tracts related to the home literacy  
816 environment went untested in the current study.

817 This study had five main limitations. First, consistent with prior work (36), the models we  
818 fit to early brain development generated smooth longitudinal trajectories. In actuality, it is unlikely  
819 that early brain development transpires as predictably, especially during sensitive and critical  
820 periods (172) or specific learning milestones (2). Although participants in the current study were  
821 sampled over three times on average, which is preferred for modeling growth curves (173) and  
822 more than most longitudinal imaging studies (174), future studies would benefit from increased  
823 sampling, particularly around learning milestones germane to literacy development. Second, the  
824 sample size in the current study was relatively small when compared with the sample sizes used  
825 in multi-site, combined cross-sectional and longitudinal studies (e.g., 13, 36). While sensitivity  
826 analyses for the most part demonstrated the robustness of the results, future studies with larger  
827 sample sizes will be needed to confirm the findings presented here. Third, cortical thickness,  
828 mean curvature, fractional anisotropy, and mean diffusivity exhibited high correlations between  
829 random parameters (i.e., intercept-slope correlations) when modeled with logarithmic functions,  
830 which spurred concerns over the accuracy of the estimated random parameters. For the current  
831 findings, inaccurate random parameters could have generated false negatives for the former three  
832 measures and false positives for mean diffusivity. Consequently, for the former three parameters,  
833 even though they were consistently better fit with logarithmic functions, we re-analyzed intercept-  
834 outcome and slope-outcome associations using random parameters from models with quadratic  
835 functions, which had considerably lower intercept-slope correlations. Despite this, results  
836 remained non-significant. Meanwhile, the first sensitivity analysis addressed concerns for mean  
837 diffusivity by showing that nonlinear mixed effects models using asymptotic functions decoupled  
838 intercepts and slopes while maintaining the significant results observed in the main analysis. It is  
839 also important to note that this limitation does not apply to findings for gray and white matter  
840 volume or surface area. Fourth, we examined somewhat narrowly literacy-related factors that

841 could contribute to early brain development by only including FHD status and home literacy  
842 environment, and it is likely that factors not included also contribute to the longitudinal trajectories  
843 examined (e.g., teaching quality, educational opportunities, executive functioning skills (166,  
844 175). Fifth, our longitudinal analysis pipeline identifies and removes brain estimates preceding or  
845 following developmental changes that are too steep to occur neuroanatomically and more likely  
846 to emerge from region or tract mislabeling, despite our quality control efforts. Consequently, it is  
847 possible that estimates without steep developmental changes also suffer mislabeling but remain  
848 undetected. Overall, interpretations of findings should be considered in the context of these  
849 limitations.

850 In conclusion, this study examined associations between longitudinal trajectories of early  
851 brain development beginning in infancy and long-term reading acquisition, specifically literacy  
852 subskills. Longitudinal trajectories were generated using a novel, reproducible pipeline we  
853 designed specifically for examining early brain development and included familial risk of a reading  
854 difficulty and environmental covariates. Findings indicate that preschool/early kindergarten  
855 phonological processing, one of the strongest predictors of subsequent word reading  
856 development, relates to gray matter volume and surface area at birth and development of white  
857 matter volume, surface area, and mean diffusivity across early development. These results offer  
858 further evidence for a neural scaffold for literacy development, which is present at birth and  
859 continues forming across the first several years of life. The present study also provides a roadmap  
860 for future longitudinal studies to examine the relationship between early brain development and  
861 acquisition of other academic skills. Understanding when the foundations for reading emerge can  
862 deliver important insights into the development of instructional approaches and preventative, and  
863 intervention strategies.

864  
865  
866  
867  
868  
869  
870  
871  
872  
873  
874  
875  
876  
877  
878  
879

880 **Acknowledgements**

881 This work was funded by NIH–NICHD R01 HD065762 (2016-2021), the William Hearst Fund  
882 (Harvard University), and the Harvard Catalyst/NIH (5UL1RR025758) to N.G. We would like to  
883 thank all participating families for their long-term dedication to this study. We are grateful for all  
884 additional members of the research team who contributed to data acquisition and quality control,  
885 including Victoria Hue, Ja’Kala Barber, Emily Hu, Olivia Baldi, Brooke Jordan, Jade Dunstan,  
886 Clarisa Carruthers, Carolyn King, Doroteja Rubez, Kathryn Garrisi, Ally Lee, Omeed Moini, Anaïs  
887 Colin, Zumin Chen, Colby Weiss, and Olivia Oh. We also thank Rebecca Petersen for her input  
888 on psychometric assessments, Jennifer Zuk for work on infant scanning procedures, Borjan  
889 Gagoski and Ross Mair for efforts on scanning sequences, Luke Miratrix and Fernando Aguata  
890 for guidance on (non)linear mixed effects models, and Banu Ahtam for feedback.

891

892

893

894 **References**

- 895 1. R. Siegler, Children's learning. *American Psychologist* **6**, 769–778 (2005).
- 896 2. M. Bonte, S. Brem, Unraveling individual differences in learning potential: A dynamic  
897 framework for the case of reading development. *Dev Cogn Neurosci* [Preprint] (2024).
- 898 3. Y.-S. Kim, Toward Integrative Reading Science: The Direct and Indirect Effects Model of  
899 Reading. *J Learn Disabil* **53**, 469–491 (2020).
- 900 4. R. K. Wagner, J. K. Torgesen, The nature of phonological processing and its causal role  
901 in the acquisition of reading skills. *Psychol Bull* **101**, 192–212 (1987).
- 902 5. R. Wagner, *et al.*, "The Nature of Prereaders' Phonological Processing Abilities" (1987).
- 903 6. U. Goswami, A neural oscillations perspective on phonological development and  
904 phonological processing in developmental dyslexia. *Lang Linguist Compass* **13** (2019).
- 905 7. U. Goswami, "Phonological development across different languages" in *Routledge*  
906 *International Handbook of English, Language & Literacy Teaching*, (2010), pp. 98–109.
- 907 8. H. S. Scarborough, "Connecting early language and literacy to later reading (dis)abilities:  
908 Evidence, theory, and practice" in *Handbook of Early Literacy Research*, S. Neuman, D.  
909 Dickinson, Eds. (Guilford Press, 2001), pp. 97–110.
- 910 9. K. Moll, A. Loff, M. J. Snowling, Cognitive Endophenotypes of Dyslexia. *Scientific Studies*  
911 *of Reading* **17**, 385–397 (2013).
- 912 10. M. Melby-Lervåg, S.-A. H. Lyster, C. Hulme, Phonological Skills and Their Role in  
913 Learning to Read: A Meta-Analytic Review. *Psychol Bull* **138**, 322–352 (2012).
- 914 11. P. Kendeou, P. van den Broek, M. J. White, J. S. Lynch, Predicting Reading  
915 Comprehension in Early Elementary School: The Independent Contributions of Oral  
916 Language and Decoding Skills. *J Educ Psychol* **101**, 765–778 (2009).
- 917 12. Y. S. G. Kim, Why the Simple View of Reading Is Not Simplistic: Unpacking Component  
918 Skills of Reading Using a Direct and Indirect Effect Model of Reading (DIER). *Scientific*  
919 *Studies of Reading* **21**, 310–333 (2017).
- 920 13. R. A. I. Bethlehem, *et al.*, Brain charts for the human lifespan. *Nature* **604**, 525–533  
921 (2022).
- 922 14. J. Gilmore, R. C. Knickmeyer, W. Gao, Imaging structural and functional brain  
923 development in early childhood. *Nat Rev Neurosci* **19**, 123–137 (2018).
- 924 15. F. Hoeft, *et al.*, Prediction of Children's Reading Skills Using Behavioral, Functional, and  
925 Structural Neuroimaging Measures. *Behavioral Neuroscience* **121**, 602–613 (2007).
- 926 16. N. M. Raschle, M. Chang, N. Gaab, Structural brain alterations associated with dyslexia  
927 predate reading onset. *Neuroimage* **57**, 742–749 (2011).
- 928 17. N. Raschle, P. L. Stering, S. N. Meissner, N. Gaab, Altered neuronal response during  
929 rapid auditory processing and its relation to phonological processing in prereading  
930 children at familial risk for dyslexia. *Cerebral Cortex* **24**, 2489–2501 (2014).
- 931 18. N. Raschle, J. Zuk, N. Gaab, Functional characteristics of developmental dyslexia in left-  
932 hemispheric posterior brain regions predate reading onset. *Proceedings of the National*  
933 *Academy of Sciences* **109**, 2156–2161 (2012).
- 934 19. Z. M. Saygin, *et al.*, Tracking the Roots of Reading Ability: White Matter Volume and  
935 Integrity Correlate with Phonological Awareness in Prereading and Early-Reading  
936 Kindergarten Children. *Journal of Neuroscience* **33**, 13251–13258 (2013).
- 937 20. M. Vandermosten, B. Boets, J. Wouters, P. Ghesquière, A qualitative and quantitative  
938 review of diffusion tensor imaging studies in reading and dyslexia. *Neurosci Biobehav*  
939 *Rev* **36**, 1532–1552 (2012).
- 940 21. R. Romeo, *et al.*, Language Exposure Relates to Structural Neural Connectivity in  
941 Childhood. *J Neurosci* **38**, 7870–7877 (2018).
- 942 22. R. Romeo, *et al.*, Beyond the 30-million-word gap: Children's conversational exposure is  
943 associated with language-related brain function. *Psychol Sci* **29**, 700–710 (2018).

- 944 23. R. A. Marks, *et al.*, Spoken language proficiency predicts print-speech convergence in  
945 beginning readers. *Neuroimage* **201** (2019).
- 946 24. K. Davison, *et al.*, Examining the relationship between shared book reading at home,  
947 white matter organization in kindergarten, and subsequent language and reading abilities:  
948 a longitudinal investigation. *J Cogn Neurosci* **35**, 259–275 (2022).
- 949 25. H. Lyytinen, *et al.*, The development of children at familial risk for dyslexia: Birth to early  
950 school age. *Ann Dyslexia* **54**, 184–220 (2004).
- 951 26. T. K. Guttorm, P. H. T. Leppänen, J. A. Hämäläinen, K. M. Eklund, H. J. Lyytinen,  
952 Newborn event-related potentials predict poorer pre-reading skills in children at risk for  
953 dyslexia. *J Learn Disabil* **43**, 391–401 (2010).
- 954 27. T. K. Guttorm, A. Poikkeus, K. M. Eklund, P. Lyytinen, H. Lyytinen, Brain event-related  
955 potentials (ERPs) measured at birth predict later language development in children with  
956 and without familial risk for dyslexia. *Cortex* **41**, 291–303 (2005).
- 957 28. T. L. Van Zuijen, A. Plakas, B. A. M. Maassen, N. M. Maurits, A. Van der Leij, Infant  
958 ERPs separate children at risk of dyslexia who become good readers from those who  
959 become poor readers. *Dev Sci* **16**, 554–563 (2013).
- 960 29. P. H. T. Leppänen, *et al.*, Infant brain responses associated with reading-related skills  
961 before school and at school age. *Neurophysiologie Clinique* **42**, 35–41 (2012).
- 962 30. X. Yu, *et al.*, Functional Connectivity in Infancy and Toddlerhood Predicts Long-Term  
963 Language and Preliteracy Outcomes. *Cerebral Cortex* **32**, 725–736 (2021).
- 964 31. J. Zuk, *et al.*, White matter in infancy is prospectively associated with language outcomes  
965 in kindergarten. *Dev Cogn Neurosci* **50** (2021).
- 966 32. X. Tang, *et al.*, Longitudinal associations between language network characteristics in the  
967 infant brain and school-age reading abilities are mediated by early-developing  
968 phonological skills. *Dev Cogn Neurosci* **68** (2024).
- 969 33. R. Cusack, M. Ranzato, C. J. Charvet, Helpless infants are learning a foundation model.  
970 *Trends Cogn Sci* (2024). <https://doi.org/10.1016/j.tics.2024.05.001>.
- 971 34. E. Roy, *et al.*, White matter and literacy: A dynamic system in flux. *Dev Cogn Neurosci* **65**  
972 (2024).
- 973 35. J. H. Gilmore, *et al.*, Longitudinal development of cortical and subcortical gray matter  
974 from birth to 2 years. *Cerebral Cortex* **22**, 2478–2485 (2012).
- 975 36. A. M. Alex, *et al.*, A global multicohort study to map subcortical brain development and  
976 cognition in infancy and early childhood. *Nat Neurosci* **27**, 176–186 (2024).
- 977 37. M. Prastawa, J. H. Gilmore, W. Lin, G. Gerig, Automatic segmentation of MR images of  
978 the developing newborn brain. *Med Image Anal* **9**, 457–466 (2005).
- 979 38. N. Raschle, *et al.*, Pediatric neuroimaging in early childhood and infancy: Challenges and  
980 practical guidelines. *Ann N Y Acad Sci* **1252**, 43–50 (2012).
- 981 39. A. Makropoulos, S. J. Counsell, D. Rueckert, A review on automatic fetal and neonatal  
982 brain MRI segmentation. *Neuroimage* **170**, 231–248 (2018).
- 983 40. L. Zöllei, J. E. Iglesias, Y. Ou, P. E. Grant, B. Fischl, Infant FreeSurfer: An automated  
984 segmentation and surface extraction pipeline for T1-weighted neuroimaging data of  
985 infants 0–2 years. *Neuroimage* **218**, 116946 (2020).
- 986 41. M. Pietsch, *et al.*, A framework for multi-component analysis of diffusion MRI data over  
987 the neonatal period. *Neuroimage* **186**, 321–337 (2019).
- 988 42. M. Grotheer, *et al.*, White matter myelination during early infancy is linked to spatial  
989 gradients and myelin content at birth. *Nat Commun* **13**, 1–12 (2022).
- 990 43. T. K. Turesky, J. Vanderauwera, N. Gaab, Imaging the rapidly developing brain: Current  
991 challenges for MRI studies in the first five years of life. *Dev Cogn Neurosci* **47**, 100893  
992 (2021).
- 993 44. W. Gao, *et al.*, Functional network development during the first year: Relative sequence  
994 and socioeconomic correlations. *Cerebral Cortex* **25**, 2919–2928 (2015).

- 995 45. N. Vijayakumar, K. L. Mills, A. Alexander-Bloch, C. K. Tamnes, S. Whittle, Structural brain  
996 development: A review of methodological approaches and best practices. *Dev Cogn*  
997 *Neurosci* **33**, 129–148 (2018).
- 998 46. R. C. Knickmeyer, *et al.*, A Structural MRI Study of Human Brain Development from Birth  
999 to 2 Years. *Journal of Neuroscience* **28**, 12176–12182 (2008).
- 1000 47. G. Li, *et al.*, Mapping region-specific longitudinal cortical surface expansion from birth to 2  
1001 years of age. *Cerebral Cortex* **23**, 2724–2733 (2013).
- 1002 48. J. Reynolds, M. N. Grohs, D. Dewey, C. Lebel, Global and regional white matter  
1003 development in early childhood. *Neuroimage* **196**, 49–58 (2019).
- 1004 49. F. Wang, *et al.*, Developmental topography of cortical thickness during infancy. *Proc Natl*  
1005 *Acad Sci U S A* **116**, 15855–15860 (2019).
- 1006 50. M. Ben-Shachar, R. F. Dougherty, G. K. Deutsch, B. A. Wandell, “The Development of  
1007 Cortical Sensitivity to Visual Word Forms” (2011).
- 1008 51. S. V. Di Pietro, I. I. Karipidis, G. Pleisch, S. Brem, Neurodevelopmental trajectories of  
1009 letter and speech sound processing from preschool to the end of elementary school. *Dev*  
1010 *Cogn Neurosci* **61** (2023).
- 1011 52. S. Brem, *et al.*, Brain sensitivity to print emerges when children learn letter-speech sound  
1012 correspondences. *Proc Natl Acad Sci U S A* **107**, 7939–7944 (2010).
- 1013 53. X. Yu, *et al.*, Emergence of the neural network underlying phonological processing from  
1014 the prereading to the emergent reading stage: A longitudinal study. *Hum Brain Mapp* **39**,  
1015 2047–2063 (2018).
- 1016 54. J. Reynolds, X. Long, M. N. Grohs, D. Dewey, C. Lebel, Structural and functional  
1017 asymmetry of the language network emerge in early childhood. *Dev Cogn Neurosci* **39**  
1018 (2019).
- 1019 55. G. Dehaene-Lambertz, K. Monzalvo, S. Dehaene, The emergence of the visual word  
1020 form: Longitudinal evolution of category-specific ventral visual areas during reading  
1021 acquisition. *PLoS Biol* **16** (2018).
- 1022 56. J. Yeatman, R. F. Dougherty, M. Ben-Shachar, B. A. Wandell, Development of white  
1023 matter and reading skills. *Proc Natl Acad Sci U S A* **109**, E3045–E3053 PNAS (2012).
- 1024 57. Y. Wang, *et al.*, Development of tract-specific white matter pathways during early reading  
1025 development in at-risk children and typical controls. *Cerebral Cortex* **27**, 2469–2485  
1026 (2017).
- 1027 58. O. Ozernov-Palchik, D. Sury, T. K. Turesky, X. Yu, N. Gaab, Longitudinal changes in  
1028 brain activation underlying reading fluency. *Hum Brain Mapp* **44**, 18–34 (2023).
- 1029 59. E. Huber, A. Mezer, J. D. Yeatman, Neurobiological underpinnings of rapid white matter  
1030 plasticity during intensive reading instruction. *Neuroimage* **243** (2021).
- 1031 60. E. Eising, *et al.*, Genome-wide analyses of individual differences in quantitatively  
1032 assessed reading- and language-related skills in up to 34,000 people. *Proc Natl Acad Sci*  
1033 *U S A* **119** (2022).
- 1034 61. A. Carrión-Castillo, P. M. Paz-Alonso, M. Carreiras, Brain structure, phenotypic and  
1035 genetic correlates of reading performance. *Nat Hum Behav* **7**, 1120–1134 (2023).
- 1036 62. G. P. Vogler, J. C. DeFries, S. N. Decker, Family history as an indicator of risk for reading  
1037 disability. *J Learn Disabil* **18**, 419–421 (1985).
- 1038 63. M. J. Snowling, M. Melby-Lervåg, Oral language deficits in familial dyslexia: A meta-  
1039 analysis and review. *Psychol Bull* **142**, 498–545 (2016).
- 1040 64. F. Hoeft, *et al.*, Functional and morphometric brain dissociation between dyslexia and  
1041 reading ability. *Proceedings of the National Academy of Sciences* **104**, 4234–4239  
1042 (2007).
- 1043 65. F. Richlan, M. Kronbichler, H. Wimmer, Meta-analyzing brain dysfunctions in dyslexic  
1044 children and adults. *Neuroimage* **56**, 1735–42 (2011).

- 1045 66. F. Richlan, M. Kronbichler, H. Wimmer, Structural abnormalities in the dyslexic brain: A  
1046 meta-analysis of voxel-based morphometry studies. *Hum Brain Mapp* **34**, 3055–3065  
1047 (2013).
- 1048 67. F. Richlan, M. Kronbichler, H. Wimmer, Functional abnormalities in the dyslexic brain: a  
1049 quantitative meta-analysis of neuroimaging studies. *Hum Brain Mapp* **30**, 3299–308  
1050 (2009).
- 1051 68. C. Steinbrink, *et al.*, The contribution of white and gray matter differences to  
1052 developmental dyslexia: Insights from DTI and VBM at 3.0 T. *Neuropsychologia* **46**,  
1053 3170–3178 (2008).
- 1054 69. K. M. Hasan, *et al.*, Diffusion tensor quantification and cognitive correlates of the  
1055 macrostructure and microstructure of the corpus callosum in typically developing and  
1056 dyslexic children. *NMR Biomed* **25**, 1263–1270 (2012).
- 1057 70. E. Temple, *et al.*, Disrupted neural responses to phonological and orthographic  
1058 processing in dyslexic children: an fMRI study. *Neuroreport* **12**, 299–307 (2001).
- 1059 71. N. Langer, *et al.*, White Matter Alterations in Infants at Risk for Developmental Dyslexia.  
1060 *Cereb Cortex* **27**, 1027–1036 (2017).
- 1061 72. X. Yu, *et al.*, Patterns of Neural Functional Connectivity in Infants at Familial Risk of  
1062 Developmental Dyslexia. *JAMA Netw Open* **5**, E2236102 (2022).
- 1063 73. T. K. Guttorm, P. H. T. Leppänen, A. Tolvanen, H. Lyytinen, Event-related potentials in  
1064 newborns with and without familial risk for dyslexia: Principal component analysis reveals  
1065 differences between the groups. *J Neural Transm* **110**, 1059–1074 (2003).
- 1066 74. T. K. Guttorm, P. H. T. Leppänen, U. Richardson, H. Lyytinen, Event-Related Potentials  
1067 and Consonant Differentiation in Newborns with Familial Risk for Dyslexia. *J Learn*  
1068 *Disabil* **34**, 534–544 (2001).
- 1069 75. M. van Herten, *et al.*, Differences in AERP responses and atypical hemispheric  
1070 specialization in 17-month-old children at risk of dyslexia. *Brain Res* **1201**, 100–105  
1071 (2008).
- 1072 76. C. Doust, *et al.*, Discovery of 42 genome-wide significant loci associated with dyslexia.  
1073 *Nat Genet* **54**, 1621–1629 (2022).
- 1074 77. K. M. Price, *et al.*, Hypothesis-driven genome-wide association studies provide novel  
1075 insights into genetics of reading disabilities. *Transl Psychiatry* **12** (2022).
- 1076 78. M. Watabe-Uchida, K. A. John, J. A. Janas, S. E. Newey, L. Van Aelst, The Rac Activator  
1077 DOCK7 Regulates Neuronal Polarity through Local Phosphorylation of Stathmin/Op18.  
1078 *Neuron* **51**, 727–739 (2006).
- 1079 79. A. C. Payne Grover, W. L. Andrea Angel, “The Role of Home Literacy Environment in the  
1080 Development of Language Ability in Preschool Children from Low-income Families”  
1081 (1994).
- 1082 80. A. G. Bus, M. H. van IJzendoorn, A. D. Pellegrini, Joint book reading makes for success  
1083 in learning to read: A meta-analysis on intergenerational transmission of literacy. *Rev*  
1084 *Educ Res* **65**, 1–21 (1995).
- 1085 81. S. R. Burgess, S. A. Hecht, C. J. Lonigan, Relations of the home literacy environment  
1086 (HLE) to the development of reading-related abilities: A one-year longitudinal study. *Read*  
1087 *Res Q* **37**, 408–426 (2002).
- 1088 82. M. A. Foster, R. Lambert, M. Abbott-Shim, F. McCarty, S. Franze, A model of home  
1089 learning environment and social risk factors in relation to children’s emergent literacy and  
1090 social outcomes. *Early Child Res Q* **20**, 13–36 (2005).
- 1091 83. S. A. Schmitt, A. M. Simpson, M. Friend, A longitudinal assessment of the home literacy  
1092 environment and early language. *Infant Child Dev* **20**, 409–431 (2011).
- 1093 84. L. G. Hamilton, M. E. Hayiou-Thomas, C. Hulme, M. J. Snowling, The Home Literacy  
1094 Environment as a Predictor of the Early Literacy Development of Children at Family-Risk  
1095 of Dyslexia. *Scientific Studies of Reading* **20**, 401–419 (2016).

- 1096 85. J. Karrass, J. M. Braungart-Rieker, Effects of shared parent-infant book reading on early  
1097 language acquisition. *J Appl Dev Psychol* **26**, 133–148 (2005).
- 1098 86. E. Hoff, The Specificity of Environmental Influence: Socioeconomic Status Affects Early  
1099 Vocabulary Development Via Maternal Speech. *Child Dev* **74**, 1368–1378 (2003).
- 1100 87. A. Muhinyi, M. L. Rowe, Shared reading with preverbal infants and later language  
1101 development. *J Appl Dev Psychol* **64** (2019).
- 1102 88. M.-L. Laakso, A.-M. Poikkeus, P. Lyytinen, Shared reading interaction in families with and  
1103 without genetic risk for dyslexia: implications for toddlers' language development. *Infant*  
1104 *Child Dev* **8**, 179–195 (1999).
- 1105 89. J. L. Malin, N. J. Cabrera, M. L. Rowe, Low-income minority mothers' and fathers' reading  
1106 and children's interest: Longitudinal contributions to children's receptive vocabulary skills.  
1107 *Early Child Res Q* **29**, 425–432 (2014).
- 1108 90. Ö. E. Demir-Lira, L. R. Applebaum, S. Goldin-Meadow, S. C. Levine, Parents' early book  
1109 reading to children: Relation to children's later language and literacy outcomes controlling  
1110 for other parent language input. *Dev Sci* **22** (2019).
- 1111 91. S. J. Powers, Y. Wang, S. D. Beach, G. D. Sideridis, N. Gaab, Examining the relationship  
1112 between home literacy environment and neural correlates of phonological processing in  
1113 beginning readers with and without a familial risk for dyslexia: an fMRI study. *Ann*  
1114 *Dyslexia* **66**, 337–360 (2016).
- 1115 92. J. S. Hutton, J. Dudley, T. Horowitz-Kraus, T. DeWitt, S. K. Holland, Associations  
1116 between home literacy environment, brain white matter integrity and cognitive abilities in  
1117 preschool-age children. *Acta Paediatr* **109**, 1376–1386 (2020).
- 1118 93. J. S. Hutton, T. Horowitz-Kraus, A. L. Mendelsohn, T. DeWitt, S. K. Holland, Home  
1119 reading environment and brain activation in preschool children listening to stories.  
1120 *Pediatrics* **136**, 466–478 (2015).
- 1121 94. J. S. Hutton, *et al.*, Shared Reading Quality and Brain Activation during Story Listening in  
1122 Preschool-Age Children. *Journal of Pediatrics* **191**, 204-211.e1 (2017).
- 1123 95. L. S. King, M. C. Camacho, D. F. Montez, K. L. Humphreys, I. H. Gotlib, Naturalistic  
1124 language input is associated with resting-state functional connectivity in infancy. *Journal*  
1125 *of Neuroscience* **41**, 424–434 (2021).
- 1126 96. T. K. Turesky, *et al.*, Home language and literacy environment and its relationship to  
1127 socioeconomic status and white matter structure in infancy. *Brain Struct Funct* **227**,  
1128 2633–2645 (2022).
- 1129 97. J. Zuk, J. Vanderauwera, T. Turesky, X. Yu, N. Gaab, Neurobiological predispositions for  
1130 musicality: White matter in infancy predicts school-age music aptitude. *Dev Sci* **26** (2023).
- 1131 98. C. Lebel, *et al.*, Prepartum and Postpartum Maternal Depressive Symptoms Are Related  
1132 to Children's Brain Structure in Preschool. *Biol Psychiatry* **80**, 859–868 (2016).
- 1133 99. C. Thieba, *et al.*, Factors Associated With Successful MRI Scanning in Unsedated Young  
1134 Children. *Front Pediatr* **6**, 1–5 (2018).
- 1135 100. D. Paniukov, R. M. Lebel, G. Giesbrecht, C. Lebel, Cerebral blood flow increases across  
1136 early childhood. *Neuroimage* **204** (2020).
- 1137 101. M. Walton, D. Dewey, C. Lebel, Brain white matter structure and language ability in  
1138 preschool-aged children. *Brain Lang* **176**, 19–25 (2018).
- 1139 102. J. Reynolds, X. Long, D. Paniukov, M. Bagshawe, C. Lebel, Calgary Preschool magnetic  
1140 resonance imaging (MRI) dataset. *Data Brief* **29** (2020).
- 1141 103. L. M. Betancourt, *et al.*, Effect of socioeconomic status (SES) disparity on neural  
1142 development in female African-American infants at age 1 month. *Dev Sci* **19**, 947–956  
1143 (2016).
- 1144 104. N. H. Brito, W. P. Fifer, M. M. Myers, A. J. Elliott, K. G. Noble, Associations among family  
1145 socioeconomic status, EEG power at birth, and cognitive skills during infancy. *Dev Cogn*  
1146 *Neurosci* **19**, 144–151 (2016).

- 1147 105. G. M. Lawson, J. T. Duda, B. B. Avants, J. Wu, M. J. Farah, Associations between  
1148 children's socioeconomic status and prefrontal cortical thickness. *Dev Sci* **16**, 641–652  
1149 (2013).
- 1150 106. E. C. Merz, N. Tottenham, K. G. Noble, Socioeconomic Status, Amygdala Volume, and  
1151 Internalizing Symptoms in Children and Adolescents. *Journal of Clinical Child and*  
1152 *Adolescent Psychology* **47**, 312–323 (2018).
- 1153 107. K. G. Noble, *et al.*, Family income, parental education and brain structure in children and  
1154 adolescents. *Nat Neurosci* **18**, 773–778 (2015).
- 1155 108. O. Ozernov-Palchik, *et al.*, The relationship between socioeconomic status and white  
1156 matter microstructure in pre-reading children: A longitudinal investigation. *Hum Brain*  
1157 *Mapp* **40**, 741–754 (2018).
- 1158 109. M. K. Denney, J. P. English, M. M. Gerber, J. Leafstedt, M. L. Ruz, Family and home  
1159 literacy practices: mediating factors for preliterate English learners at risk in *Annual*  
1160 *Meeting of the American Educational Research Associations*, (2001), pp. 1–17.
- 1161 110. Y. S. G. Kim, Executive Functions and Morphological Awareness Explain the Shared  
1162 Variance between Word Reading and Listening Comprehension. *Scientific Studies of*  
1163 *Reading* **27**, 451–474 (2023).
- 1164 111. F. A. Schrank, K. S. McGrew, N. Mather, *Woodcock-Johnson IV Tests of Cognitive*  
1165 *Abilities* (Riverside, 2014).
- 1166 112. M. Korkman, U. Kirk, S. Kemp, *NEPSY–Second Edition (NEPSY-II)*, 2nd Ed. (The  
1167 Psychological Corporation, 2007).
- 1168 113. F. Schrank, N. Mather, K. McGrew, *Woodcock-Johnson IV Tests of Oral Language*  
1169 (Riverside Publishing Co, 2014).
- 1170 114. R. W. Woodcock, *Woodcock Reading Mastery Tests (WRMT-III)* (NCS Pearson, 2011).
- 1171 115. A. S. Kaufman, N. L. Kaufman, Kaufman Brief Intelligence Test, Second Edition.  
1172 *PsycTESTS Dataset* [Preprint] (2004).
- 1173 116. L. L. Backhausen, *et al.*, Quality control of structural MRI images applied using  
1174 FreeSurfer—a hands-on workflow to rate motion artifacts. *Front Neurosci* **10** (2016).
- 1175 117. V. S. Natu, *et al.*, Infants' cortex undergoes microstructural growth coupled with  
1176 myelination during development. *Commun Biol* **4** (2021).
- 1177 118. L. Wang, *et al.*, iBEAT V2.0: a multisite-applicable, deep learning-based pipeline for infant  
1178 cerebral cortical surface reconstruction. *Nat Protoc* **18**, 1488–1509 (2023).
- 1179 119. G. Li, *et al.*, Measuring the dynamic longitudinal cortex development in infants by  
1180 reconstruction of temporally consistent cortical surfaces. *Neuroimage* **90**, 266–279  
1181 (2014).
- 1182 120. G. Li, *et al.*, Computational neuroanatomy of baby brains: A review. *Neuroimage*  
1183 [Preprint] (2019).
- 1184 121. C. S. McCarthy, *et al.*, A comparison of FreeSurfer-generated data with and without  
1185 manual intervention. *Front Neurosci* **9** (2015).
- 1186 122. E. P. Pulli, *et al.*, Feasibility of FreeSurfer Processing for T1-Weighted Brain Images of 5-  
1187 Year-Olds: Semiautomated Protocol of FinnBrain Neuroimaging Lab. *Front Neurosci* **16**  
1188 (2022).
- 1189 123. B. Ahtam, *et al.*, Morphological Features of Language Regions in Individuals with  
1190 Tuberos Sclerosis Complex. *J Autism Dev Disord* **54**, 3155–3175 (2024).
- 1191 124. K. Chyl, G. Fraga-González, S. Brem, K. Jednoróg, Brain dynamics of (a)typical reading  
1192 development—a review of longitudinal studies. *NPJ Sci Learn* [Preprint] (2021).
- 1193 125. M. Bastiani, *et al.*, Automated processing pipeline for neonatal diffusion MRI in the  
1194 developing Human Connectome Project. *Neuroimage* **185**, 750–763 (2019).
- 1195 126. L. Cordero-Grande, D. Christiaens, J. Hutter, A. N. Price, J. V. Hajnal, Complex diffusion-  
1196 weighted image estimation via matrix recovery under general noise models. *Neuroimage*  
1197 **200**, 391–404 (2019).

- 1198 127. J. Veraart, *et al.*, Denoising of diffusion MRI using random matrix theory. *Neuroimage*  
1199 **142**, 394–406 (2016).
- 1200 128. J. Veraart, E. Fieremans, D. S. Novikov, Diffusion MRI noise mapping using random  
1201 matrix theory. *Magn Reson Med* **76**, 1582–1593 (2016).
- 1202 129. J. L. R. Andersson, S. Skare, J. Ashburner, How to correct susceptibility distortions in  
1203 spin-echo echo-planar images: Application to diffusion tensor imaging. *Neuroimage* **20**,  
1204 870–888 (2003).
- 1205 130. J. L. R. Andersson, *et al.*, Towards a comprehensive framework for movement and  
1206 distortion correction of diffusion MR images: Within volume movement. *Neuroimage* **152**,  
1207 450–466 (2017).
- 1208 131. J. L. R. Andersson, S. N. Sotiropoulos, An integrated approach to correction for off-  
1209 resonance effects and subject movement in diffusion MR imaging. *Neuroimage* **125**,  
1210 1063–1078 (2016).
- 1211 132. S. Skare, R. Bammer, Jacobian weighting of distortion corrected EPI data in *Proceedings*  
1212 *of the International Society for Magnetic Resonance in Medicine*, (2010).
- 1213 133. S. M. Smith, *et al.*, Advances in functional and structural MR image analysis and  
1214 implementation as FSL. *Neuroimage* **23**, 208–219 (2004).
- 1215 134. N. J. Tustison, *et al.*, N4ITK: Improved N3 bias correction. *IEEE Trans Med Imaging* **29**,  
1216 1310–1320 (2010).
- 1217 135. T. Dhollander, R. Mito, D. Raffelt, A. Connelly, Improved white matter response function  
1218 estimation for 3-tissue constrained spherical deconvolution in *Proc Intl Soc Mag Reson*  
1219 *Med*, (2019).
- 1220 136. B. Jeurissen, J. D. Tournier, T. Dhollander, A. Connelly, J. Sijbers, Multi-tissue  
1221 constrained spherical deconvolution for improved analysis of multi-shell diffusion MRI  
1222 data. *Neuroimage* **103**, 411–426 (2014).
- 1223 137. J. D. Tournier, F. Calamante, D. G. Gadian, A. Connelly, Direct estimation of the fiber  
1224 orientation density function from diffusion-weighted MRI data using spherical  
1225 deconvolution. *Neuroimage* **23**, 1176–1185 (2004).
- 1226 138. J. D. Tournier, F. Calamante, A. Connelly, MRtrix: Diffusion tractography in crossing fiber  
1227 regions. *Int J Imaging Syst Technol* **22**, 53–66 (2012).
- 1228 139. R. E. Smith, J. D. Tournier, F. Calamante, A. Connelly, Anatomically-constrained  
1229 tractography: Improved diffusion MRI streamlines tractography through effective use of  
1230 anatomical information. *Neuroimage* **62**, 1924–1938 (2012).
- 1231 140. J. Yeatman, R. Dougherty, N. Myall, B. Wandell, H. Feldman, Tract profiles of white  
1232 matter properties: automating fiber-tract quantification. *PLoS One* **7**, e49790 (2012).
- 1233 141. J. Kruper, *et al.*, Evaluating the Reliability of Human Brain White Matter Tractometry.  
1234 *Aperture Neuro* **1**, 1–25 (2021).
- 1235 142. M. Grotheer, *et al.*, Human white matter myelinates faster in utero than ex utero. (2023).  
1236 <https://doi.org/10.1073/pnas>.
- 1237 143. S. M. Smith, T. E. Nichols, Threshold-free cluster enhancement: Addressing problems of  
1238 smoothing, threshold dependence and localisation in cluster inference. *Neuroimage* **44**,  
1239 83–98 (2009).
- 1240 144. J. Frossard, O. Renaud, Permutation tests for regression, anova, and comparison of  
1241 signals: The permuco package. *J Stat Softw* **99**, 1–32 (2021).
- 1242 145. J. Pinheiro, D. Bates, S. DebRoy, D. Sarkar, R Core Team, nlme: Linear and Nonlinear  
1243 Mixed Effects Models. *R Package Version 3* [Preprint] (2017). Available at: [https://bugs.r-](https://bugs.r-project.org)  
1244 [project.org](https://bugs.r-project.org).
- 1245 146. A. F. G. Rosen, *et al.*, Quantitative assessment of structural image quality. *Neuroimage*  
1246 **169**, 407–418 (2018).

- 1247 147. T. Turesky, *et al.*, Brain Morphometry and Diminished Physical Growth in Bangladeshi  
1248 Children Growing up in Extreme Poverty: a Longitudinal Study. *Dev Cogn Neurosci* **52**,  
1249 101029 (2021).
- 1250 148. T. K. Turesky, *et al.*, Brain morphometry and chronic inflammation in Bangladeshi  
1251 children growing up in extreme poverty. *Imaging Neuroscience* **2**, 1–16 (2024).
- 1252 149. J. Monereo-Sánchez, *et al.*, Quality control strategies for brain MRI segmentation and  
1253 parcellation: Practical approaches and recommendations - insights from the Maastricht  
1254 study. *Neuroimage* **237** (2021).
- 1255 150. J. Matsuzawa, M. Matsui, T. Konishi, Age-related Volumetric Changes of Brain Gray and  
1256 White Matter in Healthy Infants and Children. *Cerebral Cortex* **11**, 335–342 (2001).
- 1257 151. S. Groeschel, B. Vollmer, M. D. King, A. Connelly, Developmental changes in cerebral  
1258 grey and white matter volume from infancy to adulthood. *International Journal of*  
1259 *Developmental Neuroscience* **28**, 481–489 (2010).
- 1260 152. S. C. L. Deoni, D. C. Dean, J. O. Muircheartaigh, H. Dirks, B. A. Jerskey, Investigating  
1261 white matter development in infancy and early childhood using myelin water fraction and  
1262 relaxation time mapping. **63**, 1038–1053 (2012).
- 1263 153. S. C. L. Deoni, *et al.*, Breastfeeding and early white matter development: A cross-  
1264 sectional study. *Neuroimage* **82**, 77–86 (2013).
- 1265 154. J. Remer, *et al.*, Quantifying cortical development in typically developing toddlers and  
1266 young children, 1–6 years of age. *Neuroimage* **153**, 246–261 (2017).
- 1267 155. C. E. Sanchez, J. E. Richards, C. R. Almli, Neurodevelopmental MRI brain templates for  
1268 children from 2 weeks to 4 years of age. *Dev Psychobiol* **54**, 77–91 (2011).
- 1269 156. X. Geng, *et al.*, NeuroImage Quantitative tract-based white matter development from birth  
1270 to age 2 years. *Neuroimage* **61**, 542–557 (2012).
- 1271 157. K. Im, N. Raschle, S. A. Smith, P. Ellen Grant, N. Gaab, Atypical Sulcal Pattern in  
1272 Children with Developmental Dyslexia and At-Risk Kindergarteners. *Cerebral Cortex* **26**,  
1273 1138–1148 (2016).
- 1274 158. C. A. Myers, *et al.*, White Matter Morphometric Changes Uniquely Predict Children’s  
1275 Reading Acquisition. *Psychol Sci* **25**, 1870–1883 (2014).
- 1276 159. K. Hannula-Jouppi, *et al.*, The axon guidance receptor gene ROBO1 is a candidate gene  
1277 for developmental dyslexia. *PLoS Genet* **1**, 0467–0474 (2005).
- 1278 160. L. Reiche, *et al.*, C21orf91 Regulates Oligodendroglial Precursor Cell Fate—A Switch in  
1279 the Glial Lineage? *Front Cell Neurosci* **15** (2021).
- 1280 161. A. M. Fjell, *et al.*, The relationship between diffusion tensor imaging and volumetry as  
1281 measures of white matter properties. *Neuroimage* **42**, 1654–1668 (2008).
- 1282 162. A. D. Friederici, The cortical language circuit: From auditory perception to sentence  
1283 comprehension. *Trends Cogn Sci* [Preprint] (2012).
- 1284 163. J. Wang, M. L. Rice, J. R. Booth, Syntactic and semantic specialization and integration in  
1285 5-to 6-year-old children during auditory sentence processing. *J Cogn Neurosci* **32**, 36–49  
1286 (2019).
- 1287 164. P. K. Kuhl, Early language acquisition: Cracking the speech code. *Nat Rev Neurosci*  
1288 [Preprint] (2004).
- 1289 165. X. Yu, J. Zuk, N. Gaab, What Factors Facilitate Resilience in Developmental Dyslexia?  
1290 Examining Protective and Compensatory Mechanisms Across the Neurodevelopmental  
1291 Trajectory. *Child Dev Perspect* **12**, 240–246 (2018).
- 1292 166. O. Ozernov-Palchik, X. Yu, Y. Wang, N. Gaab, Lessons to be learned: How a  
1293 comprehensive neurobiological framework of atypical reading development can inform  
1294 educational practice. *Curr Opin Behav Sci* **10**, 45–58 (2016).
- 1295 167. H. Catts, Y. Petscher, Early identification of dyslexia: Current advancements and future  
1296 directions. *Perspect Lang Lit* **44**, 33–36 (2018).

- 1297 168. S. A. Hart, C. Little, E. van Bergen, Nurture might be nature: cautionary tales and  
1298 proposed solutions. *NPJ Sci Learn* **6**, 1–12 (2021).  
1299 169. J. Zuk, *et al.*, Multifactorial pathways facilitate resilience among kindergarteners at risk for  
1300 dyslexia: A longitudinal behavioral and neuroimaging study. *Dev Sci* **24**, 1–18 (2021).  
1301 170. X. Yu, *et al.*, Putative protective neural mechanisms in prereaders with a family history of  
1302 dyslexia who subsequently develop typical reading skills. *Hum Brain Mapp* **41**, 2827–  
1303 2845 (2020).  
1304 171. F. Hoeft, *et al.*, Neural systems predicting long-term outcome in dyslexia. *Proceedings of*  
1305 *the National Academy of Sciences* **108**, 361–366 (2011).  
1306 172. C. A. Nelson, L. J. Gabard-Durnam, Early Adversity and Critical Periods :  
1307 Neurodevelopmental Consequences of Violating the Expectable Environment. *Trends*  
1308 *Neurosci* **43**, 133–143 (2020).  
1309 173. P. J. Curran, K. Obeidat, D. Losardo, Twelve frequently asked questions about growth  
1310 curve modeling. *Journal of Cognition and Development* **11**, 121–136 (2010).  
1311 174. E. H. Telzer, *et al.*, Methodological considerations for developmental longitudinal fMRI  
1312 research. *Dev Cogn Neurosci* [Preprint] (2018).  
1313 175. E. Roy, *et al.*, Differences in educational opportunity predict white matter development.  
1314 *Dev Cogn Neurosci* **67** (2024).  
1315

## Supplementary Methods

### 1. Participants

#### *New England cohort*

Children participated in a longitudinal investigation of brain and literacy development from infancy to school age (NIH–NICHD R01 HD065762). Families of these children were recruited from the New England Area using the Research Participant Registry provided by the Division of Developmental Medicine at Boston Children’s Hospital, and with flyers and ads disseminated in local schools and newspapers, at community events, and on social media. Children were enrolled as infants with the expectation that participation would continue at subsequent developmental stages across the first decade of life. Children were excluded from the study if at any timepoint they were diagnosed with neurological, sensory, or motor disorders or had contraindications for MRI evaluation (e.g., metal implants). All children included were from English-speaking families and were born at gestational week 37 or later. Race demographics, whose reporting is encouraged to improve equitability in neuroscience (1), are as follows: 70% White/Caucasian, 6% Black/African American, 5% Asian, 16% Multiracial, and 5% Hispanic. Neuroimaging and behavioral testing were conducted at Boston Children’s Hospital prior to 2021 and at the Center for Brain Science at Harvard University from 2021 onward. At Boston Children’s Hospital, children’s anatomical MRI scans (please see parameters below) did not show any potentially malignant brain features, as reviewed by a pediatric neuroradiologist. This study was approved by the Institutional Review Boards of Boston Children’s Hospital (IRB-P00023182) and Harvard University (IRB21-0916). Informed written consent was provided by each participating infant’s parent(s) and children gave verbal assent for participation after 50 months of age.

#### *Calgary cohort*

Children in the Calgary, Alberta area were recruited from the ongoing study on pregnancy outcomes and nutrition (2). Children in this study were predominantly (roughly 90%) from Caucasian families, but also included Asian/Pacific Islander, African, Filipino, Latino/Hispanic, and Multiracial children. Children were born at gestational week 36 or later and did not have diagnosed genetic, neurological, or neurodevelopmental disorders. The study was approved by the University of Calgary Conjoint Health Research Ethics Board (REB13-0020). Parent and/or guardian consent and child assent were acquired for all participants. For additional information, please see the open-source repository (<https://osf.io/axz5r/>) and previous publications (3–9).

## 2. Further description for the phonological processing composite in the New England cohort

The phonological processing composite comprises three subtests: word access, word fluency, and substitution. For the word access subtest, the child is asked to provide a word that has a specific phonemic element in a specific location. For example, the child may be shown an image, told what it is, and then shown three additional images and asked to select the one that begins with the same sound as the first image. For the word fluency subtest, the child is asked to name as many words as possible that begin with a specific sound within a 1-minute time frame. For example, the child may be asked to name words that begin with the /b/ sound. Lastly, for the substitution subtest, the child is asked to substitute part of one word to create a new word. For instance, the child may be asked to say the resulting word when they replace the /b/ sound in “bunny” with the /s/ sound. Overall, these assessments are designed to probe phonological and phonemic processing/awareness.

## 3. MRI data acquisition

### *New England cohort*

All data were acquired on a 3.0 T Siemens scanner with a 32-channel head coil. Please note, sequence parameters varied to optimize acquisition for the increasing head size and neuroanatomy of the participants across the developmental window. Structural T1-weighted magnetization-prepared rapid gradient-echo (MPRAGE) scans were acquired with the following parameters: TR = 2270-2520 ms, TE = 1.66-1.73 ms, field of view = 192-224 mm, 1 mm<sup>3</sup> voxels, 144-176 sagittal slices. Diffusion echo planar images were acquired using the following parameters: TR = 3800-8320 ms, TE = 88-89 ms, flip angle = 90°, field of view = 180-256 mm, voxel size = 2 x 2 x 2 mm<sup>3</sup>, 62-78 slices, 30 b = 1000 s/mm<sup>2</sup> gradient directions, 10-11 b = 0 s/mm<sup>2</sup> non-diffusion-weighted volumes. Diffusion data were acquired with slice-acceleration (SMS/MB) factor = 2 and one reverse phase encoding (i.e., posterior-to-anterior) volume. Please note, sequence parameters varied to optimize acquisition for the increasing head size and neuroanatomy of the participants across the developmental window.

### *Calgary cohort*

All data were acquired on a 3.0 T General Electric scanner with a 32-channel head coil. Structural T1-weighted scans were acquired with the following parameters: TR = 8.23 ms, TE = 3.76 ms, field of view = 230 mm, 0.45 x 0.45 x 0.9 mm<sup>3</sup> voxels, 210 slices. Diffusion echo planar images were acquired using the following parameters: TR = 6750 ms, TE = 79 ms, flip angle = 90°, field of view = 200 mm, voxel size = 0.78 x 0.78 x 2.2 mm<sup>3</sup>, 50-55 slices, 30 b = 750 s/mm<sup>2</sup> gradient

directions,  $b = 0$  s/mm<sup>2</sup> non-diffusion-weighted volumes. Diffusion acquisition did not use a slice-acceleration factor and did not include a reverse phase encoding (i.e., posterior-to-anterior) volume.

#### 4. Algorithm for combining FreeSurfer and iBEATv2.0 segmentations

Segmentations from each software package were then hybridized using in-house MATLAB code that combined the cortical pial and white matter boundaries labeled by iBEATv2.0 with the FreeSurfer subcortical parcellations (i.e., effectively relabeling cortical gray and white matter in the FreeSurfer segmentation using iBEATv2.0 tissue-class demarcations). Herein, iBEATv2.0 3-class tissue segmentations were first resampled to the space of the aseg file. iBEATv2.0 gray matter and cerebrospinal fluid voxels that overlapped with the aseg gray matter and cerebrospinal fluid labels, respectively, inherited the latter's labels. iBEATv2.0 white matter voxels overlapping with aseg white *or* gray matter received the aseg white matter label; as iBEATv2.0 does not distinguish hemispheres in its labels and FreeSurfer generally overestimates gray matter in this age group, gray matter information was also used here for relabeling. iBEATv2.0 voxels unlabeled by these procedures were then submitted to a nearest neighbor search to identify aseg labels at minimum Euclidean distance. As FreeSurfer generally performed better compared with iBEATv2.0 on subcortical areas, all subcortical (non-cerebellum areas) were relabeled with subcortical FreeSurfer labels. Finally, hybridized segmentation files were converted to FreeSurfer-style white matter files and submitted to a modified version of the standard FreeSurfer v7.3 "recon" pipeline.

#### 5. Preparation of Euler numbers

Similar to Bethlehem and colleagues 2022, for further quality control, we also extracted Euler numbers (10), which quantify topological defects in FreeSurfer's cortical reconstruction and have been shown to correlate with visual ratings and mark artifactual images (11). Euler numbers from each hemisphere were averaged across observations for each participant (average: (11); sum: (12)) and used in sensitivity analyses.

#### 6. Implementations of pyAFQ and pyBabyAFQ

Whole-brain tractography was then submitted for fiber tract segmentation to the open-source instantiation of Automated Fiber Quantification (AFQ; (13, 14)). Herein, waypoint regions-of-interest (ROIs) and a probabilistic fiber atlas were mapped from a standard template to the

individual brain. Fibers were delineated into separate tracts according to the waypoint ROIs through which they passed and the tract they were most likely to belong based on the probability atlas. Additional fibers were removed (i.e., outlier detection) if they deviated sufficiently from the core of the tract. While all diffusion data underwent the above processes, parameters differed by age group. For brains > 25 months, the standard pyAFQ pipeline was used, in which ROIs and the probability fiber atlas were mapped from an adult MNI template and fibers were removed if they were more than five standard deviations from the core of the tract (14). In contrast, for brains  $\leq$  24 months, we used pyBabyAFQ (15), an implementation in the pyAFQ suite designed to accommodate the smaller neuroanatomy in infants. Accordingly, ROIs and the probabilistic fiber atlas are mapped from an infant template (16), the ROIs are smaller compared to those used by standard pyAFQ, an additional ROI was used for tracts with acute curves, and the fiber outlier detection threshold was reduced to four standard deviations from the tract core. Importantly, varying the parameters used to segment the tracts by age group preserves the accuracy with which tracts are segmented and reduces age-related bias that would emerge if using standard (i.e., suboptimal) parameters for younger children.

#### 7. Quality control procedures for longitudinal trajectory estimation

Prior to modeling, estimates of brain structure and white matter organization, excepting cortical thickness and mean curvature, underwent a final quality control procedure to remove neuroanatomically implausible observations by setting annual change thresholds. For instance, it was unlikely that gray matter volume in any particular brain area changed by more than 10% per year in children over 25 months. Accordingly, for brains > 25 months, observations for brain regions and tracts of interest (please see above) were flagged if they were preceded or followed by  $\geq$  10% annual change (positive or negative). To improve model convergence in the first sensitivity analysis (with nonlinear mixed effects models), the threshold for mean diffusivity was lowered from 10% to 5%. To mitigate data loss, we next identified which timepoint—the earlier timepoint or later timepoint—was more likely to be inaccurate, using an outlier detection procedure. Herein, we generated average (across participants) estimates for each brain area/tract and each brain measure by timepoint (roughly, grade level) to which to compare the observations flagged in the previous step. Out of the pair of flagged observations, the one farther from the average estimate corresponding to its timepoint was discarded and the other flagged observation was preserved. This process was done iteratively to handle cases in which children over 50 months had MRI observations from more than two timepoints. A similar quality control procedure was used for brains  $\leq$  24 months, but it needed to account for the rapid brain growth already

thoroughly reported (17, 18). Consequently, observations were only flagged when inter-timepoint changes were negative for gray/white matter volume, surface area, or fractional anisotropy, or positive for mean diffusivity. No inter-timepoint threshold was used for cortical thickness or mean curvature for brains  $\leq 24$  months. All remaining participants after these additional quality control procedures had multiple observations (i.e., longitudinal datasets), including one from  $\leq 24$  months.

## 8. Sensitivity analyses

To test the reliability of our results, we performed a replication analysis on gray/white matter volume, and surface area with nonlinear mixed effects models using asymptotic functions from the R 'nlme' package (19), similar to that described in Alex and colleagues (18); [https://github.com/knickmeyer-lab/ORIGINS\\_ICV-and-Subcortical-volume-development-in-early-childhood](https://github.com/knickmeyer-lab/ORIGINS_ICV-and-Subcortical-volume-development-in-early-childhood)). Intercepts and asymptotes were modeled as fixed and random effects; rate constants were modeled as fixed effects. The reason that this model was not used in the main analysis is that it does not use a random slopes term, and a key aspect of the current study is to examine the relation between brain growth and literacy subskills. However, it should be noted that the nonlinear model does provide an indirect examination of the relation between growth and literacy subskills; e.g., if there is no association between the intercept and the literacy subskill, but there is an association between the asymptote and the literacy subskill, then it could be inferred that there is an association between brain growth and the literacy subskill. Although both linear and nonlinear models have different requirements (e.g., linear models require relationships between predictors and outcomes to be linear), the functional forms used on the current dataset in both cases fit the data closely (Supplementary Figure 8), suggesting random parameters were similar or proportional across models.

For the main analysis, we opted to model brain development prior to testing brain-behavior associations because this comports with the temporal order theorized, that brain development effects subsequent behavioral skills. Also, our sample size is larger for longitudinal brain data alone compared with longitudinal brain data plus reading-related outcomes; therefore, longitudinal models of brain development would be improved if not including outcomes in the model. However, in practice, contributions of phonological processing main and age x phonological interaction terms should be analogous to associations between phonological processing and curve intercepts and slopes, respectively. Consequently, we also examined phonological processing main and age x phonological processing interaction terms included in the linear mixed effects models.

In addition, we did not initially control for total intracranial volume (TIV) when modeling longitudinal trajectories of brain structure, consistent with other work examining developmental

trajectories of brain structure beginning in infancy (12, 18, 20–23). Further, recent work has shown that TIV correction may be problematic, reducing brain-behavior predictive accuracies for gray matter volume and surface area or potentially generating spurious predictions for cortical thickness (24). Given these concerns and recommendations to report both raw and TIV-corrected results (25), we thought that an appropriate use of TIV would be to recompute brain-behavior associations for volumetric and surface-based measures using semipartial correlations (Pearson) with the random terms from longitudinal modeling with TIV as covariates of no interest. We report results of the linear mixed model run on brain-behavior relations with TIV.

Lastly, for volumetric and surface-based measures, visual ratings of cortical surfaces were used to identify sub-optimal datasets (visual ratings of tract reconstructions were for measures of white matter organization). However, Euler numbers, which quantify the number the topological defects in FreeSurfer's cortical surface reconstruction (10), have been shown to consistently correlate with quality ratings (11) and to serve as reproducible alternatives to manual quality control, including manual editing (26). Comparable to Rosen and colleagues, visual ratings and Euler numbers were highly correlated after controlling for age and biological sex ( $r = 0.44$ ,  $p < 0.001$ ). Therefore, to account for residual variance due to segmentation quality in a data-driven, reproducible manner, we submitted volumetric and surface-based brain-behavior associations to semipartial correlations (Pearson) with average (across timepoint) Euler numbers.

## 9. References for the Supplement

1. E. K. Webb, J. A. Etter, J. A. Kwasa, Addressing racial and phenotypic bias in human neuroscience methods. *Nat Neurosci* **25**, 410–414 (2022).
2. B. J. Kaplan, *et al.*, The Alberta Pregnancy Outcomes and Nutrition (APrON) cohort study: Rationale and methods. *Matern Child Nutr* **10**, 44–60 (2014).
3. D. Paniukov, R. M. Lebel, G. Giesbrecht, C. Lebel, Cerebral blood flow increases across early childhood. *Neuroimage* **204** (2020).
4. M. Walton, D. Dewey, C. Lebel, Brain white matter structure and language ability in preschool-aged children. *Brain Lang* **176**, 19–25 (2018).
5. J. Reynolds, M. N. Grohs, D. Dewey, C. Lebel, Global and regional white matter development in early childhood. *Neuroimage* **196**, 49–58 (2019).
6. J. Reynolds, X. Long, D. Paniukov, M. Bagshawe, C. Lebel, Calgary Preschool magnetic resonance imaging (MRI) dataset. *Data Brief* **29** (2020).
7. J. Reynolds, X. Long, M. N. Grohs, D. Dewey, C. Lebel, Structural and functional asymmetry of the language network emerge in early childhood. *Dev Cogn Neurosci* **39** (2019).
8. C. Lebel, *et al.*, Prepartum and Postpartum Maternal Depressive Symptoms Are Related to Children's Brain Structure in Preschool. *Biol Psychiatry* **80**, 859–868 (2016).
9. C. Thieba, *et al.*, Factors Associated With Successful MRI Scanning in Unsedated Young Children. *Front Pediatr* **6**, 1–5 (2018).
10. A. M. Dale, B. Fischl, M. I. Sereno, "Cortical Surface-Based Analysis I. Segmentation and Surface Reconstruction" (1999).

11. A. F. G. Rosen, *et al.*, Quantitative assessment of structural image quality. *Neuroimage* **169**, 407–418 (2018).
12. R. A. I. Bethlehem, *et al.*, Brain charts for the human lifespan. *Nature* **604**, 525–533 (2022).
13. J. Yeatman, R. Dougherty, N. Myall, B. Wandell, H. Feldman, Tract profiles of white matter properties: automating fiber-tract quantification. *PLoS One* **7**, e49790 (2012).
14. J. Kruper, *et al.*, Evaluating the Reliability of Human Brain White Matter Tractometry. *Aperture Neuro* **1**, 1–25 (2021).
15. M. Grotheer, *et al.*, Human white matter myelinates faster in utero than ex utero. (2023). <https://doi.org/10.1073/pnas>.
16. F. Shi, *et al.*, Infant brain atlases from neonates to 1- and 2-year-olds. *PLoS One* **6** (2011).
17. J. Gilmore, R. C. Knickmeyer, W. Gao, Imaging structural and functional brain development in early childhood. *Nat Rev Neurosci* **19**, 123–137 (2018).
18. A. M. Alex, *et al.*, A global multicohort study to map subcortical brain development and cognition in infancy and early childhood. *Nat Neurosci* **27**, 176–186 (2024).
19. J. Pinheiro, D. Bates, S. DebRoy, D. Sarkar, R Core Team, nlme: Linear and Nonlinear Mixed Effects Models. *R Package Version 3* [Preprint] (2017). Available at: <https://bugs.r-project.org>.
20. S. Groeschel, B. Vollmer, M. D. King, A. Connelly, Developmental changes in cerebral grey and white matter volume from infancy to adulthood. *International Journal of Developmental Neuroscience* **28**, 481–489 (2010).
21. J. Matsuzawa, M. Matsui, T. Konishi, Age-related Volumetric Changes of Brain Gray and White Matter in Healthy Infants and Children. *Cerebral Cortex* **11**, 335–342 (2001).
22. S. C. L. Deoni, D. C. Dean, J. O. Muircheartaigh, H. Dirks, B. A. Jerskey, Investigating white matter development in infancy and early childhood using myelin water fraction and relaxation time mapping. **63**, 1038–1053 (2012).
23. J. Remer, *et al.*, Quantifying cortical development in typically developing toddlers and young children, 1–6 years of age. *Neuroimage* **153**, 246–261 (2017).
24. E. Dhamala, *et al.*, Proportional intracranial volume correction differentially biases behavioral predictions across neuroanatomical features, sexes, and development. *Neuroimage* **260** (2022).
25. N. Vijayakumar, K. L. Mills, A. Alexander-Bloch, C. K. Tamnes, S. Whittle, Structural brain development: A review of methodological approaches and best practices. *Dev Cogn Neurosci* **33**, 129–148 (2018).
26. J. Monereo-Sánchez, *et al.*, Quality control strategies for brain MRI segmentation and parcellation: Practical approaches and recommendations - insights from the Maastricht study. *Neuroimage* **237** (2021).

## Supplemental Tables

<b>Supplementary Table 1. Participant demographics</b>			
		Structure	Diffusion
<i>General information</i>	N. participants	98	128
	N. observations	276	396
	N. observations per participant	3 ± 1	3 ± 1
	Age at literacy-related subskill testing (months)	63 ± 5.3	63 ± 5.1
	Age at decoding/word reading testing (months)	82 ± 6.4	82 ± 6.4
<i>Covariates</i>	Biological sex (F/M)	46/52	67/61
	Maternal education (years)	17 ± 2.1	17 ± 2.1
	Cohort ([New England]/Calgary)	59/39	77/51
	Family history of reading difficulty (+/-)	30/29	39/38
	Home literacy environment (a.u.)	0.073 ± 0.40	0.041 ± 0.42
<i>Literacy-related subskills</i>	Phonological processing standard score	108 ± 13	106 ± 14
	Oral language standard score	115 ± 13	113 ± 13
<i>Decoding/word reading</i>	Word attack standard score	115 ± 13	112 ± 14
	Word identification standard score	113 ± 17	109 ± 17
<i>Cognitive abilities</i>	Nonverbal general cognitive ability	109 ± 12	106 ± 13

<b>Supplementary Table 2. Comparison of Linear Mixed Effects Models for Gray Matter Volume</b>							
Brain Region/Tract	Random Intercept			Random Intercept and Slope			
A. Gray Matter Volume	Logarithmic	Linear	Quadratic	Logarithmic	Linear	Quadratic	p
bankssts	3264	3332	3292	<b>3242</b>	3330	3283	< 0.001
fusiform	4143	4266	4160	<b>4116</b>	4270	4131	< 0.001
inferiorparietal	4459	4581	4478	<b>4456</b>	4589	4482	< 0.001
middletemporal	4265	4419	4303	<b>4233</b>	4412	4279	< 0.001
parsopercularis	3913	4016	3955	<b>3866</b>	4016	3922	< 0.001
parstriangularis	3797	3943	3812	<b>3777</b>	3946	3797	< 0.001
superiortemporal	4354	4490	4400	<b>4335</b>	4492	4387	< 0.001
supramarginal	4201	4325	4235	<b>4178</b>	4326	4207	< 0.001
<b>B. White Matter Volume</b>							
bankssts	3311	3356	3334	<b>3253</b>	3326	3292	< 0.001
fusiform	3765	3799	3772	<b>3706</b>	3777	3733	< 0.001
inferiorparietal	4030	4081	4046	<b>3968</b>	4047	4006	< 0.001
middletemporal	3735	3759	3734	<b>3664</b>	3718	3686	< 0.001
parsopercularis	3639	3685	3653	<b>3552</b>	3636	3586	< 0.001
parstriangularis	3396	3422	3399	<b>3285</b>	3360	3311	< 0.001
superiortemporal	4031	4044	4039	<b>3949</b>	3977	3966	< 0.001
supramarginal	4171	4218	4188	<b>4068</b>	4168	4103	< 0.001
<b>C. Surface Area</b>							
bankssts	2923	2970	2943	<b>2900</b>	2963	2931	< 0.001
fusiform	3523	3641	3554	<b>3503</b>	3644	3547	< 0.001
inferiorparietal	3807	3902	3831	<b>3793</b>	3903	3829	< 0.001
middletemporal	3517	3595	3552	<b>3511</b>	3595	3552	< 0.001
parsopercularis	3189	3267	3225	<b>3150</b>	3254	3207	< 0.001
parstriangularis	3110	3202	3143	<b>3072</b>	3194	3124	< 0.001
superiortemporal	3555	3639	3591	<b>3536</b>	3632	3580	< 0.001
supramarginal	3645	3724	3676	<b>3615</b>	3714	3650	< 0.001
<b>D. Cortical Thickness</b>							
bankssts	-235	-226	-225	<b>-258</b>	-233	-235	< 0.001
fusiform	-392	-372	-389	<b>-425</b>	-394	-409	< 0.001
inferiorparietal	-385	-375	-382	<b>-403</b>	-386	-395	< 0.001
middletemporal	-268	-217	-260	<b>-290</b>	-228	-288	< 0.001
parsopercularis	-335	-321	-322	<b>-361</b>	-332	-341	< 0.001
parstriangularis	-298	-277	-298	<b>-324</b>	-287	-314	< 0.001

superiortemporal	-336	-283	-319	<b>-348</b>	-286	-330	< 0.001
supramarginal	-334	-315	-330	<b>-339</b>	-314	-333	< 0.001
E. Mean Curvature							
bankssts	-1611	-1594	-1615	<b>-1649</b>	-1614	-1654	< 0.001
fusiform	-1448	-1432	-1447	<b>-1472</b>	-1439	-1471	< 0.001
inferioparietal	-1498	-1484	-1494	<b>-1554</b>	-1518	-1543	< 0.001
middletemporal	-1435	-1423	-1435	<b>-1447</b>	-1426	-1448	< 0.001
parsopercularis	-1505	-1495	-1502	<b>-1536</b>	-1513	-1526	< 0.001
parstriangularis	-1482	-1470	-1479	<b>-1502</b>	-1478	-1492	< 0.001
superiortemporal	-1525	-1513	-1525	<b>-1533</b>	-1515	-1535	< 0.001
supramarginal	-1441	-1425	-1444	<b>-1469</b>	-1440	-1475	< 0.001
F. Fractional Anisotropy							
Arcuate fasc.	<b>-1740</b>	-1564	-1685	-1733	-1557	-1685	NA
Sup. long. fasc.	<b>-1749</b>	-1530	-1700	-1742	-1525	-1713	NA
Inf. long. fasc.	-1667	-1526	-1607	<b>-1662</b>	-1523	-1611	NA
G. Mean Diffusivity							
Arcuate fasc.	-6706	-6501	-6593	<b>-6750</b>	-6525	-6647	< 0.001
Sup. long. fasc.	-6950	-6711	-6816	<b>-7001</b>	-6741	-6868	< 0.001
Inf. long. fasc.	-6384	-6214	-6294	<b>-6410</b>	-6232	-6321	< 0.001
Bold indicates lowest BIC value; I, intercept; S, slope							

<b>Supplementary Table 3. Brain-behavior associations with nonlinear mixed effects model</b>						
Brain Region/Tract	Intercept			Asymptote		
	r	p	pFDR	r	p	pFDR
<b>A. Gray Matter Volume</b>						
bankssts	0.32	0.0088	0.034	0.28	0.020	0.053
fusiform	0.02	0.86	0.86	0.08	0.48	0.48
inferiorparietal	0.28	0.013	0.034	0.28	0.013	0.051
middletemporal	0.20	0.082	0.11	0.20	0.082	0.11
parsopercularis	0.17	0.14	0.16	0.22	0.059	0.11
parstriangularis	0.29	0.0094	0.034	0.32	0.0051	0.040
superiortemporal	0.22	0.050	0.080	0.19	0.096	0.11
supramarginal	0.28	0.017	0.034	0.20	0.095	0.11
<b>B. White Matter Volume</b>						
bankssts	0.26	0.026	0.066	0.26	0.027	0.027
fusiform	0.11	0.34	0.34	0.30	0.0080	0.013
inferiorparietal	0.30	0.010	0.050	0.43	< 0.001	< 0.001
middletemporal	NA	NA	NA	NA	NA	NA
parsopercularis	0.12	0.30	0.34	0.29	0.011	0.014
parstriangularis	0.23	0.048	0.080	0.40	< 0.001	0.0012
superiortemporal	NA	NA	NA	NA	NA	NA
supramarginal	NA	NA	NA	NA	NA	NA
<b>C. Surface Area</b>						
bankssts	0.30	0.014	0.027	0.29	0.015	0.029
fusiform	0.14	0.24	0.24	0.20	0.084	0.096
inferiorparietal	0.35	0.0018	0.0072	0.39	< 0.001	0.0023
middletemporal	0.22	0.062	0.083	0.23	0.050	0.081
parsopercularis	0.21	0.078	0.089	0.21	0.072	0.096
parstriangularis	0.39	< 0.001	0.0046	0.39	< 0.001	0.0023
superiortemporal	0.30	0.011	0.027	0.30	0.010	0.027
supramarginal	0.26	0.030	0.049	0.20	0.097	0.097
<b>D. Mean Diffusivity</b>						
Arcuate fasc.*	-0.22	0.033	NA	0.03	0.65	NA
*averaged across $p_{FWE} < 0.05$ significant nodes						

<b>Supplementary Table 4. Contributions of outcomes to linear mixed effects model</b>						
Brain Region/Tract	Main Effect			Interaction		
A. Gray Matter Volume	Effect size	p	pFDR	Effect size	p	pFDR
bankssts	$1.8 \times 10^{+01}$	< 0.001	0.0044	$-1.1 \times 10^{+00}$	0.52	0.90
fusiform	$1.1 \times 10^{+01}$	0.52	0.52	$-7.4 \times 10^{-01}$	0.87	0.90
inferiorparietal	$4.0 \times 10^{+01}$	0.073	0.14	$3.1 \times 10^{+00}$	0.58	0.90
middletemporal	$2.9 \times 10^{+01}$	0.066	0.14	$-6.7 \times 10^{-01}$	0.90	0.90
parsopercularis	$1.7 \times 10^{+01}$	0.14	0.19	$-7.1 \times 10^{-01}$	0.82	0.90
parstriangularis	$8.3 \times 10^{+00}$	0.21	0.24	$2.4 \times 10^{+00}$	0.18	0.90
superiortemporal	$3.4 \times 10^{+01}$	0.087	0.14	$-3.2 \times 10^{+00}$	0.62	0.90
supramarginal	$4.5 \times 10^{+01}$	0.014	0.055	$-2.3 \times 10^{+00}$	0.70	0.90
<b>B. White Matter Volume</b>						
bankssts	$3.3 \times 10^{+00}$	0.33	0.37	$1.9 \times 10^{+00}$	0.18	0.18
fusiform	$-1.0 \times 10^{+01}$	0.35	0.37	$7.3 \times 10^{+00}$	0.015	0.017
inferiorparietal	$-2.9 \times 10^{+01}$	0.027	0.13	$2.0 \times 10^{+01}$	< 0.001	< 0.001
middletemporal	$-1.8 \times 10^{+01}$	0.092	0.17	$9.9 \times 10^{+00}$	0.0017	0.0035
parsopercularis	$-9.8 \times 10^{+00}$	0.050	0.13	$5.0 \times 10^{+00}$	0.0054	0.0072
parstriangularis	$-7.2 \times 10^{+00}$	0.11	0.17	$5.5 \times 10^{+00}$	< 0.001	< 0.001
superiortemporal	$-2.3 \times 10^{+01}$	0.033	0.13	$1.3 \times 10^{+01}$	< 0.001	< 0.001
supramarginal	$-1.1 \times 10^{+01}$	0.37	0.37	$1.2 \times 10^{+01}$	0.0049	0.0072
<b>C. Surface Area</b>						
bankssts	$4.9 \times 10^{+00}$	0.0078	0.062	$-2.1 \times 10^{-02}$	0.97	0.97
fusiform	$1.4 \times 10^{+00}$	0.73	0.73	$1.0 \times 10^{+00}$	0.35	0.56
inferiorparietal	$9.4 \times 10^{+00}$	0.21	0.42	$3.2 \times 10^{+00}$	0.11	0.43
middletemporal	$3.0 \times 10^{+00}$	0.55	0.62	$1.4 \times 10^{+00}$	0.29	0.56
parsopercularis	$1.6 \times 10^{+00}$	0.45	0.60	$4.8 \times 10^{-01}$	0.53	0.70
parstriangularis	$1.9 \times 10^{+00}$	0.20	0.42	$1.1 \times 10^{+00}$	0.026	0.21
superiortemporal	$4.5 \times 10^{+00}$	0.35	0.56	$1.8 \times 10^{+00}$	0.22	0.56
supramarginal	$1.4 \times 10^{+01}$	0.019	0.076	$-7.2 \times 10^{-01}$	0.71	0.81
<b>D. Mean Diffusivity</b>						
Arcuate fasc.*	$-2.4 \times 10^{-06}$	0.0092	NA	< 0.001	0.0069	NA
*averaged across $p_{FWE} < 0.05$ significant nodes						

<b>Supplementary Table 5. Brain-behavior associations controlling for TIV</b>				
Brain Region	Measure-Curve Feature	r	p	pFDR
bankssts	GMV-intercept	0.37	0.0021	0.017
fusiform	WMV-slope	0.21	0.068	0.11
inferiorparietal	WMV-slope	0.41	< 0.001	0.0022
middletemporal	WMV-slope	0.23	0.050	0.10
parsopercularis	WMV-slope	0.19	0.11	0.14
parstriangularis	WMV-slope	0.35	0.0030	0.012
superiortemporal	WMV-slope	0.23	0.046	0.10
supramarginal	WMV-slope	0.15	0.19	0.22
inferiorparietal	SA-intercept	0.31	0.0067	0.027
parstriangularis	SA-intercept	0.35	0.0024	0.019
superiortemporal	SA-intercept	0.26	0.029	0.075
inferiorparietal	SA-slope	0.20	0.092	0.37
parstriangularis	SA-slope	0.24	0.043	0.34
superiortemporal	SA-slope	0.01	0.96	0.99
TIV, total intracranial volume				

<b>Supplementary Table 6. Brain-behavior associations controlling for Euler numbers</b>				
Brain Region	Measure-Curve Feature	r	p	pFDR
bankssts	GMV-intercept	0.38	0.0013	0.011
fusiform	WMV-slope	0.33	0.0037	0.0049
inferiorparietal	WMV-slope	0.50	< 0.001	< 0.001
middletemporal	WMV-slope	0.36	0.0016	0.0031
parsopercularis	WMV-slope	0.30	0.0089	0.010
parstriangularis	WMV-slope	0.46	< 0.001	< 0.001
superiortemporal	WMV-slope	0.38	< 0.001	0.0016
supramarginal	WMV-slope	0.33	0.0034	0.0049
inferiorparietal	SA-intercept	0.32	0.0053	0.021
parstriangularis	SA-intercept	0.36	0.0017	0.014
superiortemporal	SA-intercept	0.28	0.016	0.042
inferiorparietal	SA-slope	0.33	0.0031	0.013
parstriangularis	SA-slope	0.37	0.0012	0.0097
superiortemporal	SA-slope	0.27	0.019	0.050

<b>Supplementary Table 7. Associations between brain measures and literacy-related and cognitive (sub)skills</b>										
Brain Region/Tract	Measure-Curve Feature	Phonological processing			Oral language			Nonverbal general cognitive ability		
		r	p	pFDR	r	p	pFDR	r	p	pFDR
bankssts	GMV-intercept	0.56	< 0.001	0.0011	0.17	0.22	0.47	0.09	0.54	0.76
fusiform	WMV-slope	0.39	0.0063	0.020	0.13	0.34	0.40	0.18	0.19	0.29
inferiorparietal	WMV-slope	0.63	< 0.001	< 0.001	0.28	0.044	0.12	0.09	0.53	0.55
middletemporal	WMV-slope	0.50	< 0.001	0.0024	0.20	0.17	0.29	0.14	0.30	0.40
parsopercularis	WMV-slope	0.41	0.0045	0.018	0.16	0.25	0.37	0.25	0.073	0.17
parstriangularis	WMV-slope	0.50	< 0.001	0.0024	0.15	0.28	0.40	0.21	0.13	0.25
superiortemporal	WMV-slope	0.56	< 0.001	< 0.001	0.14	0.33	0.40	0.13	0.36	0.40
supramarginal	WMV-slope	0.44	0.0022	0.010	0.09	0.52	0.55	0.24	0.083	0.18
inferiorparietal	SA-intercept	0.38	0.0089	0.054	0.00	1.00	0.99	0.07	0.60	0.66
parstriangularis	SA-intercept	0.41	0.0038	0.045	0.25	0.077	0.18	0.26	0.057	0.15
superiortemporal	SA-intercept	0.39	0.0067	0.054	0.19	0.18	0.39	0.30	0.027	0.096
inferiorparietal	SA-slope	0.45	0.0014	0.019	0.22	0.12	0.25	0.00	1.00	1.00
parstriangularis	SA-slope	0.43	0.0023	0.019	0.30	0.032	0.13	0.24	0.086	0.25
superiortemporal	SA-slope	0.41	0.0041	0.025	0.16	0.27	0.37	0.17	0.21	0.35
Arcuate fasc.*	MD-slope	0.24	0.015	NA	ns	ns	NA	ns	ns	NA

\*averaged across  $p_{FWE} < 0.05$  significant nodes; ns indicates no nodes were significant after FWE correction

<b>Supplementary Table 8. Contributions of literacy-related covariates to growth curves</b>					
		FHD		HLE	
Brain Region/Tract	Measure	Effect size	p	Effect size	p
bankssts	GMV	$6.8 \times 10^{+01}$	0.59	$2.2 \times 10^{+02}$	0.17
fusiform	WMV	$1.0 \times 10^{+02}$	0.51	$1.4 \times 10^{+02}$	0.48
inferiorparietal	WMV	$-1.1 \times 10^{+02}$	0.67	$3.9 \times 10^{+02}$	0.25
middletemporal	WMV	$-8.4 \times 10^{+01}$	0.65	$5.5 \times 10^{+02}$	0.021
parsopercularis	WMV	$7.0 \times 10^{+01}$	0.42	$9.6 \times 10^{+00}$	0.93
parstriangularis	WMV	$1.9 \times 10^{+02}$	0.025	$-3.0 \times 10^{+01}$	0.79
superiortemporal	WMV	$3.4 \times 10^{+01}$	0.86	$1.8 \times 10^{+02}$	0.48
supramarginal	WMV	$-2.7 \times 10^{+02}$	0.32	$3.5 \times 10^{+02}$	0.32
inferiorparietal	SA	$1.0 \times 10^{+01}$	0.95	$2.2 \times 10^{+02}$	0.28
parstriangularis	SA	$8.2 \times 10^{+01}$	0.031	$5.3 \times 10^{+00}$	0.92
superiortemporal	SA	$6.5 \times 10^{+01}$	0.51	$1.0 \times 10^{+02}$	0.42
Arcuate fasc.	MD	ns	ns	ns	ns
FHD, family history of reading difficulty					
HLE, home literacy environment					
ns indicates no nodes were significant after FWE correction					

<b>Supplementary Table 9. Comparison of Linear Mixed Effects Models with versus without Literacy-Related Covariates</b>				
Brain Region/Tract	Measure	without covariate	with covariate	p
<b>A. Family history of reading difficulty</b>				
bankssts	GMV	<b>2328.2</b>	2332.5	0.37
fusiform	WMV	<b>2505.3</b>	2509.9	0.51
inferiorparietal	WMV	<b>2670.1</b>	2675.0	0.67
middletemporal	WMV	<b>2496.7</b>	2501.6	0.66
parsopercularis	WMV	<b>2311.7</b>	2315.9	0.34
parstriangularis	WMV	<b>2274.7</b>	2275.0	0.028
superiortemporal	WMV	<b>2530.3</b>	2535.3	0.86
supramarginal	WMV	<b>2647.6</b>	2651.3	0.24
inferiorparietal	SA	<b>2451.3</b>	2456.4	0.97
parstriangularis	SA	<b>2012.9</b>	2013.6	0.036
superiortemporal	SA	<b>2354.4</b>	2359.0	0.50
Arcuate fasc.	MD	<b>-3358.7</b>	-3354.7	0.26
<b>B. Home literacy Environment</b>				
bankssts	GMV	<b>2328.2</b>	2331.4	0.17
fusiform	WMV	<b>2505.3</b>	2509.9	0.49
inferiorparietal	WMV	<b>2670.1</b>	2673.9	0.25
middletemporal	WMV	2496.7	<b>2496.4</b>	0.021
parsopercularis	WMV	<b>2311.7</b>	2316.8	0.93
parstriangularis	WMV	<b>2274.7</b>	2279.7	0.79
superiortemporal	WMV	<b>2530.3</b>	2534.8	0.48
supramarginal	WMV	<b>2647.6</b>	2651.8	0.32
inferiorparietal	SA	<b>2451.3</b>	2455.3	0.29
parstriangularis	SA	<b>2012.9</b>	2018.0	0.92
superiortemporal	SA	<b>2354.4</b>	2358.8	0.42
Arcuate fasc.	MD	<b>-3358.7</b>	-3353.4	1.00
Bold indicates lower BIC value				

<b>Supplementary Table 10. Indirect effects between brain structure and decoding via phonological processing</b>					
Brain Region/Tract	Measure-Curve Feature	Effect size	Lower CI	Upper CI	p
bankssts	GMV-intercept	$1.7 \times 10^{-02}$	$3.4 \times 10^{-03}$	$3.8 \times 10^{-02}$	0.011
fusiform	WMV-slope	$6.8 \times 10^{-03}$	$-1.0 \times 10^{-03}$	$1.9 \times 10^{-02}$	0.094
inferiorparietal	WMV-slope	$9.1 \times 10^{-03}$	$5.5 \times 10^{-04}$	$2.2 \times 10^{-02}$	0.032
middletemporal	WMV-slope	$9.4 \times 10^{-03}$	$6.1 \times 10^{-04}$	$2.3 \times 10^{-02}$	0.034
parsopercularis	WMV-slope	$2.0 \times 10^{-02}$	$3.0 \times 10^{-03}$	$4.1 \times 10^{-02}$	0.016
parstriangularis	WMV-slope	$2.2 \times 10^{-02}$	$2.8 \times 10^{-03}$	$4.9 \times 10^{-02}$	0.016
superiortemporal	WMV-slope	$8.3 \times 10^{-03}$	$7.8 \times 10^{-04}$	$2.2 \times 10^{-02}$	0.020
supramarginal	WMV-slope	$5.0 \times 10^{-03}$	$-1.3 \times 10^{-03}$	$1.3 \times 10^{-02}$	0.12
inferiorparietal	SA-intercept	$8.5 \times 10^{-03}$	$-9.7 \times 10^{-04}$	$1.5 \times 10^{-02}$	0.088
parstriangularis	SA-intercept	$4.6 \times 10^{-02}$	$2.3 \times 10^{-03}$	$1.0 \times 10^{-01}$	0.036
superiortemporal	SA-intercept	$1.6 \times 10^{-02}$	$-1.9 \times 10^{-03}$	$3.6 \times 10^{-02}$	0.083
inferiorparietal	SA-slope	$2.3 \times 10^{-02}$	$2.0 \times 10^{-03}$	$5.9 \times 10^{-02}$	0.024
parstriangularis	SA-slope	$7.4 \times 10^{-02}$	$3.7 \times 10^{-03}$	$1.8 \times 10^{-01}$	0.034
superiortemporal	SA-slope	$1.8 \times 10^{-02}$	$-3.8 \times 10^{-03}$	$4.6 \times 10^{-02}$	0.11
Arcuate fasc.*	MD-slope	$2.6 \times 10^{+05}$	$6.8 \times 10^{+04}$	$6.2 \times 10^{+05}$	0.014
*averaged across $p_{FWE} < 0.05$ significant nodes					

**Supplementary Table 11. Indirect effects between brain structure and word reading via phonological processing**

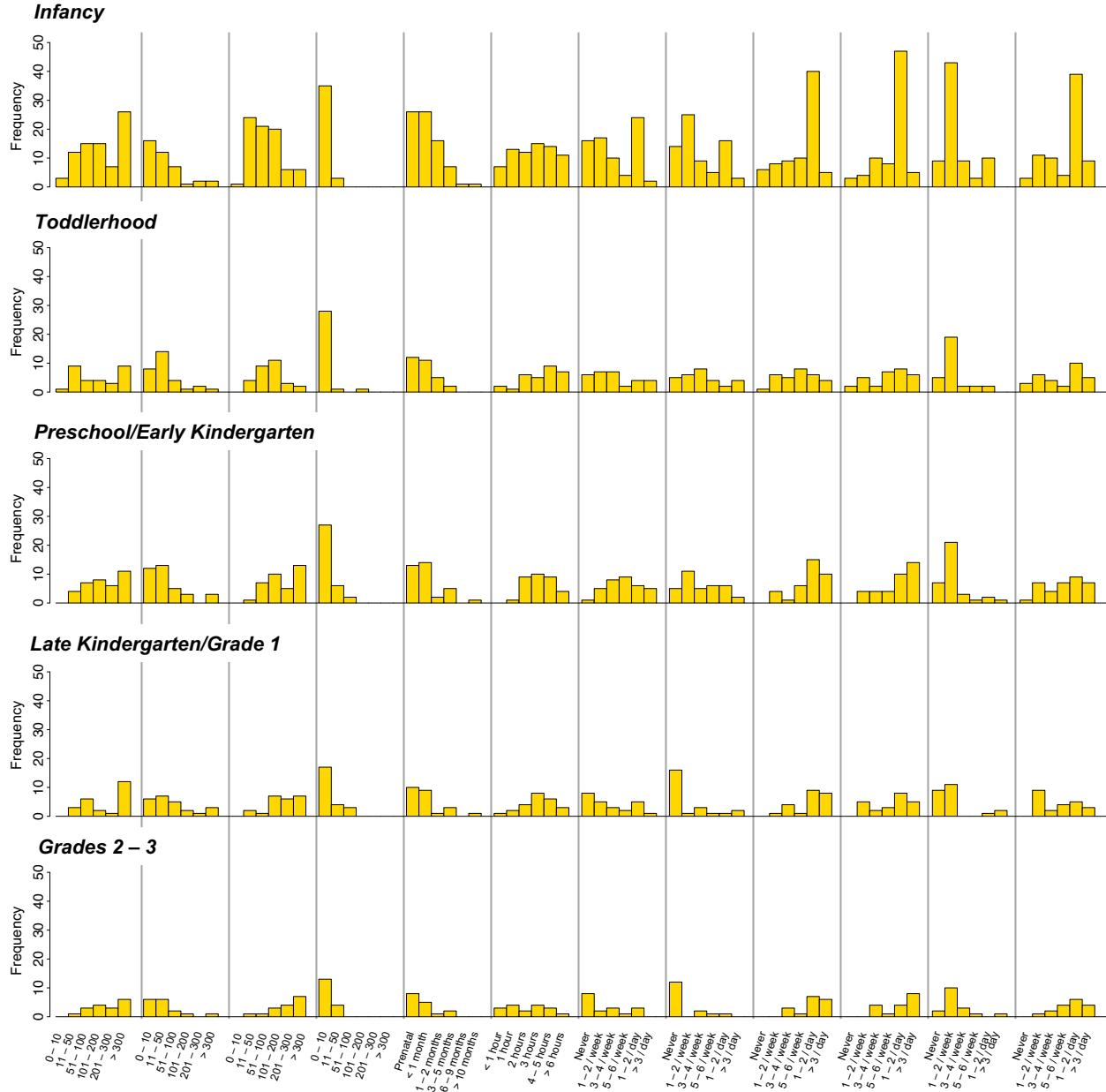
Brain Region/Tract	Measure-Curve Feature	Effect size	Lower CI	Upper CI	p
bankssts	GMV-intercept	$2.6 \times 10^{-02}$	$9.2 \times 10^{-03}$	$5.4 \times 10^{-02}$	< 0.001
fusiform	WMV-slope	$9.7 \times 10^{-03}$	$-1.3 \times 10^{-03}$	$2.5 \times 10^{-02}$	0.083
inferiorparietal	WMV-slope	$1.4 \times 10^{-02}$	$2.7 \times 10^{-03}$	$3.2 \times 10^{-02}$	0.0070
middletemporal	WMV-slope	$1.4 \times 10^{-02}$	$1.6 \times 10^{-03}$	$3.3 \times 10^{-02}$	0.026
parsopercularis	WMV-slope	$2.9 \times 10^{-02}$	$6.2 \times 10^{-03}$	$5.8 \times 10^{-02}$	0.011
parstriangularis	WMV-slope	$3.4 \times 10^{-02}$	$6.9 \times 10^{-03}$	$7.2 \times 10^{-02}$	0.013
superiortemporal	WMV-slope	$1.3 \times 10^{-02}$	$3.2 \times 10^{-03}$	$3.2 \times 10^{-02}$	0.0042
supramarginal	WMV-slope	$7.1 \times 10^{-03}$	$-1.6 \times 10^{-03}$	$1.8 \times 10^{-02}$	0.10
inferiorparietal	SA-intercept	$1.2 \times 10^{-02}$	$3.8 \times 10^{-04}$	$2.1 \times 10^{-02}$	0.045
parstriangularis	SA-intercept	$6.6 \times 10^{-02}$	$3.3 \times 10^{-03}$	$1.4 \times 10^{-01}$	0.041
superiortemporal	SA-intercept	$2.6 \times 10^{-02}$	$3.1 \times 10^{-03}$	$4.9 \times 10^{-02}$	0.026
inferiorparietal	SA-slope	$3.7 \times 10^{-02}$	$7.1 \times 10^{-03}$	$8.6 \times 10^{-02}$	0.013
parstriangularis	SA-slope	$1.1 \times 10^{-01}$	$5.3 \times 10^{-03}$	$2.5 \times 10^{-01}$	0.039
superiortemporal	SA-slope	$3.1 \times 10^{-02}$	$-3.0 \times 10^{-04}$	$6.6 \times 10^{-02}$	0.052
Arcuate fasc.*	MD-slope	$3.1 \times 10^{+05}$	$7.0 \times 10^{+04}$	$6.8 \times 10^{+05}$	0.020

\*averaged across  $p_{FWE} < 0.05$  significant nodes

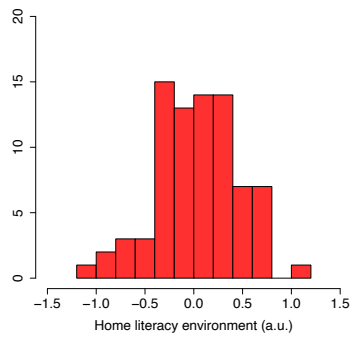
<b>Supplementary Table 12. Indirect effects between brain and decoding via phonological processing controlling for TIV</b>					
Brain Region	Measure-Curve Feature	Effect size	Lower CI	Upper CI	p
bankssts	GMV-intercept	$1.7 \times 10^{-02}$	$3.2 \times 10^{-03}$	$3.8 \times 10^{-02}$	0.010
fusiform	WMV-slope	$3.5 \times 10^{-03}$	$-4.6 \times 10^{-03}$	$1.6 \times 10^{-02}$	0.37
inferiorparietal	WMV-slope	$8.5 \times 10^{-03}$	$-1.5 \times 10^{-05}$	$2.5 \times 10^{-02}$	0.051
middletemporal	WMV-slope	$7.1 \times 10^{-03}$	$-3.1 \times 10^{-03}$	$2.3 \times 10^{-02}$	0.16
parsopercularis	WMV-slope	$1.4 \times 10^{-02}$	$-5.3 \times 10^{-04}$	$3.7 \times 10^{-02}$	0.065
parstriangularis	WMV-slope	$1.7 \times 10^{-02}$	$-1.7 \times 10^{-03}$	$4.6 \times 10^{-02}$	0.085
superiortemporal	WMV-slope	$7.7 \times 10^{-03}$	$-5.2 \times 10^{-04}$	$2.2 \times 10^{-02}$	0.079
supramarginal	WMV-slope	$2.2 \times 10^{-03}$	$-5.9 \times 10^{-03}$	$1.1 \times 10^{-02}$	0.56
inferiorparietal	SA-intercept	$8.4 \times 10^{-03}$	$-1.2 \times 10^{-03}$	$1.5 \times 10^{-02}$	0.10
parstriangularis	SA-intercept	$4.5 \times 10^{-02}$	$1.6 \times 10^{-03}$	$1.1 \times 10^{-01}$	0.039
superiortemporal	SA-intercept	$1.6 \times 10^{-02}$	$-3.4 \times 10^{-03}$	$3.7 \times 10^{-02}$	0.10
inferiorparietal	SA-slope	$1.8 \times 10^{-02}$	$-1.4 \times 10^{-03}$	$5.9 \times 10^{-02}$	0.078
parstriangularis	SA-slope	$5.2 \times 10^{-02}$	$-1.2 \times 10^{-02}$	$1.7 \times 10^{-01}$	0.14
superiortemporal	SA-slope	$8.3 \times 10^{-03}$	$-3.1 \times 10^{-02}$	$4.3 \times 10^{-02}$	0.67

<b>Supplementary Table 13. Indirect effects between brain and word reading via phonological processing controlling for TIV</b>					
Brain Region	Measure-Curve Feature	Effect size	Lower CI	Upper CI	p
bankssts	GMV-intercept	$2.6 \times 10^{-02}$	$8.4 \times 10^{-03}$	$5.3 \times 10^{-02}$	0.0017
fusiform	WMV-slope	$5.0 \times 10^{-03}$	$-6.6 \times 10^{-03}$	$2.0 \times 10^{-02}$	0.38
inferiorparietal	WMV-slope	$1.3 \times 10^{-02}$	$1.4 \times 10^{-03}$	$3.3 \times 10^{-02}$	0.020
middletemporal	WMV-slope	$1.0 \times 10^{-02}$	$-4.9 \times 10^{-03}$	$3.2 \times 10^{-02}$	0.15
parsopercularis	WMV-slope	$2.1 \times 10^{-02}$	$-8.0 \times 10^{-04}$	$4.9 \times 10^{-02}$	0.060
parstriangularis	WMV-slope	$2.6 \times 10^{-02}$	$-3.8 \times 10^{-03}$	$6.3 \times 10^{-02}$	0.093
superiortemporal	WMV-slope	$1.2 \times 10^{-02}$	$-2.4 \times 10^{-04}$	$3.2 \times 10^{-02}$	0.056
supramarginal	WMV-slope	$2.9 \times 10^{-03}$	$-8.7 \times 10^{-03}$	$1.4 \times 10^{-02}$	0.57
inferiorparietal	SA-intercept	$1.2 \times 10^{-02}$	$-6.5 \times 10^{-05}$	$2.1 \times 10^{-02}$	0.051
parstriangularis	SA-intercept	$6.6 \times 10^{-02}$	$2.5 \times 10^{-03}$	$1.4 \times 10^{-01}$	0.042
superiortemporal	SA-intercept	$2.6 \times 10^{-02}$	$5.2 \times 10^{-04}$	$5.1 \times 10^{-02}$	0.047
inferiorparietal	SA-slope	$2.8 \times 10^{-02}$	$-1.3 \times 10^{-03}$	$8.5 \times 10^{-02}$	0.061
parstriangularis	SA-slope	$7.2 \times 10^{-02}$	$-2.6 \times 10^{-02}$	$2.2 \times 10^{-01}$	0.17
superiortemporal	SA-slope	$1.4 \times 10^{-02}$	$-4.3 \times 10^{-02}$	$6.4 \times 10^{-02}$	0.60

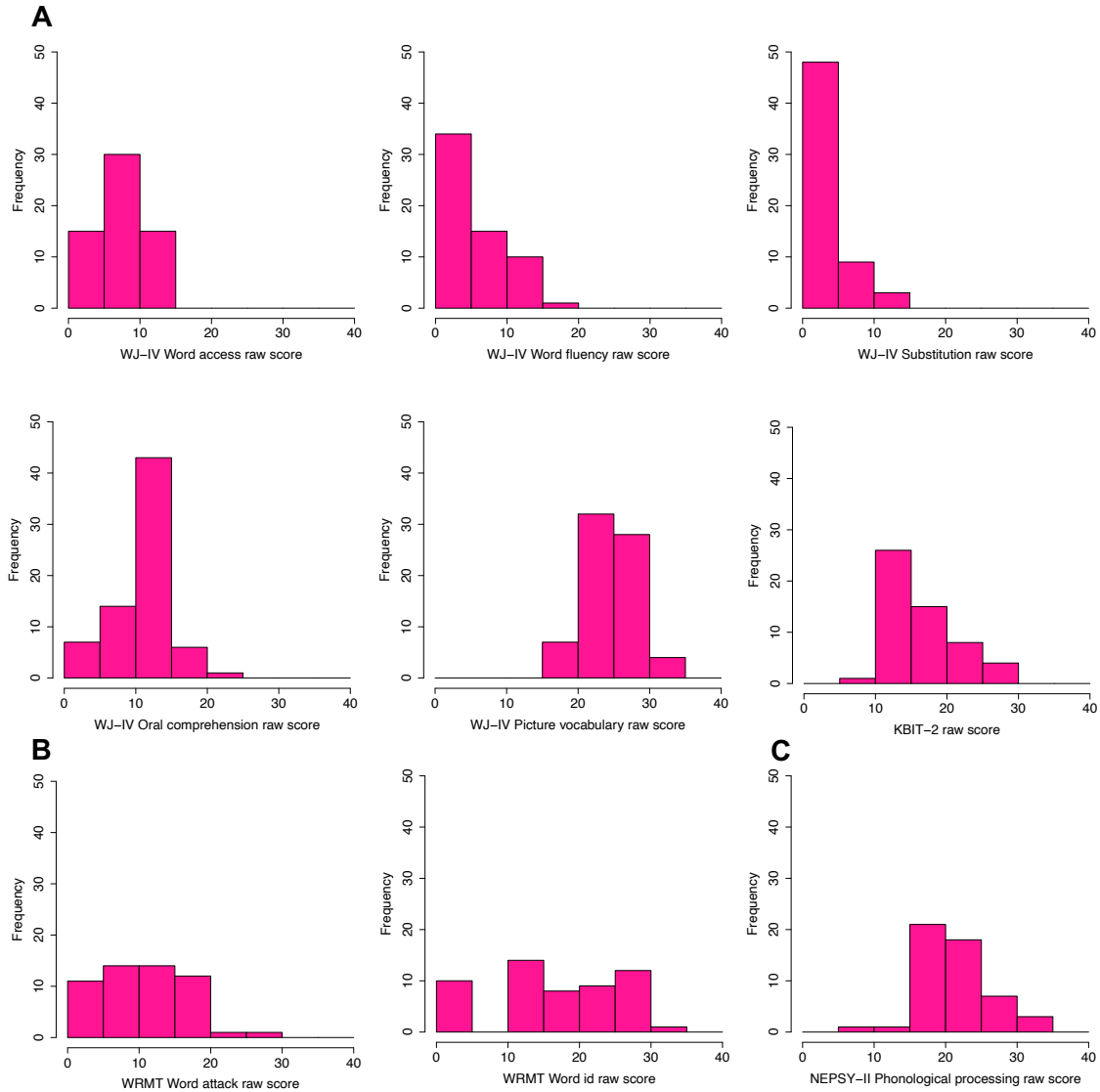
## Supplementary Figures



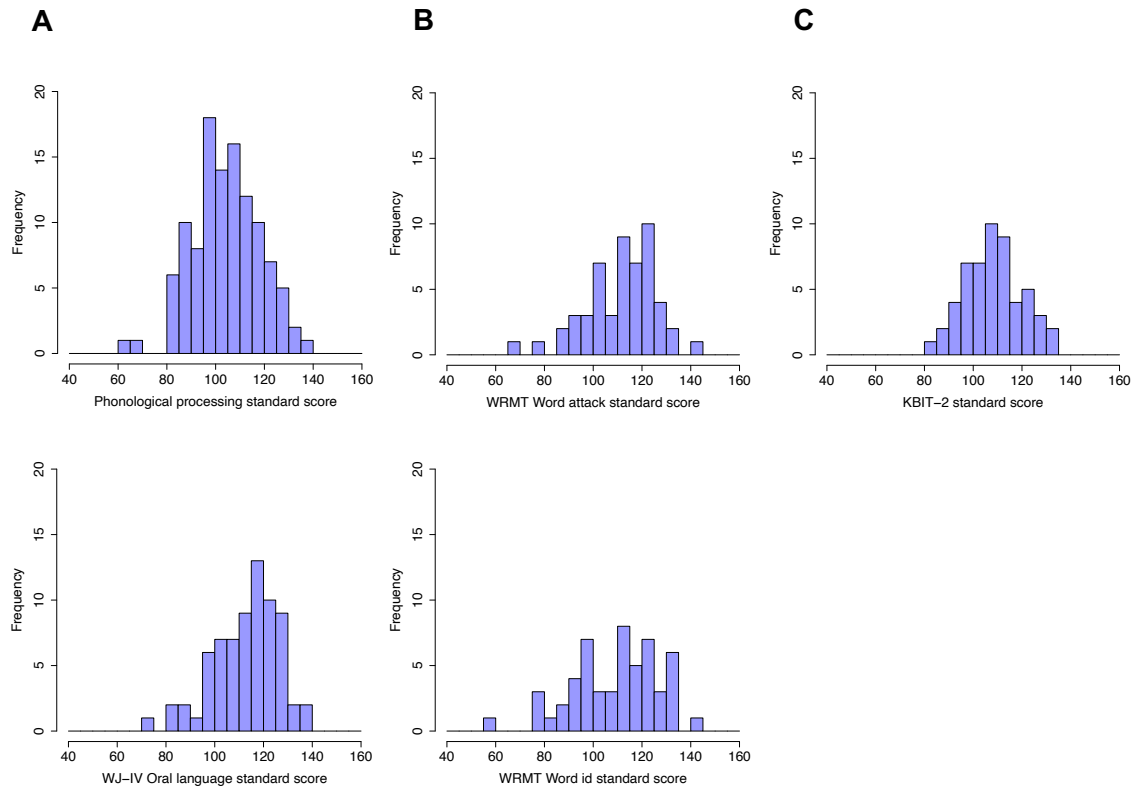
**Supplementary Figure 1.** Distribution of home literacy environment variables. Histograms depict the distribution of home literacy environment questionnaire responses across five developmental timepoints. New England data only, as these data were not collected in the Calgary dataset.



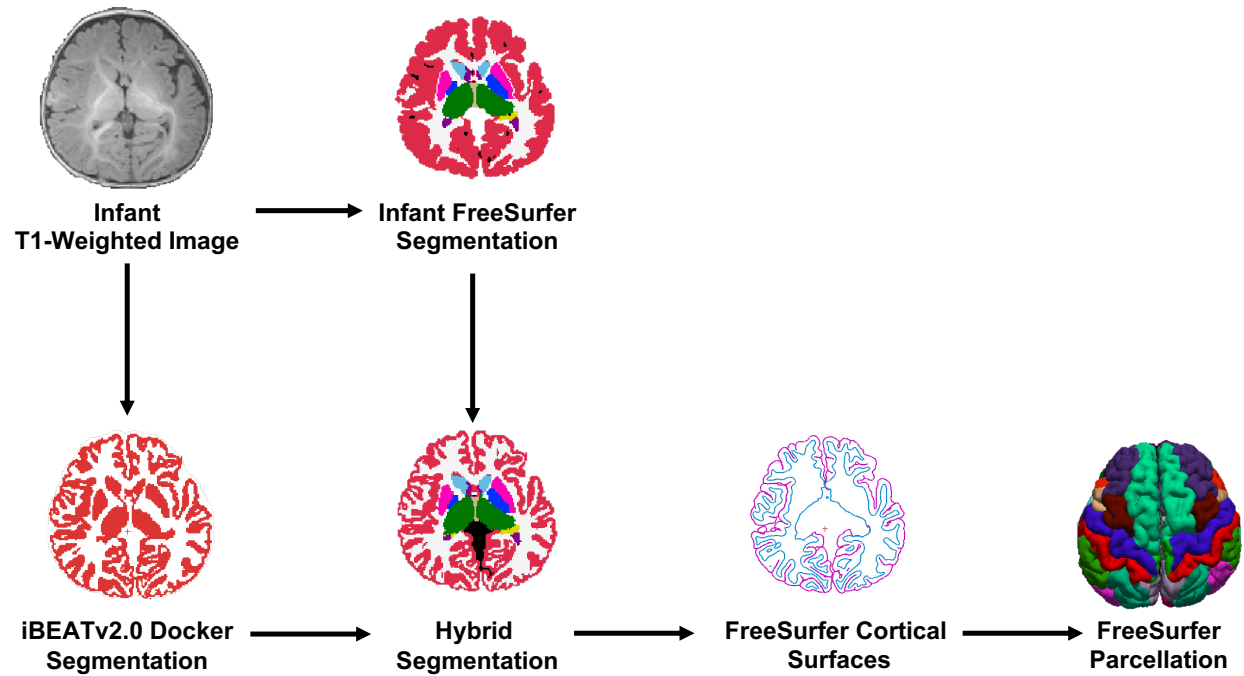
**Supplementary Figure 2.** Distribution of home literacy environment scores. Histogram depicts the distribution of home literacy environment scores normalized from the responses shown in Supplementary Figure 1. New England data only, as these data were not collected in the Calgary dataset.



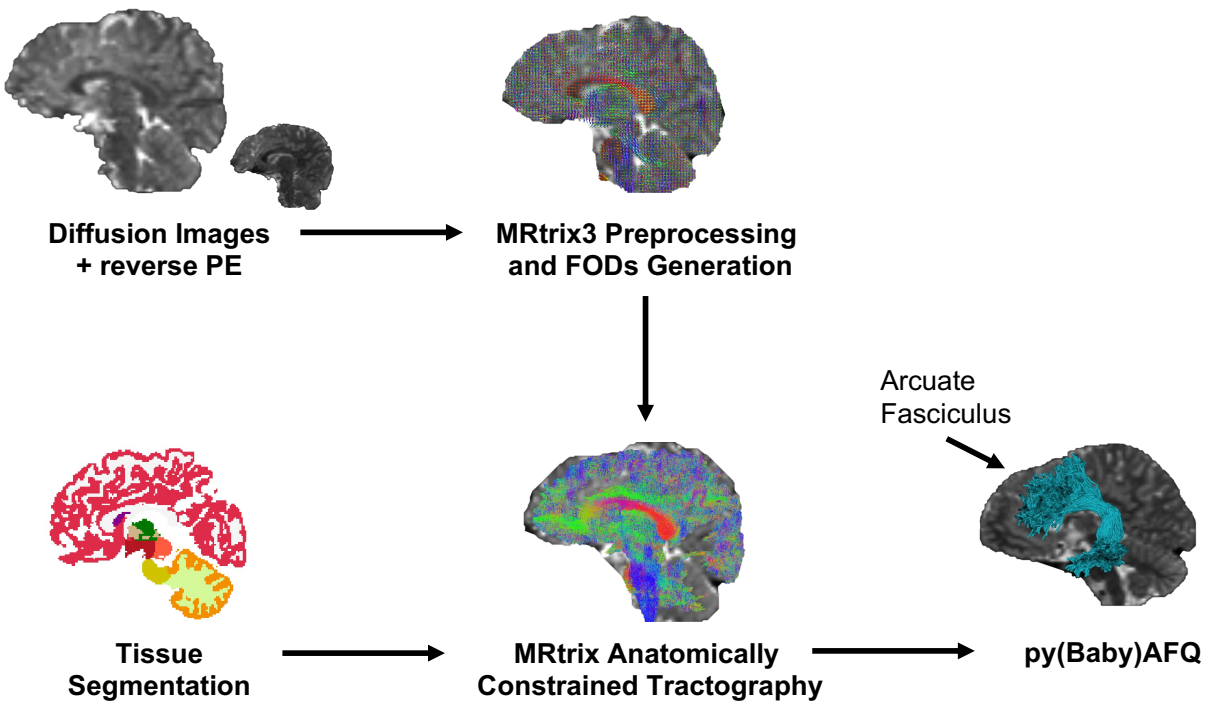
**Supplementary Figure 3.** Distribution of raw literacy-related outcomes. Histograms depict the distributions of New England data for (A) subtests constituting phonological processing and oral language composite scores and KBIT-2, and (B) word ID and word attack assessments. (C) Histogram for raw phonological processing scores from the Calgary dataset. WJ-IV, Woodcock-Johnson edition IV; KBIT-2, Kaufman Brief Intelligence Test edition 2; WRMT, Woodcock Reading Mastery Tests; NEPSY-II, Neuropsychological Assessment.



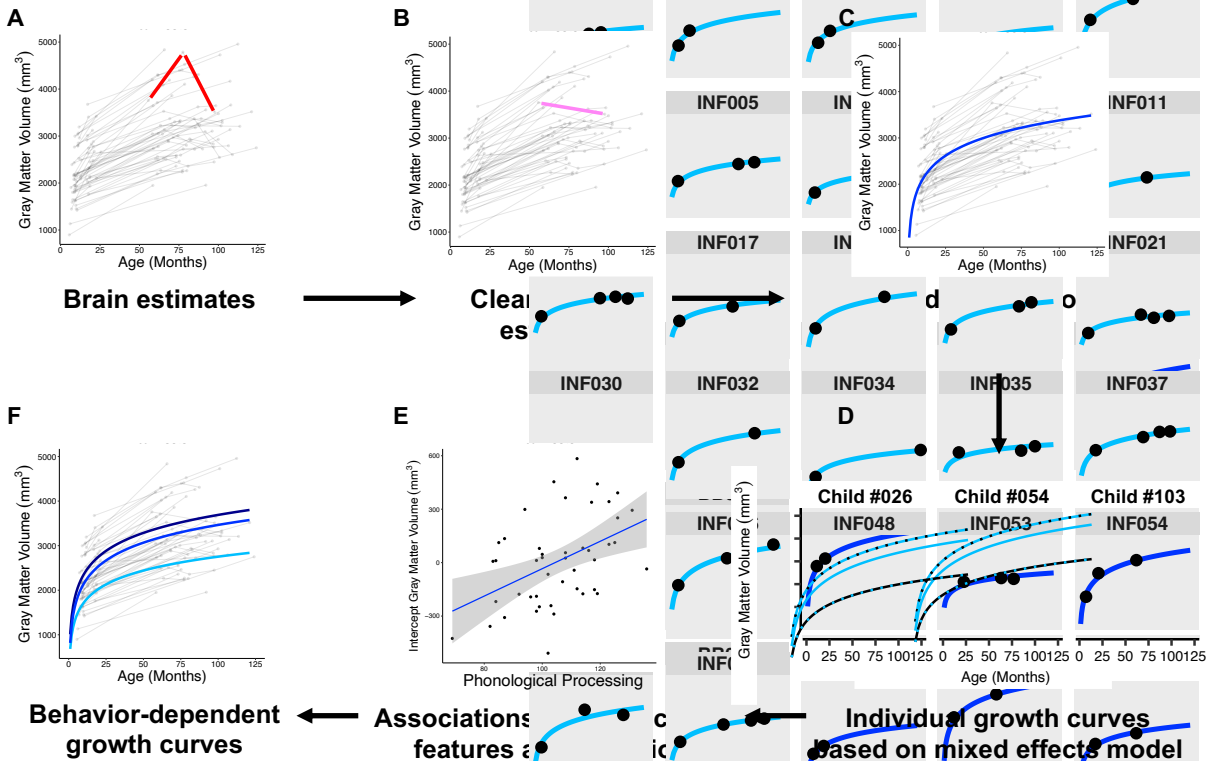
**Supplementary Figure 4.** Distribution of standardized literacy-related outcomes. Histograms depict the distributions of for (A) literacy-related subskills, (B) decoding/word reading assessments and (C) nonverbal general cognitive abilities. Phonological processing scores sum WJ-IV estimates from the New England dataset and NEPSY-II estimates from the Calgary dataset. WJ-IV, Woodcock-Johnson edition IV; NEPSY-II, Neuropsychological Assessment; WRMT, Woodcock Reading Mastery Tests; KBIT-2, Kaufman Brief Intelligence Test edition 2.



**Supplementary Figure 5.** Infant Structural Processing Pipeline Overview. Raw images without visual artifacts were processed using a combination of iBEATv2.0 Docker, Infant FreeSurfer, FreeSurfer, and in-house scripts. Cortical surfaces were visually inspected for tissue classification accuracy (please see Methods section for details).

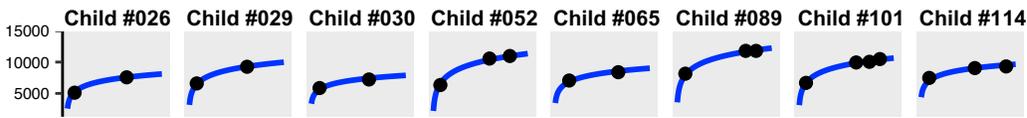


**Supplementary Figure 6.** Diffusion Processing Pipeline Overview. Diffusion data were denoised and then corrected for susceptibility distortions, eddy currents, head motion, and intensity inhomogeneity using MRtrix with FSL and ANTs implementations. Fiber orientation densities (FODs) were generated using constrained spherical deconvolution. Fibers were tracked with Anatomically Constrained Tractography, which leveraged the tissue segmentations from the structural processing pipeline (Supplementary Figure 1): the hybrid segmentation for brains < 50 months and the standard FreeSurfer segmentation for brains > 50 months. Fibers were segmented into tracts using pyBabyAFQ for brains  $\leq$  24 months and pyAFQ for brains > 50 months (the left arcuate fasciculus is depicted as an example). PE, phase encoding.

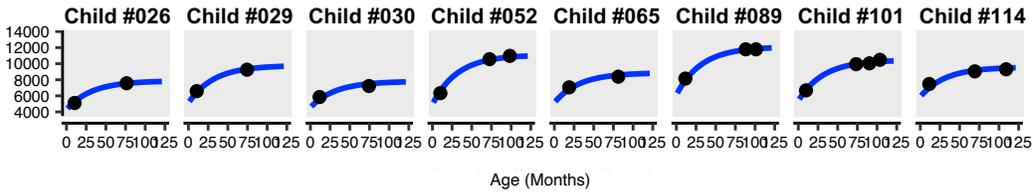


**Supplementary Figure 7. Statistical Analysis Overview.** (A, B) Structural and diffusion brain estimates for regions and tracts of interest are first cleaned to remove observations with annual changes that are not neurophysiologically plausible (example inter-observation segments in red); remaining observations are then bridged (pink segment). Please see Methods for determining whether to remove the estimate preceding or following the problematic annual change. (C) Mixed effects models, here using logarithmic functions and random intercept and slope terms, were used to generate (D) individual growth curves. (E) Brain-behavior associations were tested using curve features (i.e., random intercepts and slopes). (F) Individual growth curves for measures and regions/tracts with significant brain-behavior associations were divided into low (< 85, dotted line), average (85 – 115, solid line), and high (> 115, dashed line) behavioral performance, meaned within groups, and plotted.

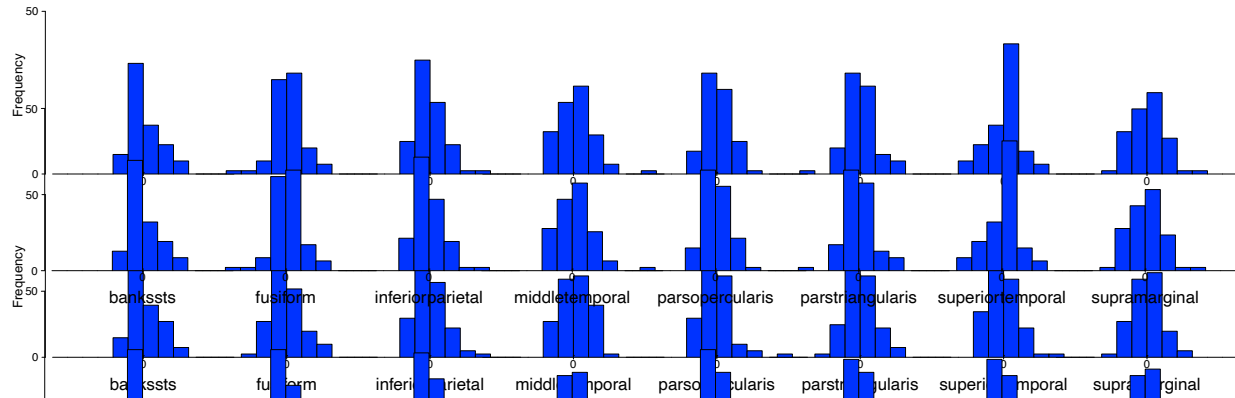
### Linear model with logarithmic function



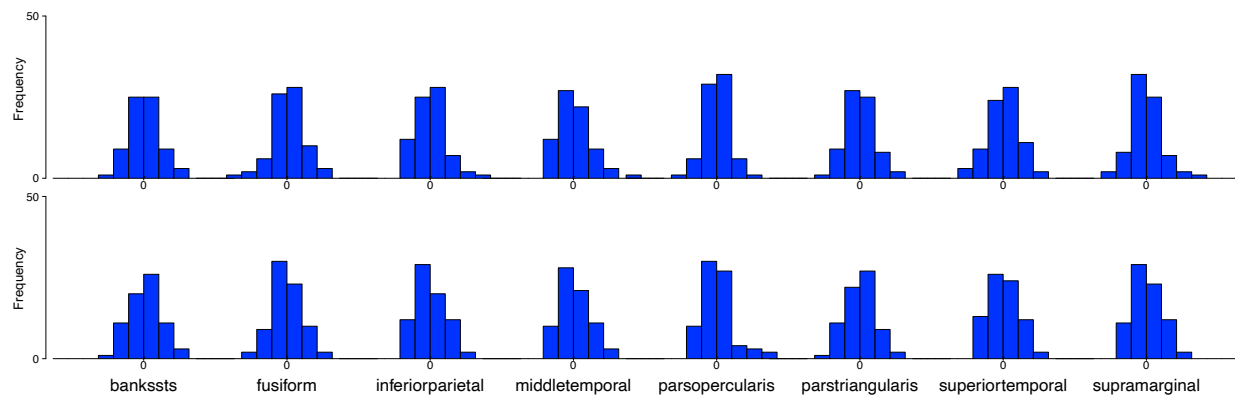
### Nonlinear model with asymptotic function



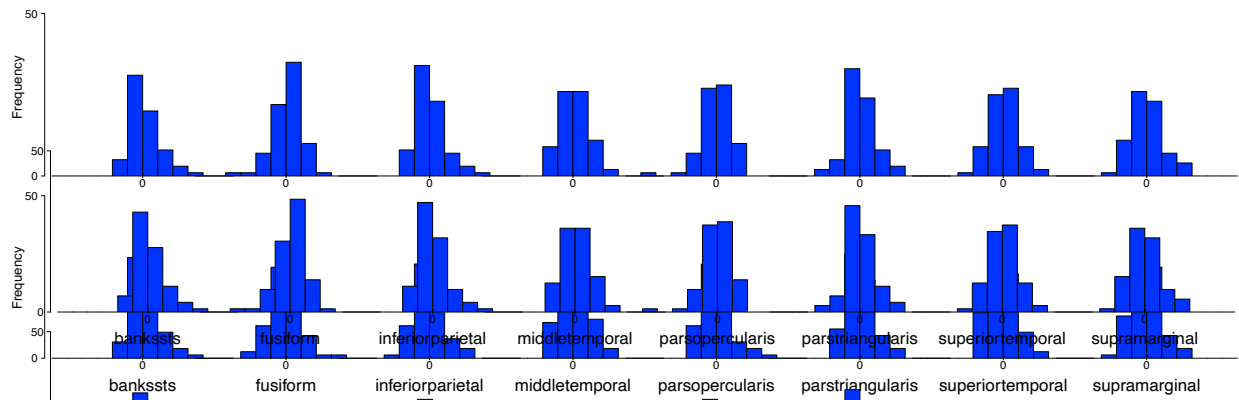
**Supplementary Figure 8.** Individual growth curves for inferior parietal white matter in a subset of participants. Projected longitudinal trajectories (blue lines) show close fits to raw brain estimates (black dots) for both linear and nonlinear models.



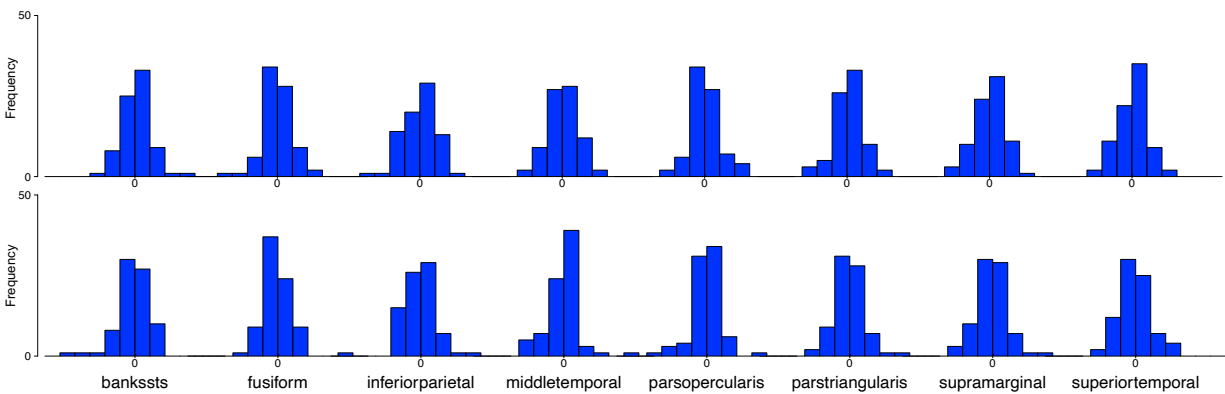
**Supplementary Figure 9.** Distribution of curve features of gray matter volume. Top row depicts histograms for curve intercepts. Bottom row depicts histograms for curve slopes. Brain estimates were scaled for visualization purposes, but skewness was not altered.



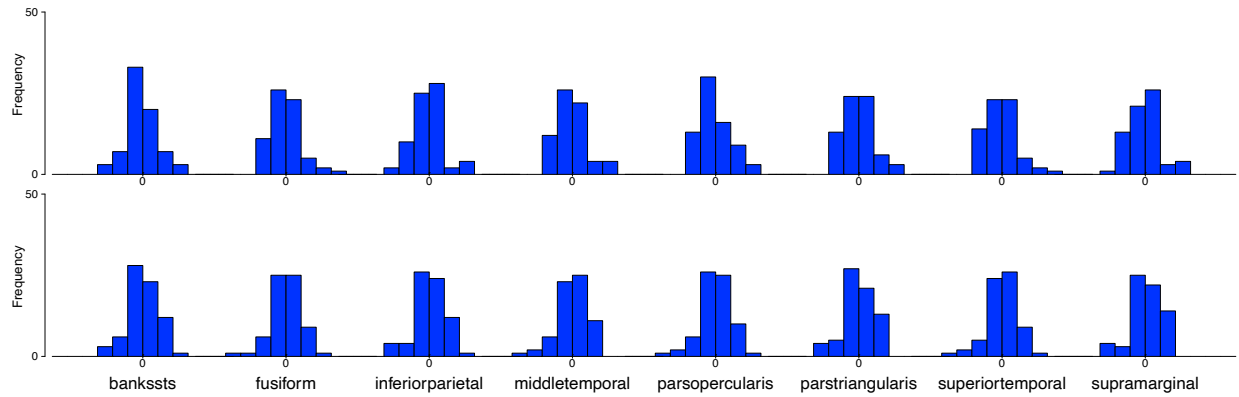
**Supplementary Figure 10.** Distribution of curve features of white matter volume. Top row depicts histograms for curve intercepts. Bottom row depicts histograms for curve slopes. Brain estimates were scaled for visualization purposes, but skewness was not altered.



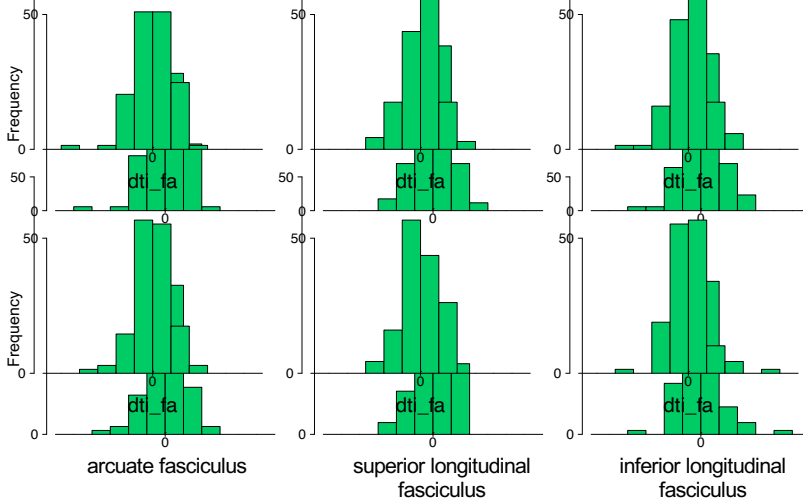
**Supplementary Figure 11.** Distribution of curve features of surface area. Top row depicts histograms for curve intercepts. Bottom row depicts histograms for curve slopes. Brain estimates were scaled for visualization purposes, but skewness was not altered.



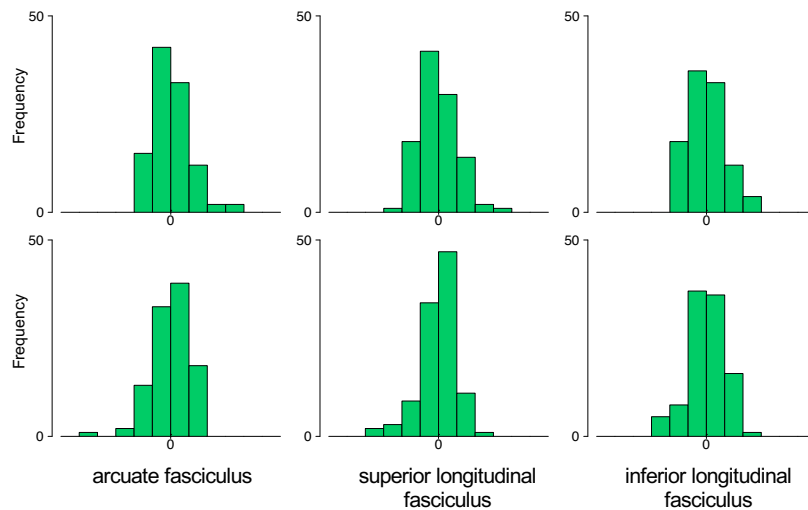
**Supplementary Figure 12.** Distribution of curve features of cortical thickness. Top row depicts histograms for curve intercepts. Bottom row depicts histograms for curve slopes. Brain estimates were scaled for visualization purposes, but skewness was not altered.



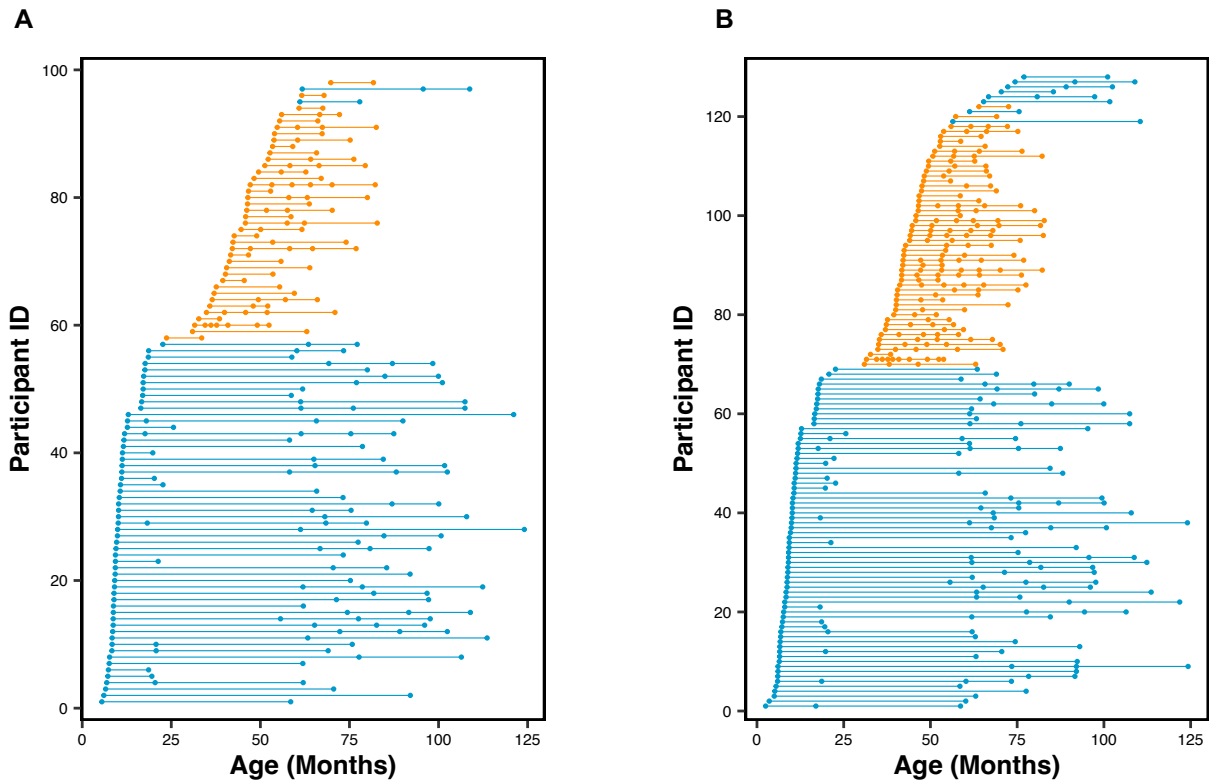
**Supplementary Figure 13.** Distribution of curve features of mean curvature. Top row depicts histograms for curve intercepts. Bottom row depicts histograms for curve slopes. Brain estimates were scaled for visualization purposes, but skewness was not altered.



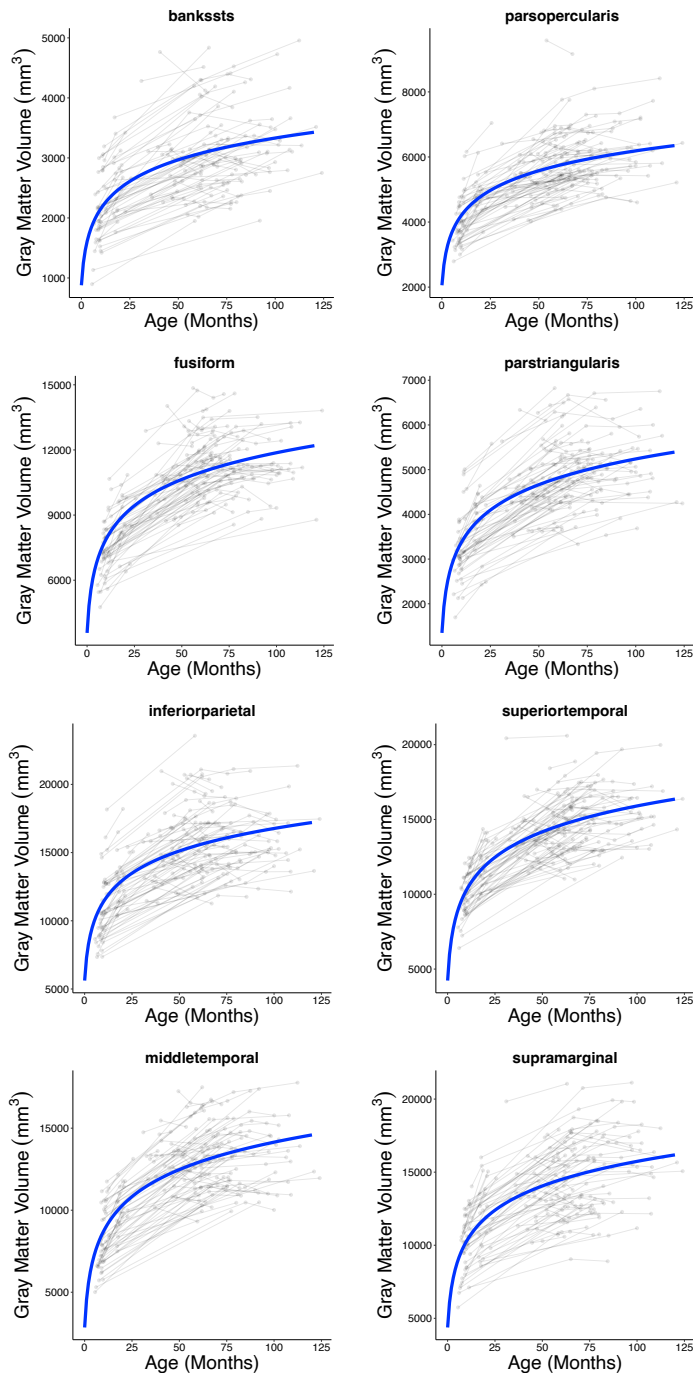
**Supplementary Figure 14.** Distribution of curve features of fractional anisotropy. Top row depicts histograms for curve intercepts. Bottom row depicts histograms for curve slopes. Brain estimates were scaled for visualization purposes, but skewness was not altered.



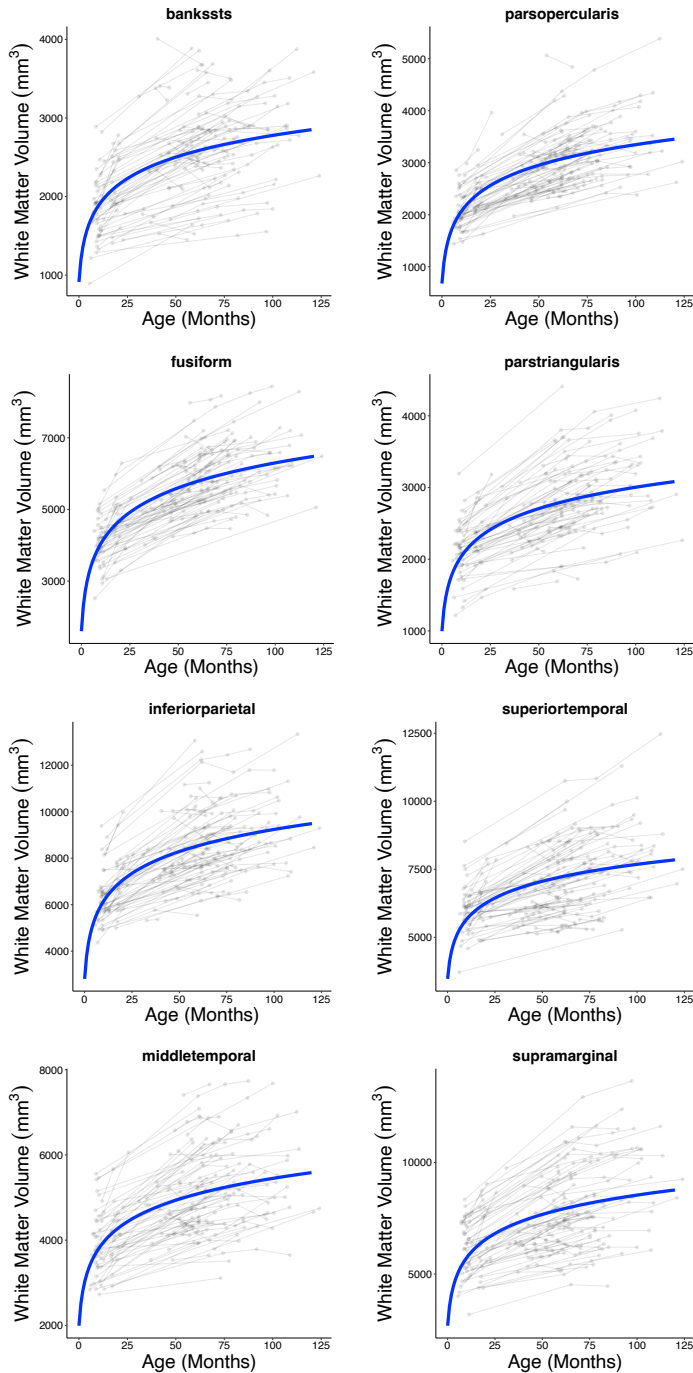
**Supplementary Figure 15.** Distribution of curve features of mean diffusivity. Top row depicts histograms for curve intercepts. Bottom row depicts histograms for curve slopes. Brain estimates were scaled for visualization purposes, but skewness was not altered.



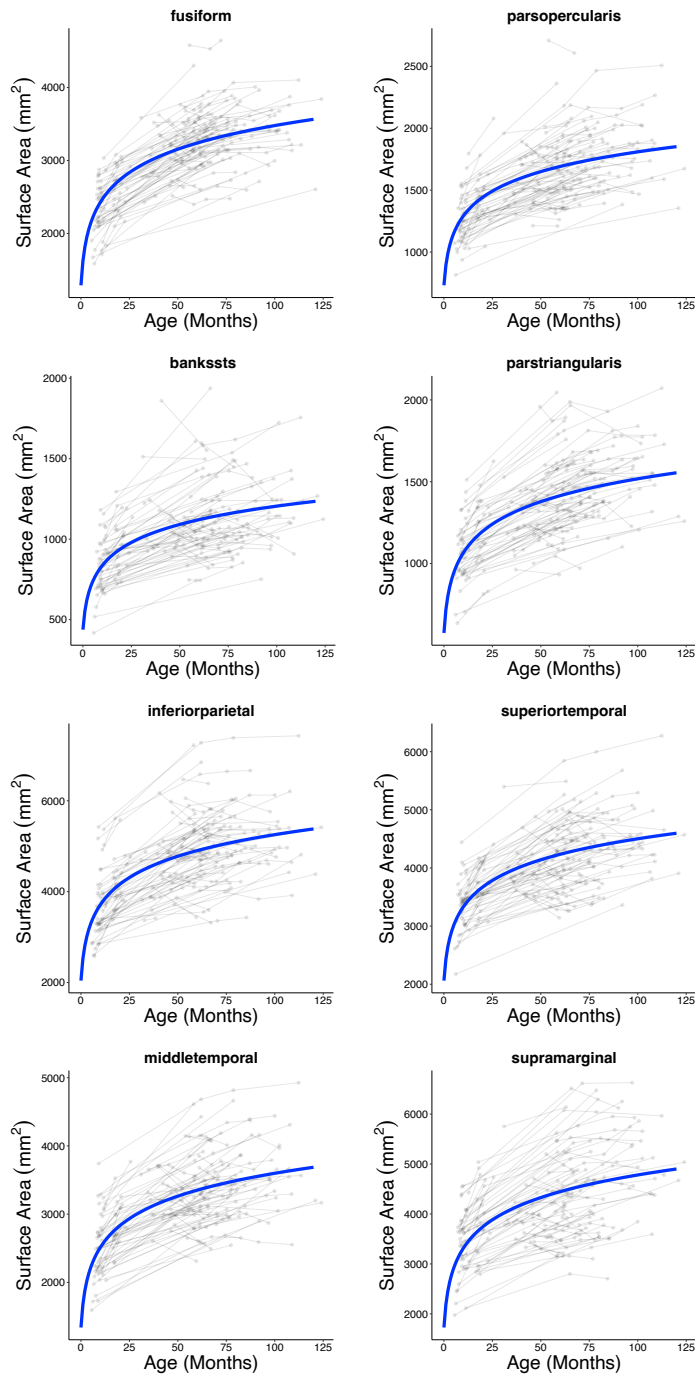
**Supplementary Figure 16.** Age distributions by modality of longitudinal datasets from infancy to late childhood. All children had (A) structural and/or (B) diffusion MRI data from at least two observations (dots). Blue, New England cohort; orange, Calgary cohort.



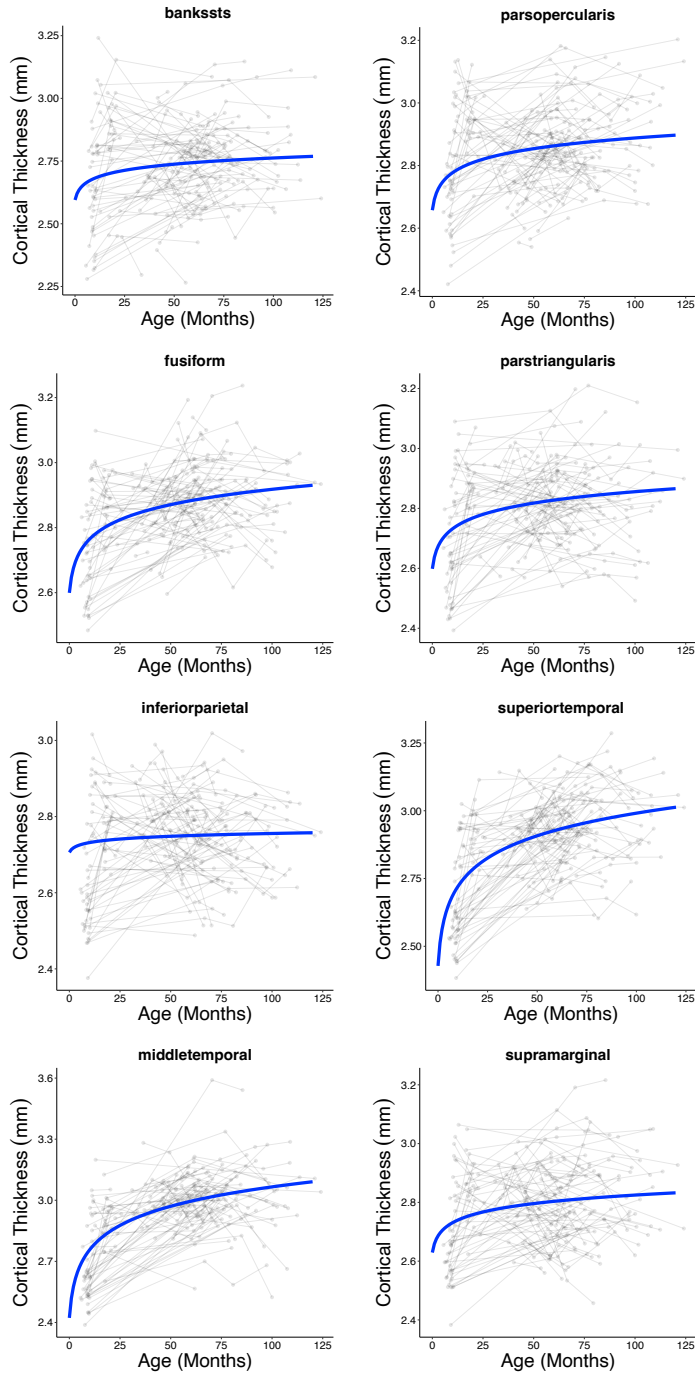
**Supplementary Figure 17.** Longitudinal trajectories of gray matter volume between infancy and late childhood. Raw estimates of gray matter volume (gray spaghetti plot backdrop) were submitted to linear mixed effects models using a logarithmic function. Individual growth curves predicted by this model were averaged to show the overall longitudinal trajectory of the sample (blue line).



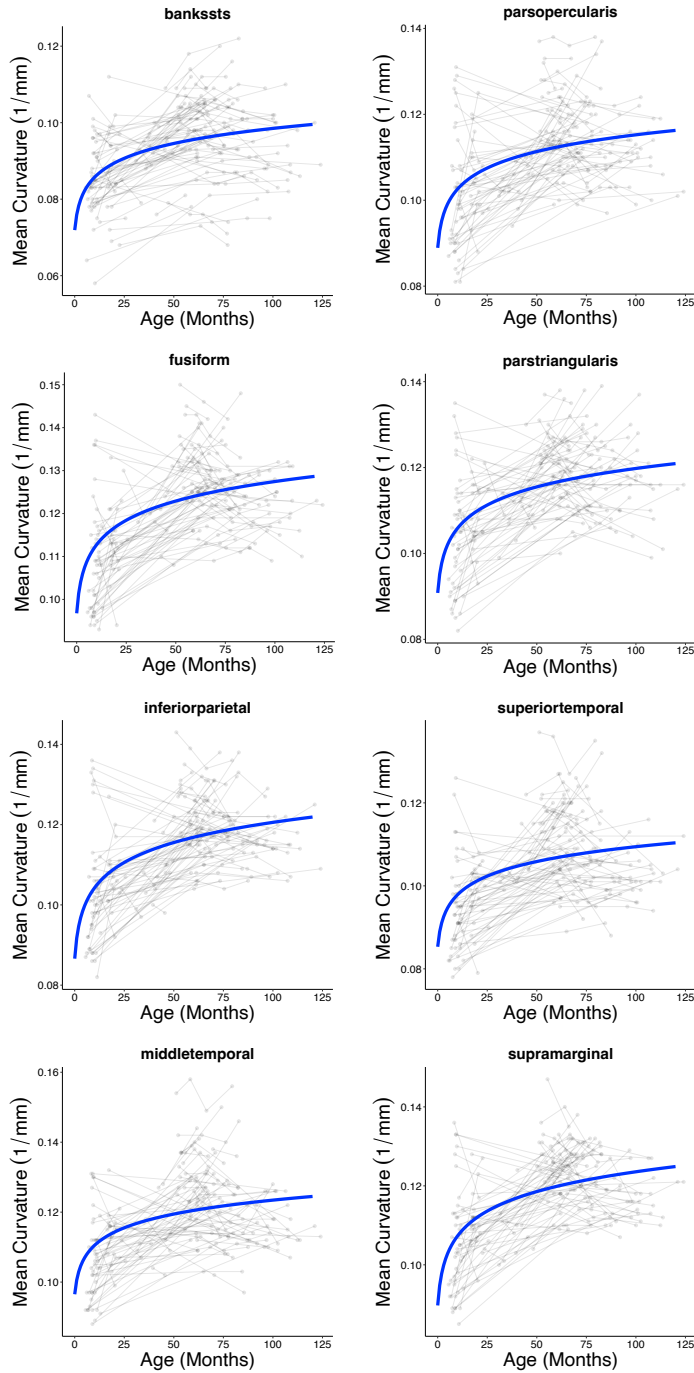
**Supplementary Figure 18.** Longitudinal trajectories of white matter volume between infancy and late childhood. Raw estimates of white matter volume (gray spaghetti plot backdrop) were submitted to linear mixed effects models using a logarithmic function. Individual growth curves predicted by this model were averaged to show the overall longitudinal trajectory of the sample (blue line).



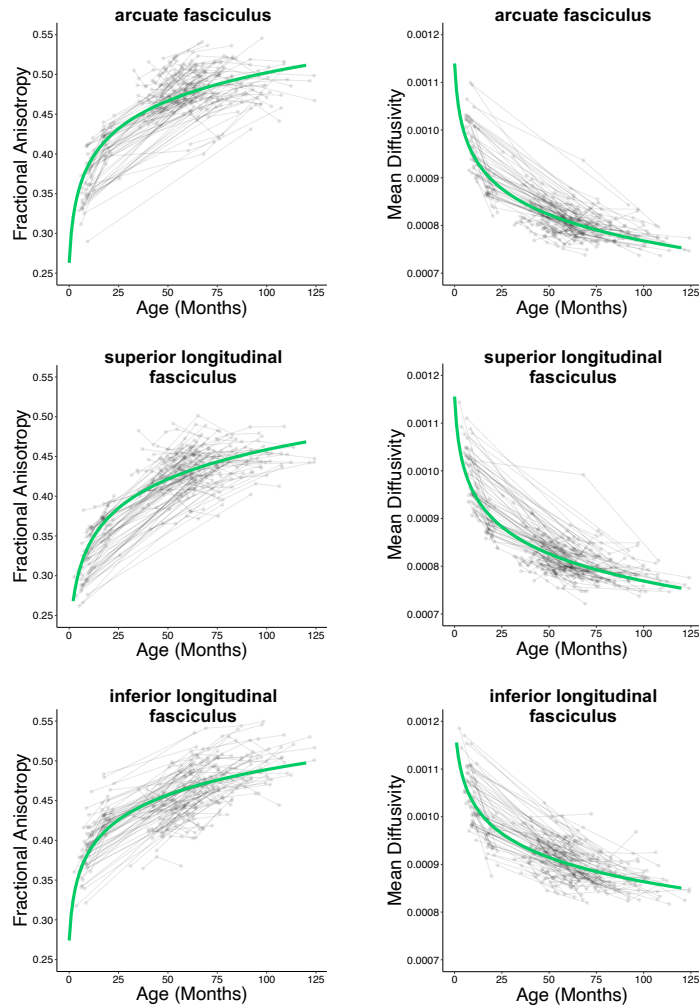
**Supplementary Figure 19.** Longitudinal trajectories of surface area between infancy and late childhood. Raw estimates of surface area (gray spaghetti plot backdrop) were submitted to linear mixed effects models using a logarithmic function. Individual growth curves predicted by this model were averaged to show the overall longitudinal trajectory of the sample (blue line).



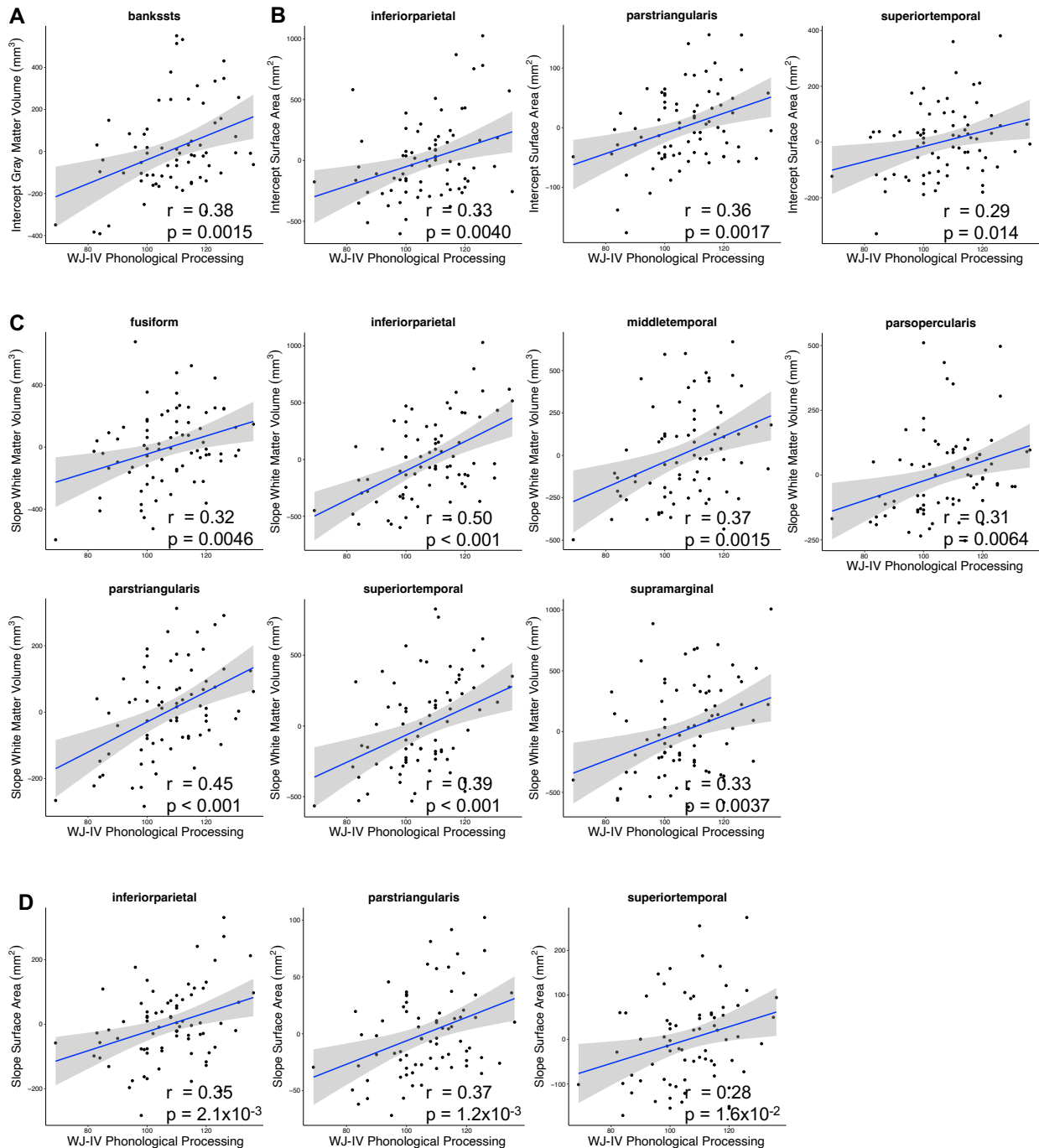
**Supplementary Figure 20.** Longitudinal trajectories of cortical thickness between infancy and late childhood. Raw estimates of cortical thickness (gray spaghetti plot backdrop) were submitted to linear mixed effects models using a logarithmic function. Individual growth curves predicted by this model were averaged to show the overall longitudinal trajectory of the sample (blue line).



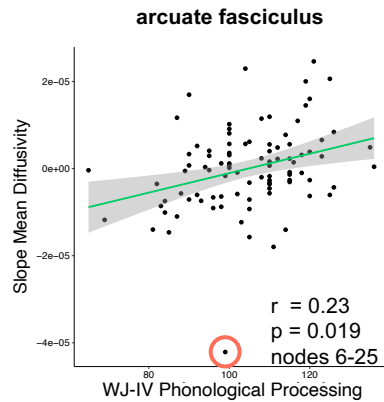
**Supplementary Figure 21.** Longitudinal trajectories of mean curvature between infancy and late childhood. Raw estimates of mean curvature (gray spaghetti plot backdrop) were submitted to linear mixed effects models using a logarithmic function. Individual growth curves predicted by this model were averaged to show the overall longitudinal trajectory of the sample (blue line).



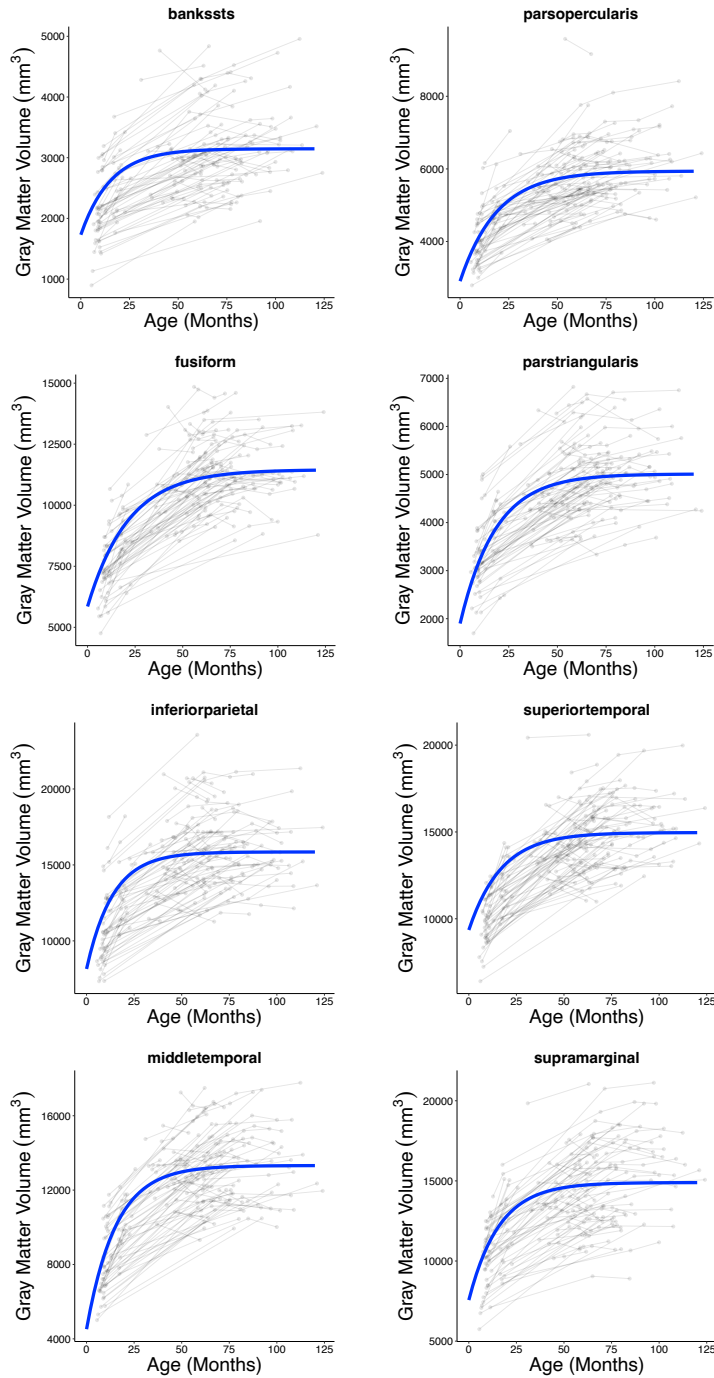
**Supplementary Figure 22.** Longitudinal trajectories of fractional anisotropy and mean diffusivity between infancy and late childhood. Raw diffusion estimates (gray spaghetti plot backdrop) were submitted to linear mixed effects models using a logarithmic function. Individual growth curves predicted by this model were averaged to show the overall longitudinal trajectory of the sample (green line).



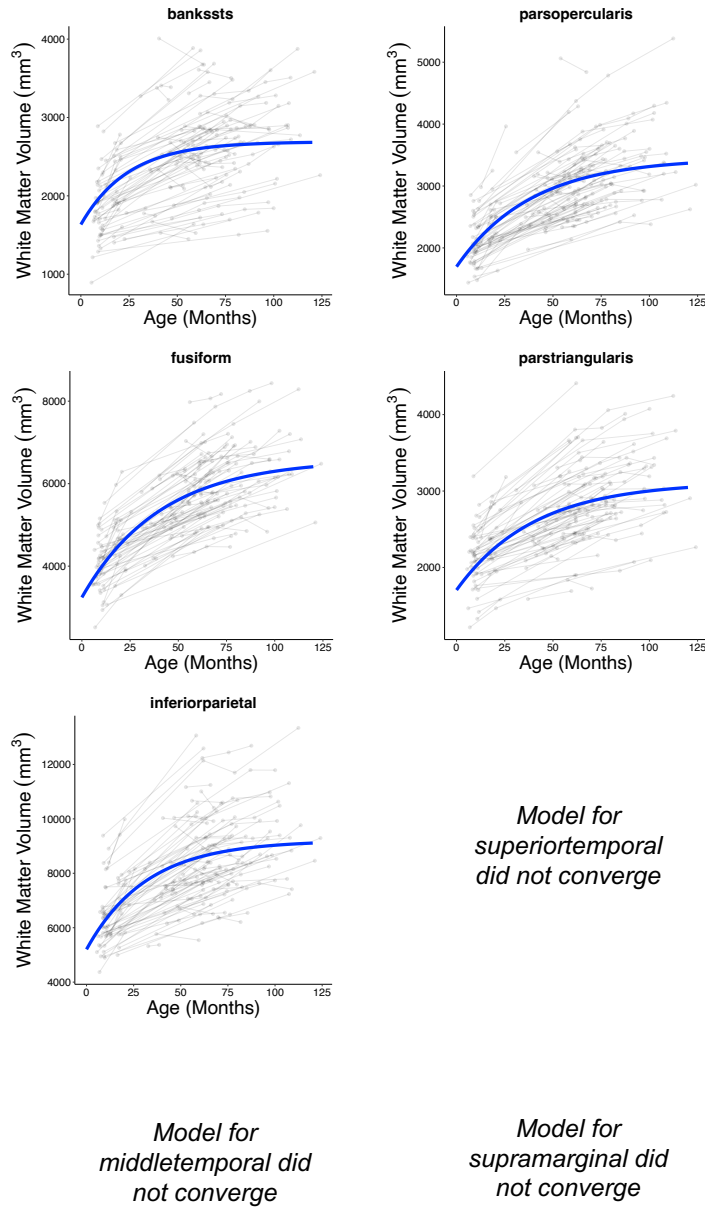
**Supplementary Figure 23.** Statically significant associations between growth curve features of brain volume and surface area and preschool/early kindergarten phonological processing. (A) Gray matter volume in the left banks of the superior temporal sulcus exhibited an association between growth curve intercepts and phonological processing, whereas (C) all associations with white matter volume were between growth curve slopes and phonological processing. Both surface area intercepts (B) and slopes (D) exhibited associations with phonological processing. All associations pass  $p_{FDR} < 0.05$ . WJ-IV, Woodcock-Johnson IV.



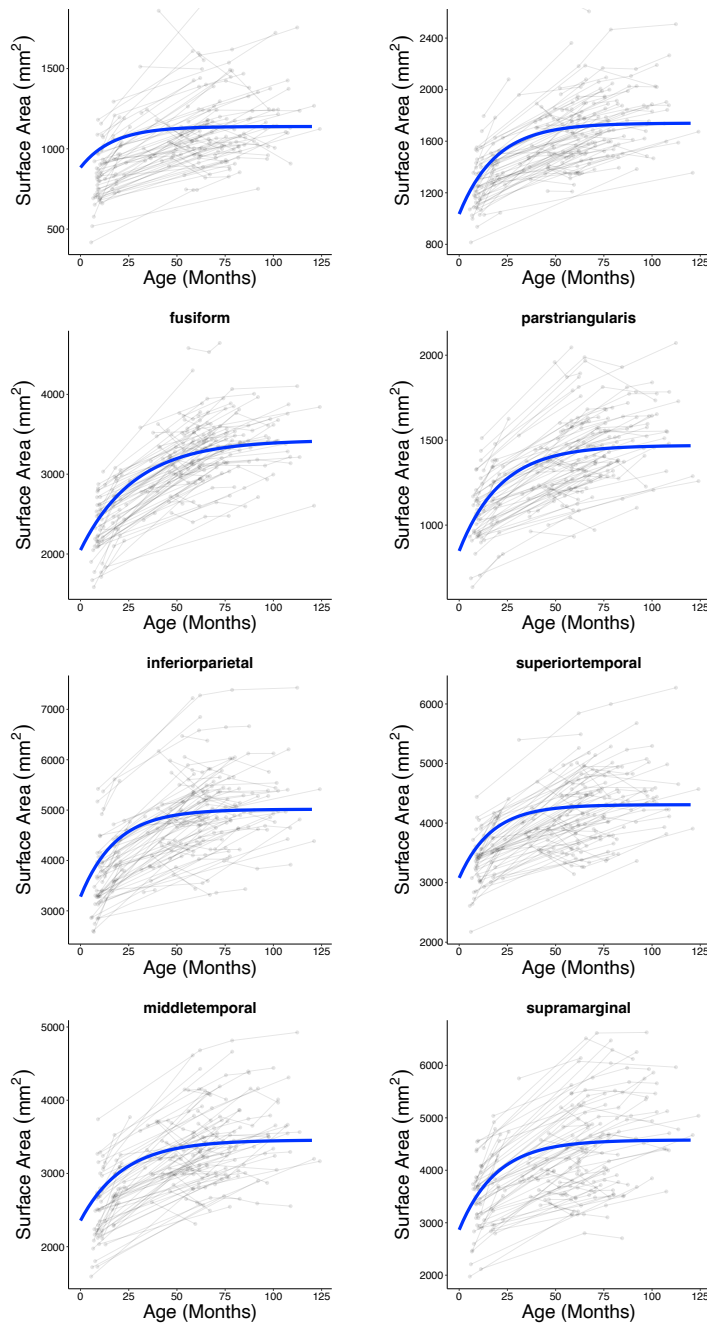
**Supplementary Figure 24.** Statistically significant associations between growth curve features of white matter organization and preschool/early kindergarten phonological processing skill. Mean diffusivity in the left arcuate fasciculus exhibited associations between growth curve slopes and phonological processing. Association is cluster-level corrected at  $p_{FWE} < 0.05$ . Note: removal of outlier (orange circle) did not abolish cluster-level significance. WJ-IV, Woodcock-Johnson IV.



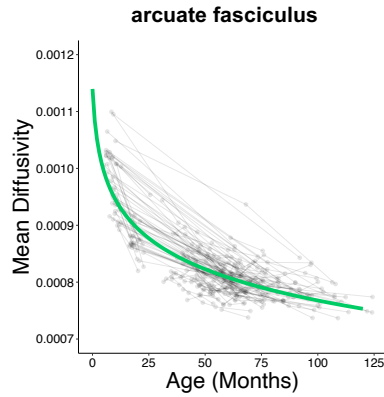
**Supplementary Figure 25.** Longitudinal trajectories of gray matter volume between infancy and late childhood generated for sensitivity analyses. Raw estimates of gray matter volume (gray spaghetti plot backdrop) were submitted to nonlinear mixed effects models using an asymptotic function. Individual growth curves predicted by this model were averaged to show the overall longitudinal trajectory of the sample (blue lines).



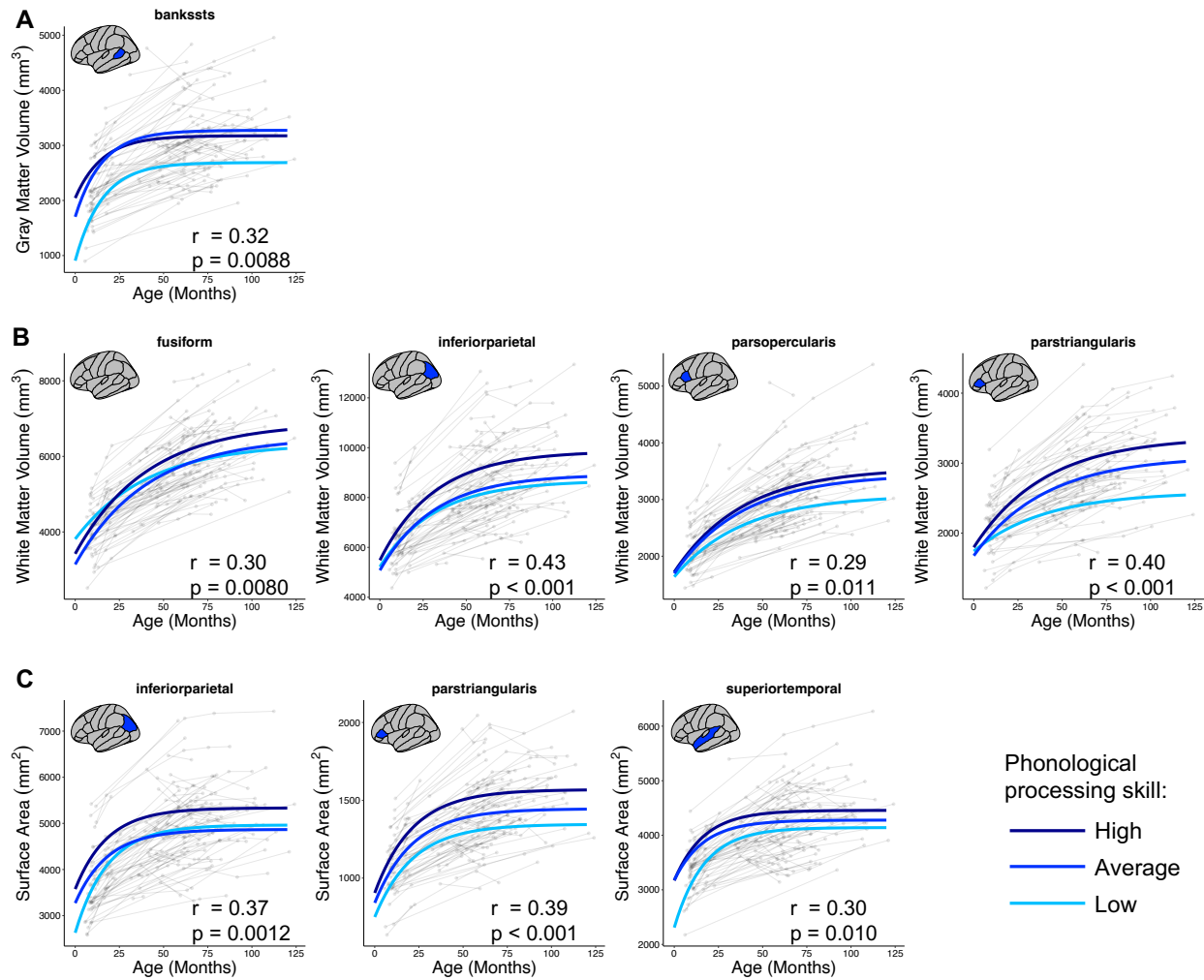
**Supplementary Figure 26.** Longitudinal trajectories of white matter volume between infancy and late childhood generated for sensitivity analyses. Raw estimates of white matter volume (gray spaghetti plot backdrop) were submitted to nonlinear mixed effects models using an asymptotic function. Individual growth curves predicted by this model were averaged to show the overall longitudinal trajectory of the sample (blue lines).



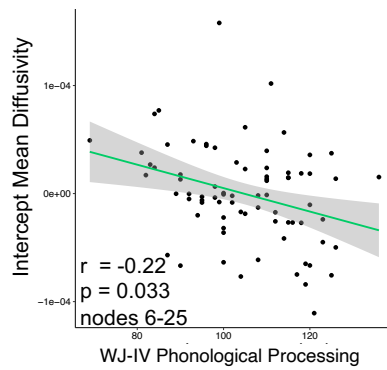
**Supplementary Figure 27.** Longitudinal trajectories of surface area between infancy and late childhood generated for sensitivity analyses. Raw estimates of surface area (gray spaghetti plot backdrop) were submitted to nonlinear mixed effects models using an asymptotic function. Individual growth curves predicted by this model were averaged to show the overall longitudinal trajectory of the sample (blue lines).



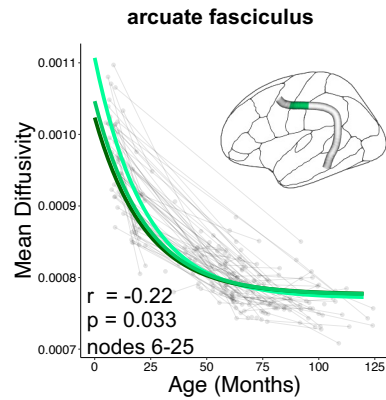
**Supplementary Figure 28.** Longitudinal trajectories of mean diffusivity between infancy and late childhood generated for sensitivity analyses. Raw estimates of mean diffusivity (gray spaghetti plot backdrop) were submitted to a nonlinear mixed effects model using an asymptotic function. Individual growth curves predicted by this model were averaged to show the overall longitudinal trajectory of the sample (green lines).



**Supplementary Figure 29.** Longitudinal trajectories of brain structure from infancy to late childhood according to phonological processing skill in preschool/early kindergarten for sensitivity analyses. Graphs depict average trajectories for children with low (< 85), average (85 – 115), and high (> 115) standardized phonological processing scores for measures and regions whose (A) intercepts, (B) slopes, or (C) both intercepts and asymptotes correlated with phonological processing ( $p_{\text{FDR}} < 0.05$ ). Correlation statistics are reported adjacent to their corresponding plots; intercept and asymptote statistics for surface area averaged here for visualization purposes but reported separately in Supplemental Table 3.

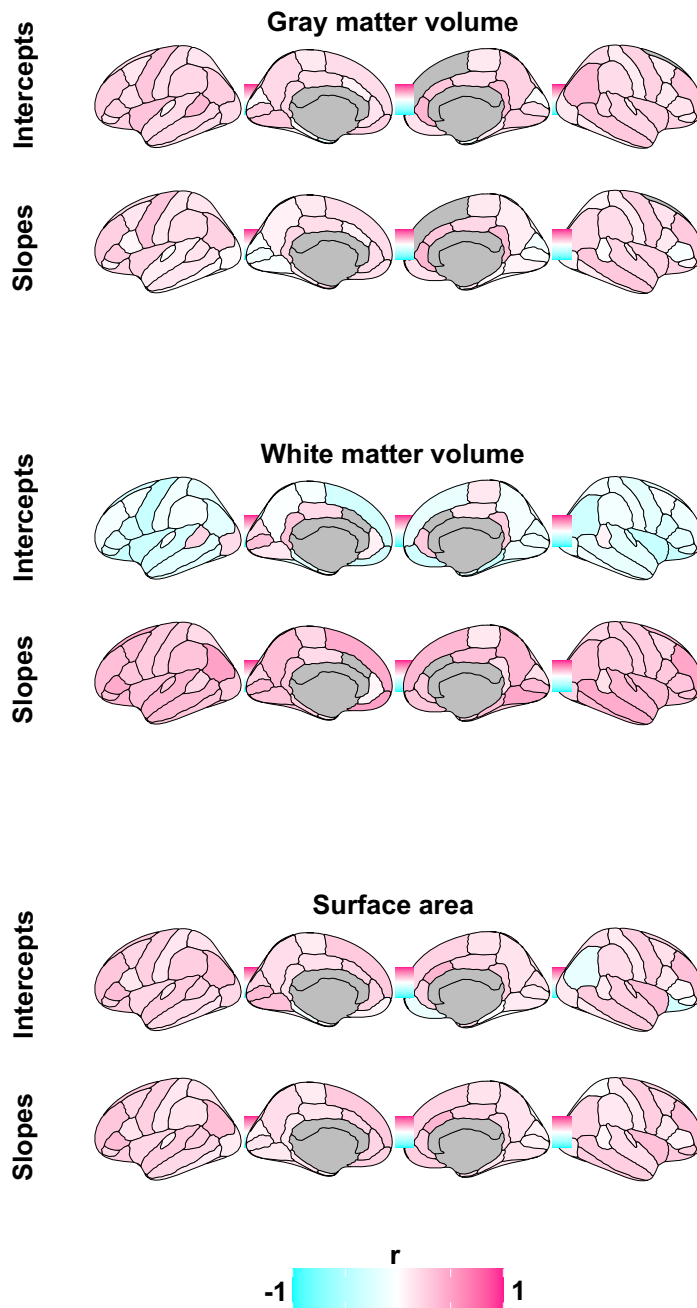


**Supplementary Figure 30.** Statistically significant associations between growth curve features of white matter organization and preschool/early kindergarten phonological processing for sensitivity analyses. Mean diffusivity in the left arcuate fasciculus exhibited a negative association between growth curve intercepts and phonological processing. Association is cluster-level corrected at  $p_{FWE} < 0.05$ . WJ-IV, Woodcock-Johnson IV.



Phonological processing skill: Low Average High

**Supplementary Figure 31.** Longitudinal trajectories of mean diffusivity from infancy to late childhood according to phonological processing skill in preschool/early kindergarten for sensitivity analyses. Graph depicts average trajectories for children with low (< 85), average (85 – 115), and high (> 115) standardized phonological processing scores for the left arcuate fasciculus nodes whose intercepts correlated negatively with phonological processing ( $p_{FWE}$  cluster-level < 0.05).



**Supplementary Figure 32.** Maps of brain-behavior associations. Brain maps show associations between curve features (intercepts and slopes) and preschool/early kindergarten phonological processing across brain regions in the Desikan-Killiany atlas for gray matter volume, white matter volume, and surface area. Note: no model convergence for superior frontal volume and no white matter volume measures were available for anterior cingulate cortex.